Optimizing Ternary Nanocarriers for Stable and Non-Toxic Delivery of Rictor/mTORC2 RNAi Against Triple Negative Breast Cancer

By

Shrusti Shailesh Patel

Dissertation

Submitted to the Faculty of the

Graduate School of Vanderbilt University

in partial fulfillment of the requirements

for the degree of

DOCTOR OF PHILOSOPHY

in

Biomedical Engineering

May 10, 2024

Nashville, Tennessee

Approved:

Craig L. Duvall, Ph.D.

Rebecca S. Cook, Ph.D.

Todd D. Giorgio, Ph.D.

John T. Wilson, Ph.D.

Dana M. Brantley-Sieders, Ph.D.

Dedication

This work is dedicated to my siblings, Shivani and Smit,
who were always just a phone call away.

Acknowledgements

I am incredibly lucky to have the support of many individuals throughout my PhD career. I would first like to thank my favorite lab mate and graduate advisor, Dr. Craig Duvall, for his exceptional mentorship and guidance. There were many tough days that were improved by his constant encouragement and willingness to aid me both emotionally as well as in my research. I am tremendously grateful for all our easy conversations and his trust in me to improve myself as well as those around me. I already know that I will never have a boss as amazing as him and will miss having him in my corner.

I am also extremely thankful to Dr. Rebecca Cook and Dr. Dana Brantley-Sieders for their wealth of knowledge on Rictor and cancer biology. Rictor biology has been Dr. Cook's passion for a long time, and I feel honored to have borrowed it for these past years. I am also grateful to Dr. John Wilson and Dr. Todd Giorgio, who always paused for a greeting and a chat when they would run into me in the hallway.

My sincerest gratitude also goes out to the members of Duvall Lab, who have been like a tightknit family to me. Dr. Meredith Jackson was responsible for my mentorship at the very start of my graduate career and was incredibly patient as I learned the ropes. Much of this work would not have been possible without Dr. Fang Yu and Dr. Ella Hoogenboezem, who supported me through many odd hours of animal work. Ella, in particular, always included me in her own studies, giving me the chance to learn. Dr. Prarthana Patil always made it a point to support me both within the lab and my personal life; this has not changed even as she moved on beyond Vanderbilt. Dr. Nora Francini is a brilliant mind that improved my work in so many ways but, more importantly, taught me to celebrate my successes. I could always count on Dr. Justin Lo and Dr. Richard d'Arcy to answer even the most niche questions on cancer biology and polymer chemistry, respectively,

among their many other responsibilities. Working with younger PhD students within the Duvall Lab brought me an endless source of energy; they have truly kept me young these past years. I also had the opportunity to mentor brilliant student, Fiona Cherry, in her undergraduate research, and it gave me the greatest joy to watch her succeed.

My PhD also granted me life-long friends who made even the hardest days something to look forward to. Dr. Carli DeJulius included me in every aspect of her life, and she and her husband, Jesse Beckner, have been so generous to open their home and family to me countless times. Dr. Jenna Poole has been the greatest roommate and dearest friend who made our cozy Nashville apartments feel like home. I have never known a greater kindred spirit who shared so many of my interests, opinions, and life experiences.

Finally, I would like to thank my family for patiently waiting for me to complete my graduate work, which often left little time to dedicate to those existing outside my PhD. My parents, in particular, trusted me to strike out to Nashville on my own, and their faith carried me through many daunting adult tasks. Finally, thank you to my older sister and younger brother, Shivani and Smit; our sibling group chat, mostly filled with useless chatter, has been pinned in my messages for years now and a greater source of strength than you could ever know.

I would also like to acknowledge my funding sources, National Institutes of Health (NIH R01 CA224241) and the National Science Foundation (NSF GRF 1937963).

TABLE OF CONTENTS

LIST OF FIGURES

LIST OF TABLES

Chapter 1: Introduction

1.1. Background and Significance

1.1.i. Therapies for triple negative breast cancer

Basal-like breast cancer, or triple negative breast cancer (TNBC), makes up 15-20% of all BCs and is considered a particularly aggressive subtype of the disease.[1, 2] TNBC is given its name because it lacks expression of estrogen receptor (ER), progesterone receptor (PR), and human epidermal growth factor receptor 2 (HER2), key biomarkers that aid in the clinical evaluation and targeted treatment of BC in a subtype-specific manner. Few molecularly-targeted clinical therapies are available for the treatment of TNBC, making cytotoxic neoadjuvant chemotherapy (NAC) and tumor resection surgery the most readily available options.[3, 4] Despite displaying a clinical response to neoadjuvant chemotherapy,[5] TNBC patients, when compared to those harboring other BC subtypes, are more likely to experience distant recurrence and death within the first 5 years following surgical tumor resection.[3] TNBC is furthermore characterized as a more aggressive subtype compared to other BCs due to earlier and higher rates of metastasis as well as an overall reduction in disease-free survival.[2, 6, 7] While chemotherapy provides significant therapeutic benefit, as low as 30% of TNBC patients experience a pathologic complete response (pCR).[4] Overall, there remains a critical clinically unmet need for potent, targeted therapies against TNBC.

Despite TNBCs displaying some of the greatest rates of pCR, compared to other BC subtypes,[4, 8] nearly 70% of NAC-treated TNBC patients harbor residual disease (RD). Identification of the molecular culprits of tumor cell survival in the face of chemotherapy could guide the use of medicines to target these molecular pathways and consequently enable a greater response to NAC. Close to 50% of TNBC RDs harbor genomic alterations within the phosphatidyl

inositol-3 kinase/ mechanistic target of rapamycin (PI3K/mTOR) pathway, correlating PI3K/mTOR signaling with chemoresistance. The PI3K pathway is frequently aberrantly activated in TNBCs, with a subset displaying activating mutations in PIK3CA and a much more substantial 30%-50% displaying loss of negative regulator PTEN.[9] Pan-PI3K inhibitors have achieved only limited clinical success due to associated toxicities,[10] but strategies to inhibit downstream effectors of this pathway, such as the mTOR complexes, have the potential to be more selective.

1.1.ii. Strategies for selective mTOR signaling inhibition

The protein kinase mTOR functions within two distinct protein complexes—mTORC1 and mTORC2. Previous studies show that inhibition of mTORC1, which controls many cellular processes (e.g., protein translation, autophagy, cellular metabolism) is ineffective in TNBCs. Everolimus is an allosteric inhibitor selective for mTORC1 activity blockade and is approved for the treatment of HER2+ BCs, as well as other cancer types. However, TNBC patients treated with everolimus, even when combined with chemotherapy, did not show a clinical response.[11-13] mTORC1 signaling is capable of IRS1-mediated negative feedback regulation of PI3K activity, meaning that mTORC1 inhibitors can only achieve partial blockade of this pathway, and this may explain their relative failure in the TNBC realm.

ATP-competitive dual mTOC1/2 inhibitors have been developed as a next-generation strategy to overcome the shortcomings of mTORC1 inhibition. Dual mTORC1/2 inhibitors can block resurgent PI3K activation to mTORC2 but still allow activation to other PI3K effectors, limiting their therapeutic efficacy. Though many dual mTORC1/2 inhibitors are still in clinical development and may show promise, the TORKinib, AZD2014, failed to outperform everolimus in metastatic renal cell carcinoma patients, when assessing survival outcomes in a phase 2 trial. [14] In a combination therapy setting, AZD2014 combined with fulvestrant hormone therapy failed

to improve progression-free survival in BC patients or confer an advantage over everolimus, in one such phase 2 trial in 2019.[15] Despite these failures, pre-clinical studies using dual mTORC1/2 inhibitors point to an important role for mTORC2 signaling in tumorigenesis and progression that may be independent of mTORC1, but comparatively less is known about mTORC2 in TNBCs. mTORC2 regulates tumor cell survival and motility/metastasis in other cancer types, including HER2+ breast cancers. Mechanistic understanding of mTORC2 has been difficult to acquire because small molecule inhibitors that selectively block mTORC2, without also blocking mTORC1, do not exist. The complex protein interactions of this signaling node make it relatively "undruggable" by traditional small molecules without perturbing other arms of the mTOR pathway. However, RNAi strategies using siRNAs to block expression of the mTORC2 obligate cofactor, Rictor, at the mRNA level can selectively eliminate mTORC2 activity. RNAi can therefore be a powerful tool to assess the selective therapeutic effects of mTORC2 signaling in TNBC.

TNBCs are, by definition, a particularly heterogenous BC subtype that are grouped by their distinct lack of clinically-targetable markers ER, PR, and HER2. TNBC is often further classified by 4 intrinsic molecular subtypes: basal-like 1 (BL1), basal-like 2 (BL2), mesenchymal (M), and luminal androgen receptor (LAR).[16] Distinct molecular phenotypes of TNBC may have differential response to selective mTORC2 inhibition, and it is important to ascertain which patients, with their varying genetic alterations, may benefit from this strategy. Meta-analyses performed on BC expression datasets revealed that high *RICTOR* expression correlated with decreased progression-free survival in BL1 and BL2 TNBC subtypes but not for others.[17] For certain subtypes, particularly BL1 and BL2, this suggests that selective mTORC2 inhibition via Rictor targeting could be an advantageous therapy. Using high-throughput genomic profiling

technologies that are now becoming the norm, mTORC2-targeted therapies could be leveraged towards TNBC subtypes that would experience the greatest benefit, specifically those that are aberrantly activated in mTORC2 or related pathway signaling. Therefore, siRNA-mediated Rictor targeting can be used to elucidate the relative sensitivity of various TNBC phenotypes to selective mTORC2 inhibition while also serving as a potential therapy for PI3K-active TNBC.

1.1.iii. Barriers to siRNA delivery to the tumor

Though siRNA has the potential to be a powerful tool for otherwise undruggable targets, siRNA delivery to tumors *in vivo* faces several challenges, including siRNA susceptibility to nucleases, rapid siRNA clearance through kidneys, and diminished siRNA accumulation within the tumor due to poor tumor circulation. Polymeric siRNA-encapsulating nanoparticle (si-NP) carriers have the potential to mitigate many of these delivery barriers. Negatively charged siRNA can be efficiently packaged through complexation with positively charged polymers within the si-NP, allowing for siRNA to be "carried" in circulation rather than quickly cleared through the urine based on size and charge. si-NPs can also provide stealth shielding of the siRNA through incorporation of non-fouling, hydrophilic polymers that consequently enhance pharmacokinetics. si-NPs can furthermore harbor environmentally responsive polymer elements that can aid in delivery. For example, pH responsive polymers that can induce endosome disruption can promote robust siRNA delivery to the cytosol following si-NP uptake by a given cell.[18, 19]

Despite these many advantages, abundant delivery and accumulation of si-NPs to tumor sites continues to be a major barrier to the success of RNAi nano-therapies.[20, 21] Limited tumor accumulation following systemic administration of NPs are often correlated to a lack of si-NP endurance in blood circulation.[22-24] Passive accumulation of NPs at tumor sites often depends on the enhanced permeation and retention (EPR) effect by tumors, where circulating si-NPs will

have enhanced preferential delivery to the tumor due to leaky vessel architecture and will remain entrapped in the tumor due to compromised lymphatic drainage.[25-27] By increasing circulation time of the si-NP, the window of opportunity for si-NPs to encounter the tumor is also greatly broadened and will allow for si-NP accumulation at therapeutic levels. However, long persistence within blood circulation requires siRNA delivery systems to continue to be stable and avoid immediate breakdown.

Cationic si-NP systems are usually held together by electrostatic interactions wherein the cationic polymer complexes with the negatively-charged siRNA. These weak electrostatic bonds can be easily de-complexed through interactions with other proteins in circulation. Components in the glomerular basement of the kidneys, such as negatively charged proteoglycans and heparan sulfates, can begin to bind to the polymeric carrier systems.[28] These competitive charge interactions with the polycationic carrier can ultimately destabilize the carrier system. si-NP destabilization results in release of the siRNA cargo from the nanocarrier, where it is then likely to undergo renal filtration and clearance through the bladder. Intravenously-injected si-NPs must also circumvent other destabilizing factors, such as the reticuloendothelial system (RES) where macrophages phagocytose foreign material for removal from circulation.[29, 30] In a destabilized si-NP, exposure of charged core components can lead to plasma protein adsorption and opsonization by immunoglobulins, aiding in recognition of the NP by cells of the RES.[29, 31, 32]

Furthermore, nanoparticles can result in dose-limiting toxicities,[33] often due to the pH-responsive endosome disruptive components of nanoparticles that trigger the release of siRNA into the cell cytoplasm. These toxicities are also a function of si-NP delivery to off-target organs, including off-target delivery to liver Kupffer cells. In the case of siRNA therapies, “on-target” silencing of a gene in off-target organs can result in carrier-independent toxicities. In the case of

Rictor silencing, significant inhibition of mTORC2 signaling within the liver can result in hyperglycemia.[34] There is therefore a great need for the development of si-NP systems that can prolong stability in circulation and allow for delivery of siRNA to the tumor at therapeutically-relevant doses while also mitigating toxicity.

1.2. Innovation

1.2.i. Improved ternary nanoparticles for enhanced nanocarrier stability while reducing toxicity

si-NPs can be a powerful tool for the *in vivo* delivery of RNAi technology, but their clinical translation continues to be limited due to poor biodistribution to disease sites. Many strategies have been created to improve *in vivo* polymeric NP stability.[35-37] For si-NP systems specifically, many aim to enhance core hydrophobicity, either by modifying the siRNA cargo or polymeric carrier. One such example of modifying siRNA is the inclusion of hydrophobic moieties that are directly conjugated onto the siRNA. Previous work in our lab has used conjugation of hydrophobic molecule palmitic acid,[38, 39] while other groups have improved stability using moieties such as cholesterol or other hydrophobes.[40-42]

Here, we focus our efforts on increasing stability by using a ternary si-NP system. These ternary formulations contain 50:50 DMAEMA-*co*-BMA (50B) core-forming polymers and 20kDa poly(ethylene glycol)-*block*-50B (20kPEG-50B) corona-forming polymers where the molecular weight (MW) of the 50B core-forming polymer as well as its ratio to the corona-forming polymer is varied. This system further improves previously described ternary si-NP formulations in our lab that contain the hydrophobic core-forming 50B polymer and a corona-forming 5kDa PEG-*block*-50B.[37] By increasing the ratio of the core 50B polymer to the corona-forming polymers, ternary si-NPs have shown to improve stability.[37] However, the 50B polymer—the “active” component

of the si-NP capable of complexing siRNA and inducing endosome disruption—can also be toxic at large doses.[33, 43] This work therefore tunes the MW of 50B to balance activity, toxicity, and stability to improve upon early generations of ternary si-NPs.

Ternary si-NP designs have been used in various delivery scenarios, including siRNA delivery to tumors, likely due to the versatility and multiple functionalities that they can offer. Notably, the clinically approved Onpattro comprises multiple components, including a cationic DLin-MC3-DMA core lipid and 2k PEG-lipid surface-forming unit, as well as cholesterol and DSPC phospholipids. While others have reported use of PEG-lipid amphiphiles as NP surfactants, our 20kPEG-50B diblock surface-forming polymer provides comparable charge shielding, while advantageously also contributing to both siRNA complexation and endosome escape. Importantly, the high molecular weight (20 kDa) PEG surface polymer used in our si-NP has previously shown improved *in vitro* stability in serum and *in vivo* pharmacokinetics when compared to coronas of smaller MW.[44, 45] The comparatively simple design of our si-NP, comprised of siRNA and two polymers, also offers additional flexibility for future work to separately vary the cationic block composition of the core and surface-forming polymers

While ternary si-NPs has been leveraged in the past for creation of gene delivery systems, including RNAi nanocarriers, we show here a thorough characterization of *in vitro* and *in vivo* si-NP stability and activity as a direct function of the MW and ratio of the core-forming 50B polymer. Finally, to aid in the clinical accessibility of RNAi technology, we also developed a lyophilized formulation of these si-NPs through the addition of cryo- and lyo-protective excipients such as sucrose and trehalose. Using this lyophilized formulation, si-NPs can be stored long-term and retain their activity upon rehydration.

1.2.ii. Selective mTORC2 inhibition as TNBC therapy

Mutations in the PI3K/mTOR pathway are found in up to 70% of all BCs, and these mutations often involve aberrant overexpression of downstream oncogenes such as Akt.[46-49] The high frequency of mutations in the PI3K/mTOR pathway make it very targetable for TNBC treatment, and many have focused their efforts on mTOR signaling. Clinically, mTORC1-specific inhibitors such as rapamycin analogues (or rapalogues) have been used to treat various cancers and TNBC specifically; however, the treatments have altogether been unsuccessful.[11, 12] A phase 2 study of patients with primary TNBC compared the addition of the rapalogue, Everolimus, to the standard regimen of neoadjuvant chemotherapy; addition of everolimus did downregulate mTORC1 signaling but did not significantly improve patient response rate or pCR.[11] Low treatment efficacy of mTORC1-specific targeting is likely due to the resurgence of PI3K activity and downstream oncogene (Akt) expression, a result of inhibiting the negative feedback loop between mTORC1 and IRS-1.[50]

To improve this incomplete mTOR inhibition, dual mTORC1/mTORC2 kinase inhibitors (TORKinibs) have been developed and tested in BC.[51-53] Unlike treatment with rapalogues, TORKinib-based dual mTORC1/2 treatment dampens phosphorylation of Akt, a downstream effector of mTORC2.[52, 53] However in TNBC, TORKinib treatment still gives rise to a resistant cancer stem cell-like population.[51] Despite this, TORKinibs continue to be tested clinically,[54] though there is still much to be learned about the impact of mTORC2-specific inhibition.

Sole inhibition of mTORC2 has thus far been unexplored clinically because of a lack of small molecules that selectively target the signaling complex. Here, we selectively inhibit mTORC2 signaling *in vivo* using RNAi nanocarriers carrying siRNA against the mTORC2 cofactor, Rictor. mTORC2-selective inhibition was studied across varying TNBC molecular

phenotypes, allowing for a subtype-specific exploration of mTORC2-selective therapy for the first time. Furthermore, we characterized modulations in the PI3K/mTOR pathway as well as related signaling pathways following selective mTORC2 inhibition. By elucidating the signaling effects of mTORC2 blockade, we identified potential compensatory feedback loops within the PI3K/mTOR pathway to design combination strategies that take the greatest advantage of this selective inhibition in TNBC.

1.2.iii. mTORC2 inhibition as combination therapy to improve chemotherapy cell killing

For many cancers, and TNBC specifically, combination chemotherapy is the current clinical standard of care.[55, 56] Cytotoxic chemotherapy agents such as paclitaxel and doxorubicin have provided great benefit to TNBC patients.[57-60] Further combining these agents with novel targeted therapies against TNBC can afford even greater efficacy. Nearly 50% of TNBC patients treated with neoadjuvant chemotherapy displayed aberrant activation of mTORC2 signaling in their residual tumors, making mTORC2 an important target that may be promoting resistance to chemotherapy.[61] By inhibiting mTORC2 activity in a neoadjuvant setting, we may be able to greatly reduce incidences of recurrence and metastasis in TNBC patients following tumor resection surgery.

In HER2-amplified breast cancer models, we have previously shown mTORC2 inhibition combined with lapatinib chemotherapy blocked tumor cell growth and *in vivo* tumor growth, and this effect was superior to lapatinib treatment alone.[17, 62] In HER2-amplified breast cancer cell lines with lapatinib resistance, genetic ablation of Rictor also resulted in decreased tumor cell growth.[62] Similarly, we show here that combining mTORC2 inhibition with standard of care chemotherapy, paclitaxel and doxorubicin, can raise an antitumor effect against TNBCs that possess PI3K/mTOR-related mutations. Since PI3K-active TNBCs may not be sensitive to sole

chemotherapy treatment due to resistance effects, combination with mTORC2 blockade can improve outcomes. Using our optimized si-NP system, we successfully assessed this combination effect with paclitaxel *in vivo*, in actively growing TNBC tumors.

mTORC2 inhibition and chemotherapy may also produce cooperative effects that are rooted in their respective mechanisms of action. Emerging data suggests that mTORC2 may regulate microtubule organization by way of its more well-known role in actin remodeling through Rho and Rac effector pathways.[63, 64] Studies on mTORC2 effect on endothelial cell elongation revealed that dual mTORC1/2 inhibition, but not selective mTORC1 inhibition, blocked elongation by way of impacting microtubule organization.[65] Importantly, this effect was recapitulated by microtubule stabilization induced by paclitaxel treatment, suggesting that mTORC2 inhibition may play a similar role in over-stabilization of microtubules. Thus, mTORC2 targeting could sensitize TNBCs to taxane-based chemotherapies through the convergence of these two drugs on spindle microtubule dynamics.

1.3. Specific Aims

The overall objective of our work was to develop an active and non-toxic siRNA-carrying nanoparticle complex (**si-NP**) that can serve as a molecularly-targeted therapy for TNBC patients through Rictor silencing and blockade of mTORC2 activity. Using this si-NP technology, we also sought to assess the therapeutic effect of mTORC2 inhibition in TNBC when combined with chemotherapy. To this end, we pursued the following specific aims:

Specific Aim 1: Develop ternary siRNA nanoparticle (si-NP) chemistry for improved *in vivo* nanocarrier stability, activity, and toxicity. The goal of this aim was to optimize si-NP stability and silencing activity by varying the core-forming polymer within a ternary si-NP formulation.

Using ternary si-NPs composed of a core-forming 50:50 poly(50B) polymer and a surface-forming 20kDa poly(ethylene glycol)-*block*-50B (20kPEG-50B) polymer, the 50B core-forming polymer molecular weight was iteratively varied, as was its ratio to the 20kPEG-50B polymer. Resulting si-NPs were assessed for siRNA encapsulation, stability in heparin and serum, toxicity, endosome escape ability, and gene silencing activity. Lead si-NPs were delivered intravenously (i.v.) to mice, measuring siRNA circulation time, tumor siRNA accumulation, and tumor model gene silencing. Lead si-NPs were delivered i.v. to healthy, wild-type mice to assess toxicity following an acute as well as a multi-dose si-NP treatment.

Specific Aim 2: Assess therapeutic impact of selective mTORC2 inhibition in TNBC. Using human TNBC cell lines harboring gene amplified *RICTOR* as well as PI3K pathway mutations (HCC70, CAL851) or diploid *RICTOR* (MDA-MB-157), siRNA-mediated *RICTOR* or *RAPTOR* knockdown selectively blocked mTORC2 or mTORC1, respectively. Treated cultures were assessed for target knockdown, PI3K/mTOR signaling, tumor cell growth, and tumor cell apoptosis. In parallel studies, cells were treated with a selective mTORC1 inhibitor (RAD001) or dual mTORC1/2 inhibitor (PP242) and assessed similarly. Studies repeated with paclitaxel and doxorubicin assessed if mTORC2 signaling inhibition affects TNBC chemo-response.

Specific Aim 3: Determine if siRictor-NPs selectively block mTORC2 and improve TNBC tumor cell killing *in vivo*. Selective mTORC2 inhibition in *RICTOR*-amplified TNBCs *in vivo* was achieved using optimized si-NPs (Aim 1) for i.v. delivery of *RICTOR* siRNA (siRictor-NP) to tumor bearing mice. Tumors were assessed for *RICTOR* silencing, mTORC2 signaling, cell proliferation, apoptosis, and volume. Mouse plasma was assessed to confirm a lack of si-NP mediated toxicity. These studies were repeated in combination with paclitaxel to assess if mTORC2 inhibition affects TNBC response to chemotherapy.

Chapter 2: Optimized ternary siRNA nanoparticles for active and non-toxic in vivo siRNA delivery to the tumor

Text for Chapter 2 taken from:

Patel SS, Hoogenboezem EN, Yu F, DeJulius CR, Fletcher RB, Sorets AG, Cherry FK, Lo JH, Bezold MG, Francini N, d'Arcy R, Brasuell JE, Cook RS, Duvall CL. Core Polymer Optimization of Ternary siRNA Nanoparticles Enhances In Vivo Safety, Pharmacokinetics, and Tumor Gene Silencing. 2023. *Biomaterials* 297. **DOI:** 10.1016/j.biomaterials.2023.122098.

2.1. Introduction

siRNA-based RNAi therapeutics are a promising strategy for the treatment of a variety of diseases that lack druggable targets. Systemic delivery of siRNA alone, however, is limited by rapid kidney clearance, inadequate inherent cellular uptake, and poor endosome escape. As a result, carrier free siRNAs have thus far required receptor-ligand targeting for success.[66] For a heterogeneous disease like cancer, where universal cellular receptors are lacking, nanoscale delivery vehicles can support target tissue siRNA delivery. Recent clinical success of nanocarriers for siRNA delivery was seen for Onpattro (patisiran), a lipid-based siRNA nanoparticle (LNP) formulation targeting hepatocytes for the treatment of transthyretin-mediated amyloidosis.[67, 68] While the FDA approval of Onpattro paves the way for the translation of other siRNA nano-systems, siRNA delivery to extrahepatic tissue, such as tumors, remains elusive.

LNPs such as Onpattro have been intensely investigated as systemic siRNA delivery systems.[69-73] In contrast, polymer-based siRNA nanoparticle (si-NP) systems are less studied. However, polymer-based si-NPs offer advantages in scalability, limitless chemical variations, and incorporation of "smart" components that respond to environmental stimuli or promote endosome

escape. For instance, the high tunability of cationic polymer systems was recently employed to drive tissue-selective mRNA delivery to the spleen and lymph nodes.[74]

Nanoparticle chemical physical properties can be optimized to enhance passive tumor accumulation, independent of any specific receptor-ligand targeting. However, passive NP accumulation in tumor tissue requires a stable formulation that extends circulation time following intravenous (i.v.) delivery. Cationic polymer si-NPs are typically held together by electrostatic interactions between the cationic polymer and the negatively charged siRNA. Unfortunately, these electrostatic bonds are de-complexed through serum protein interactions in circulation, or through negatively charged proteoglycans and heparan sulfates of the kidney glomerular basement membrane (GBM), resulting in siRNA loss, primarily through renal filtration.[28] Circulating si-NPs must also circumvent other factors that reduce tumor bioavailability, such as phagocytosis by the macrophages of the reticuloendothelial system (RES).[29, 30, 32, 75] Finally, nanoparticles, especially those with cationic components, have a narrow therapeutic index and can cause carrier-related off-target toxicities.[33, 76] There is a critical need to overcome siRNA carrier challenges and identify systems that provide potent silencing activity, circulation stability, and avoidance of carrier-associated toxicity.

Our lab and others have improved si-NP stability through a variety of strategies, particularly through enhancing core hydrophobic interactions in combination with canonical electrostatic interactions.[77] Shown by us and others, modification of the siRNA by conjugation with hydrophobic moieties such as palmitic acid[38, 39], cholesterol[40, 41], or other hydrophobes[42] increases carrier-cargo loading stability. Nanocarrier hydrophobicity can also be increased through ternary si-NP formulation strategies. Ternary si-NPs, to achieve a given N+/P- formulation ratio, substitute in a hydrophobic, RNA condensing core-forming polymer alongside

the PEGylated diblock surface-forming polymer to enhance carrier stability.[37] Here, we created and tested a unique library of ternary si-NPs with variations in both the core polymer molecular weight and core:surface polymer ratio. This series of candidates was formulated to test the hypothesis that core polymer molecular weight and core:surface polymer ratio interact and should be simultaneously tuned for optimization of si-NP stability, activity, and safety.

The cationic and endosomolytic polymer block of both polymers of our ternary formulations have a 50:50 monomer composition of 2-(dimethylamino)ethyl methacrylate and butyl methacrylate (poly(DMAEMA-co-BMA), 50B). This monomer composition has been established as an ideal polymer containing a balance of cationic and hydrophobic monomer in a random copolymer composition that optimizes stability, endosome escape activity, and cytocompatibility.[37, 77] The core-forming polymer our of ternary si-NPs is a single block of 50B, and the surface-forming polymer is a diblock of 20kDa poly(ethylene glycol)-block-50B (20kPEG-50B). Previous studies comparing ternary si-NPs to "binary" si-NPs, containing solely a 5kPEG-bl-50B surface-forming polymer, revealed that the inclusion of a core-forming free 50B polymer endowed ternary si-NPs with greater activity and stability; one reason for the higher activity is that the core-forming 50B single block polymer both more stably complexes siRNA and has more potent endosome disruptive function versus 5kPEG-bl-50B because its siRNA and membrane interactions are not sterically hindered by junction with a PEG block.[37]

In other related work, we have shown that for binary formulations of PEG-bl-50B, the activity and toxicity of the formulation correlate with the 50B polymer block MW.[43] The current work, therefore, simultaneously tuned both the MW of the core-forming free 50B polymer and the core:surface polymer ratio with the hypothesis that si-NP potency could be enhanced in a manner that did not necessitate the use of exceedingly large 50B polymer blocks that would cause toxicity.

MW of the core-forming 50B polymer is also a variable that has not been studied to our knowledge for this type of ternary system.

The design of ternary si-NPs comprised of core-forming and surface-forming polymers also presents the opportunity to optimize core-to-surface polymer ratio. Previous testing of the core-forming 50B polymer ratio revealed a tradeoff in si-NP performance. While a greater ratio of 50B improved activity, the consequent decrease in the surface-forming PEG polymer limited colloidal stability and charge shielding of the si-NP.[37] These studies, however, utilized a 5kPEG-bl-50B surface-forming polymer. Here, we use a 20kPEG-50B polymer with the hypothesis that a higher MW PEG will provide greater stabilization function,[44] even when it is incorporated at lower ratios in the si-NP. Previous work furthermore studied the effect of core-to-surface polymer ratio on si-NP activity solely at the *in vitro* level, and *in vitro* studies are not always predictive of *in vivo* performance.[78] In this work, we therefore screened multiple si-NP candidates *in vivo* rather than moving forward with a lead formulation identified through *in vitro* studies. In all, the library composed and tested here includes 18 ternary si-NPs that were screened for *in vitro* gene silencing, endosomolytic activity, and cargo loading stability, as well as a subset that were screened *for in vivo* si-NP tumor uptake and target gene silencing in an orthotopic breast tumor model.

2.2. Results and Discussion

2.2.i. Polymer synthesis and characterization

A library of six core-forming polymers was synthesized by reversible addition-fragmentation chain-transfer (RAFT) to create 50:50 copolymers of DMAEMA and BMA (50B). While the ratio of DMAEMA to BMA was kept equimolar (50:50), the total size was varied by iterating the degree of polymerization (DP) of 50B from 150 (DP150) to 25 (DP25) (**Figure 2.1A**).

The DP of the 50B block in the surface-forming 20kPEG-50B polymer was kept constant (**Figure 2.1B**). DP150 was synthesized as the largest 50B polymer in our library to match previously published 50B lengths used in binary si-NP (PEG-*bl*-50B diblock polymer) formulations.[38, 44] The DP of 50B was then decreased with the hypothesis that smaller 50B polymers can provide similar levels of si-NP activity while mitigating toxicity.

20kPEG-50B was synthesized as previously described where the 20 kDa PEG was conjugated to a RAFT chain transfer agent (CTA) and chain extended to add the 50B block.[44, 77] RAFT polymerization allowed for tight control of 50B DP, calculated by monomer consumption using ^{1}H nuclear magnetic resonance (NMR) spectroscopy (Figure 2.1**C-D**). A unimodal polymer population for the 50B series and 20kPEG-50B was confirmed by gel permeation chromatography (**Figure 2.1E**). Unlike early-generation ternary si-NPs that contained a surface-forming polymer made up of a 5 kDa PEG,[37] the novel si-NPs described here use a high MW (20 kDa) Y-shape PEG, shown to improve *in vitro* stability in serum, decrease protein adsorption, and enhance *in vivo* pharmacokinetics when compared to coronas of smaller MW.[44, 45] Furthermore, 20 kDa Y-shape PEG is an FDA-approved surface-forming polymer for enhancing drug pharmacokinetics and was used here as a standard to allow us to rigorously study effects of the 50B core-forming polymer.[79-81]

2.2.ii. Sucrose containing ternary si-NP formulations retain structure and silencing activity upon reconstitution following lyophilization

To generate the library of ternary si-NPs, siRNA was complexed with our panel of core-forming 50B polymers (DP150 to DP25) and mixed in different ratios with the 20kPEG-50B surface-forming polymer (**Figure 2.2A**). The relative amount of 50B and 20kPEG-50B polymers comprising the si-NP was defined based on their contribution to the overall ratio of cationic amine

(N) to anionic phosphate (P) in the formulation. The final N/P of all si-NPs was kept constant at 16, with the N contribution calculated based on the DMAEMA monomer in both the 50B core-

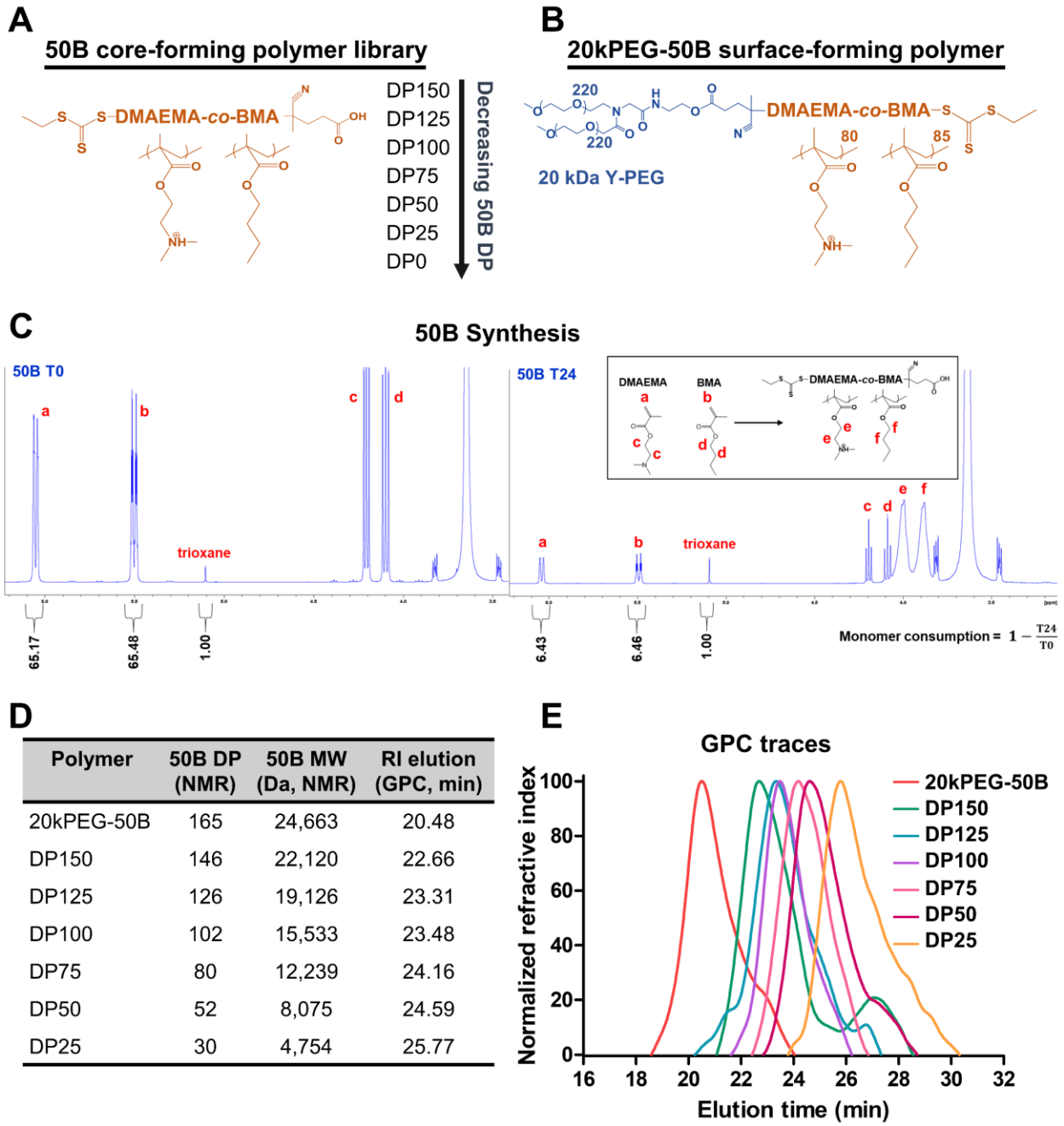

Polymer	50B DP (NMR)	50B MW (Da, NMR)	RI elution (GPC, min)
20kPEG-50B	165	24,663	20.48
DP150	146	22,120	22.66
DP125	126	19,126	23.31
DP100	102	15,533	23.48
DP75	80	12,239	24.16
DP50	52	8,075	24.59
DP25	30	4,754	25.77

Figure 2.1: Ternary si-NP polymer chemistry.
(A) The degree of polymerization (DP) was varied for the si-NP core-forming 50B polymer from DP150 to DP25. (B) si-NP surface- forming 20kPEG-50B polymer had a constant chemical structure. (C) 50B DP was quantified by NMR. (D) Table of polymer size characteristics. (E) Gel permeation chromatography confirms synthesis of 20kPEG-50B and 50B polymers with varied molecular weight.

forming polymer and the 50B block of the 20kPEG-50B polymer. We progressively increased the 50B polymer content in the si-NP ternary library from 0 to 12 (50B0, 50B4, 50B8, and 50B12) **Figure 2.2B**). Notably, this formulation strategy results in an inverse correlation between the 50B:20kPEG-50B ratio and the total PEGylation on the final ternary si-NP (**Figure 2.2C**). The respective N/P contribution from 20KPEG-50B polymer in those formulations was therefore 16, 12, 8, and 4, respectively.

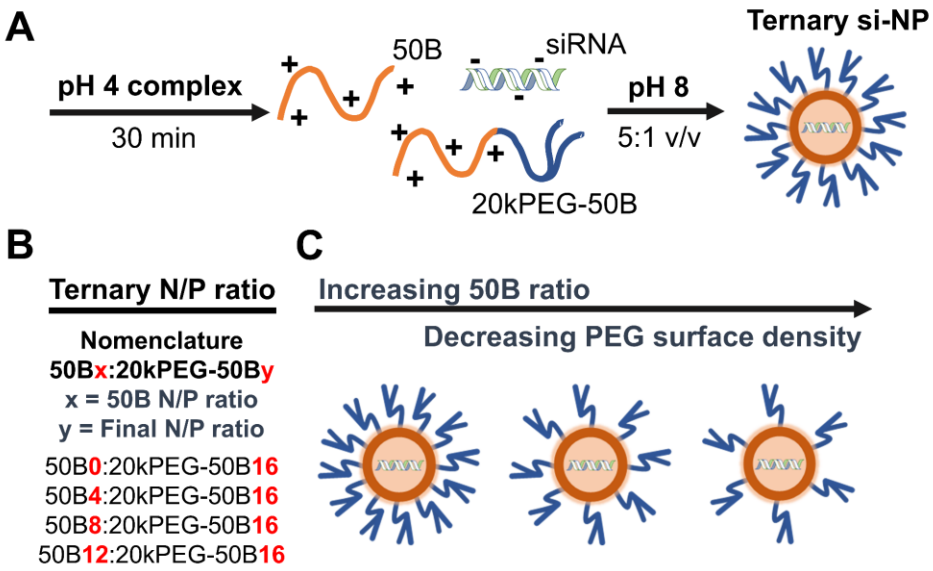

Figure 2.2: Ternary si-NP library design.
(A) Ternary si-NPs were formulated by complexing 50B and 20kPEG-50B polymers with siRNA in pH 4 buffer. The solution was brought to physiologic pH through the addition of pH 8 buffer, to stabilize the resultant ternary si-NPs. (B) si-NPs were formulated at a total N+/P- of 16, while ratio of 50B polymer was increased from N/P 4, 8, and 12. (C) Increasing 50B ratio in the si-NP results in lower amounts of 20kPEG-50B surface-forming polymer available for si-NP surface shielding.

To support large batch synthesis of si-NPs with consistent formulations across all experiments, lyophilized storage conditions were optimized for our ternary system. Lyophilized formulations also address major limitations of the siRNA nanomedicine field in that they allow for longer-term, stable storage and greater accessibility to under-developed areas in which requirement of a cold chain is a limitation.[82, 83] Prior to freezing, salt-containing buffers used during siRNA complexation and si-NP formation were exchanged for isotonic sucrose solution

(**Figure 2.3A**). Sucrose, and other sugars such as trehalose and glucose, are commonly used as cryo- and lyoprotectant agents during the freeze-drying process to prevent NP aggregation and promote cargo stabilization.[84, 85] The resulting si-NPs in sucrose were concentrated by centrifugation and freeze-dried. Following lyophilization, si-NPs were easily rehydrated by reconstitution in water.

Size characterization revealed lower size dispersity of lyophilized si-NPs than fresh, while also keeping the hydrodynamic diameter under 200 nm (**Figure 2.3B-C**). Lyophilized si-NPs were assessed for siRNA encapsulation and retention of siRNA over time and displayed virtually identical siRNA encapsulation to freshly formulated si-NPs (**Figure 2.3D**). Lyophilized si-NPs also maintained hydrodynamic size following multiple freeze-thaw cycles, demonstrating the integrity of these lyophilized formulations (**Figure 2.3E**). To determine if lyophilization-reconstitution of si-NPs affects silencing activity, we generated ternary si-NPs harboring an siRNA sequence against the model gene *LUCIFERASE* (siLuc) or a non-targeting siRNA control (siControl). Fresh si-NPs or lyophilized-reconstituted si-NPs were transfected into MDA-MB-231 cells stably expressing Luc. At 48 hours after transfection, Luc activity was measured, revealing that both fresh and previously lyophilized siLuc-NPs diminished Luc activity to <35% compared to siControl-NPs in the DP150 formulation. (**Figure 2.3F**). After confirming that lyophilized si-NPs had similar properties to freshly formulated si-NPs, all studies described in this work were completed using si-NPs that underwent the described lyophilization protocol.

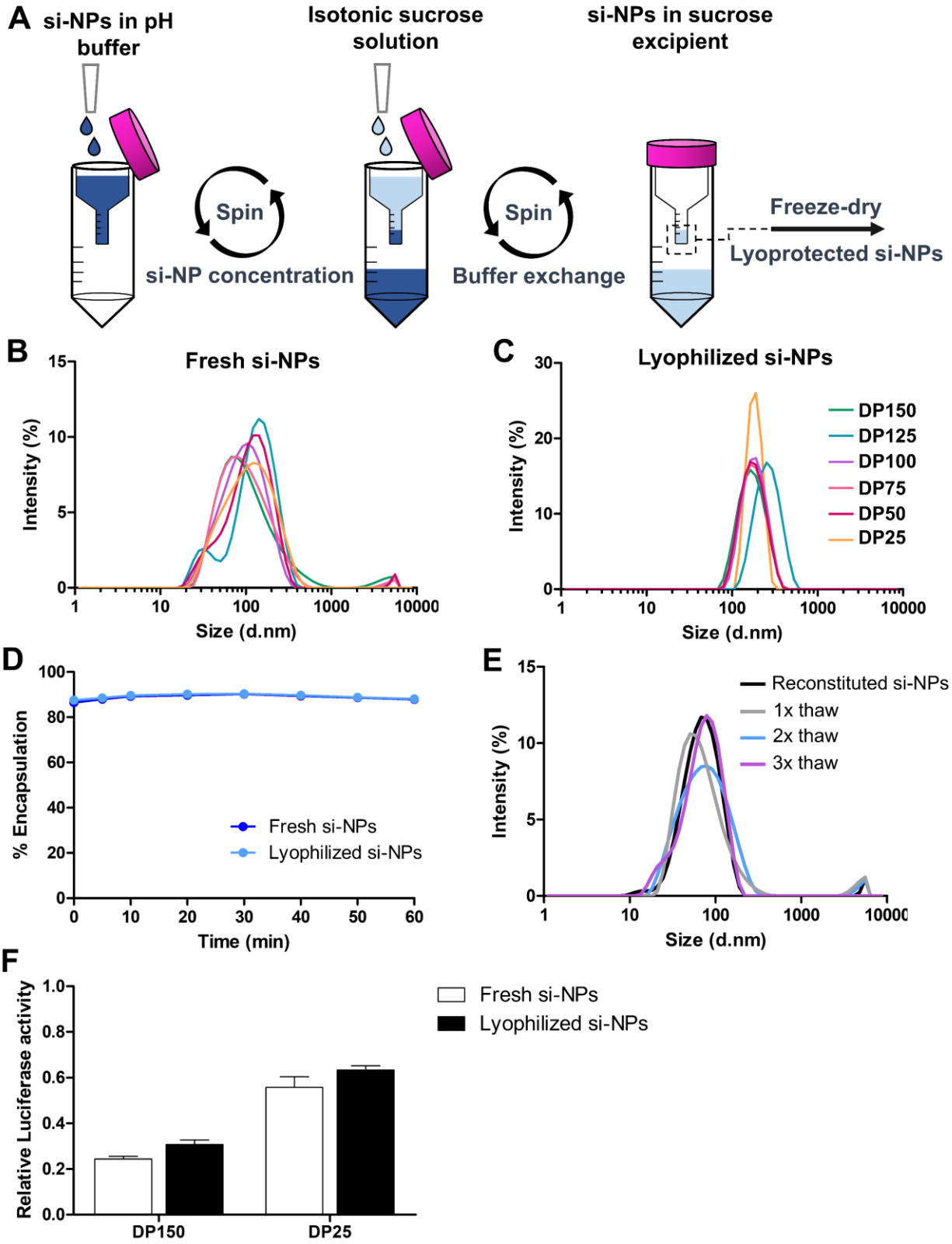

Figure 2.3: si-NP formulation and storage approach along with comparison to fresh si-NPs. (A) si-NPs were spin-concentrated to remove the majority of the buffer salts and exchanged for isotonic sucrose solution as an excipient for lyoprotection. (B) DLS analysis showed freshly formulated si-NPs had

higher polydispersity than (C) si-NPs post-lyophilization and reconstitution. (D) Lyophilized si-NPs retained siRNA cargo following freeze-drying at similar levels to freshly formulated si-NPs. (E) Lyophilized si-NPs retained size characteristics when challenged with multiple freeze-thaw cycles. (F) 50B3 lyophilized si-NPs retained similar activity levels to freshly formulated si-NPs and showed similar activity trends corresponding to 50B molecular weight.

The full ternary library, varying 50B size and ratio, was first assessed for si-NP size and zeta potential. All formulations had similar hydrodynamic diameters ranging from 150-200 nm with relatively narrow dispersity (**Figure 2.4A**). All si-NPs were slightly positive in surface charge ranging from 4 to 9 mV when assessed in deionized water. si-NPs displayed a near neutral surface charge when measured in physiologic saline (**Figure 2.4B)**. As 50B content was increased, there was no discernable increase in zeta potential for 50B8 and 50B12 si-NPs compared to the 50B0 and 50B4 si-NPs. This suggests that even the 50B12 formulations have effective PEG surface coverage contributed from the 4:1 ratio of the 20kPEG-50B polymer. Branched Y-shape PEG surface-forming polymers like the one used here are known to provide an "umbrella-like" covering that can shield larger portions of the NP surface, compared to linear PEGs of the same MW.[86] si-NPs were furthermore assessed for siRNA encapsulation, and all formulations displayed greater than 95% cargo loading (**Figure 2.4C**). As core-forming single block 50B polymer content was increased, there was an appreciable increase in siRNA encapsulation, perhaps due to lower PEG steric hindrance for siRNA complexation.

2.2.iii.In vitro si-NP activity and toxicity is correlated to 50B polymer MW and ratio

Through tuning 50B core-forming polymer size and ratio in ternary si-NP formulations, we aim to find a balance between si-NP activity and toxicity. Gene silencing activity was assessed by treating Luc-expressing MDA-MB-231 cells with 100 nM si-NPs harboring siLuc and measuring bioluminescence at 48 hr and 72 hr (**Figure 2.5A**). Overall, treatment with si-NPs harboring larger 50B core polymer sizes resulted in greater silencing activity. Within the 50B4 si-NP group, treatment with DP150 resulted in 28% remaining Luc activity at 48 hr while treatment

with DP25 had greater than double remaining Luc activity at 71%. Similar trends in activity were seen in the 50B8 and 50B12 si-NP groups.

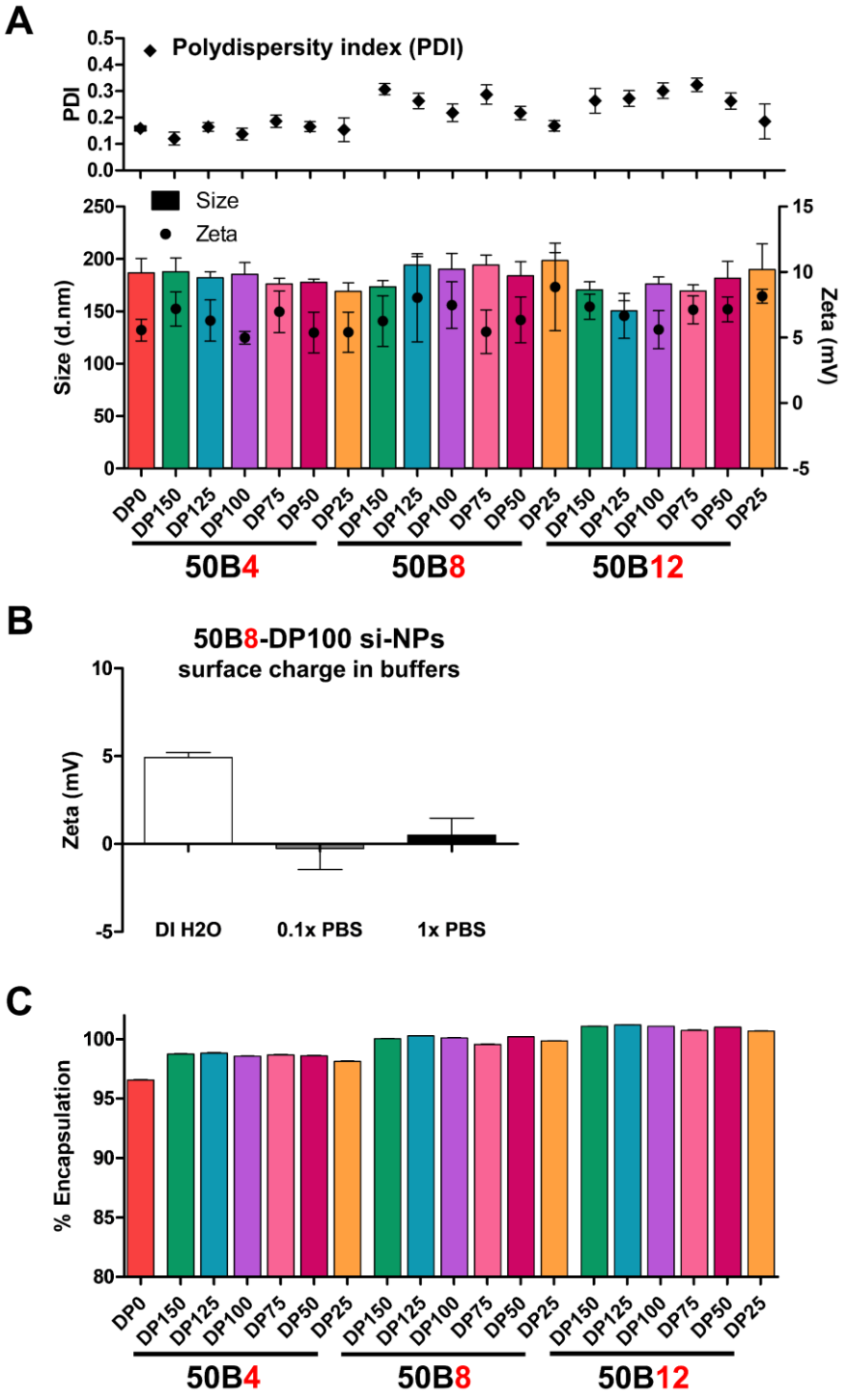

Figure 2.4: si-NP size and charge characterization.

(A) All si-NPs displayed similar hydrodynamic diameter (d.nm) and surface charge (N = 3). (B) si-NP surface charge was overall neutral. (C) All si-NPs achieved greater than 95% siRNA encapsulation efficiency (N = 3).

Level of knockdown did plateau with increasing 50B size. Compared to treatment with si-NPs harboring DP100, si-NPs harboring DP125 and DP150 did not significantly improve silencing activity. Silencing activity also improved with increasing 50B ratio, where treatment with 50B12 si-NPs resulted in the greatest Luc knockdown.

Though 50B quantity correlated with higher silencing activity, addition of 50B core-forming polymer also trended with cytotoxicity. In ternary si-NPs, these trends were apparent both with increasing 50B size and ratio. Within the 50B4 ratio group, treatment with all 50B DPs resulted in similar levels of cell viability. However, in the 50B8 and 50B12 ratio groups, cytotoxicity resulting from increasing 50B DP was apparent (**Figure 2.5B**). Independent of 50B size, increasing 50B quantity also increased si-NP toxicity. While all si-NPs in the 50B4 ratio group displayed cell viability above 95%, viability fell to approximately 85% for 50B8-DP150 si-NPs and approximately 75% for 50B12-DP150 si-NPs. Together, these data indicate that 50B content, both in terms of MW and contribution to the N/P ratio, is a critical variable in ternary si-NP tuning for maximum silencing activity and minimal toxicity. For example, though 50B12-DP25 si-NPs were the least active compared to other 50B12 formulations, these si-NPs still outperformed 50B4-DP75 and 50B8-DP75 si-NPs while having greater than 85% cell viability.

To ultimately achieve gene silencing activity, cell internalized si-NPs must trigger endosomal siRNA escape to the cytosol, which can be enhanced by carriers that respond to the acidic environment of endolysosomal vesicles.[69, 87] Endosome disruption causes diffusely dispersed Galectin 8 (Gal8) to translocate and accumulate at the inner endolysosomal leaflet. Thus, yellow fluorescent protein (YFP) fused with Gal8 serves as a reporter for endosomal

disruption,[43, 88] appearing as bright puncta.[89] Endosome disruption after treatment with si-NPs was quantified as average Gal8 puncta intensity per cell area (**Figure 2.6A).**

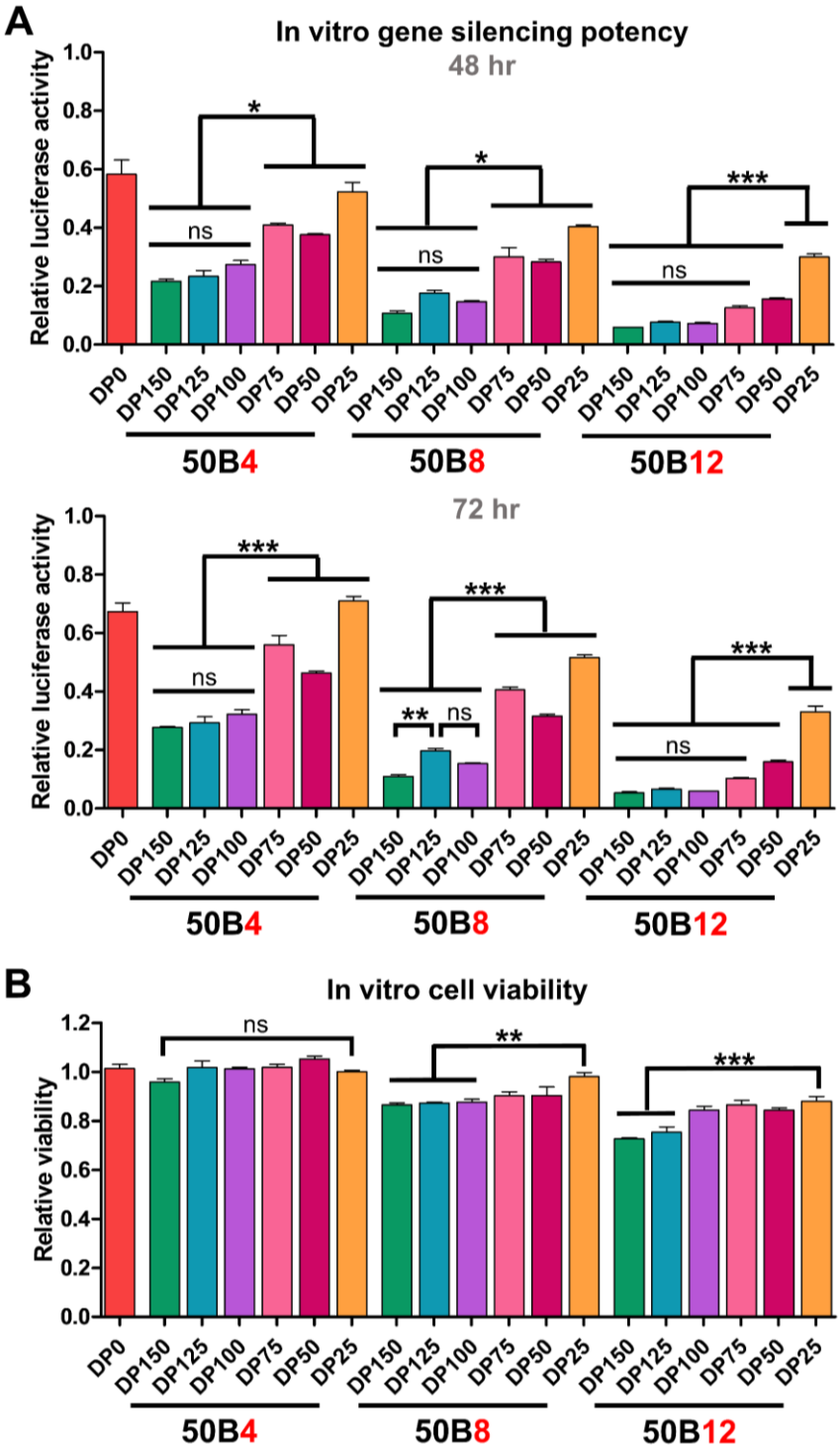

Figure 2.5: Increasing 50B polymer MW and ratio improves gene silencing activity but reduces cell viability.

(A) Luciferase activity 48 hr after siLuciferase treatment using si-NP library (N = 3). Activity assessed relative to cells treated with each si-NP formulation loaded with siControl. (B) Cell viability 24 hr after treatment with si-NP library (N = 3). Viability assessed relative to non-si-NP treated cells. One-way ANOVA analysis with Tukey's multiple comparison test was used to compare differences (*, $p < 0.05$; **, $p < 0.01$; ***, $p < 0.001$).

Processed images show Gal8 puncta recognition based on fluorescent intensity (**Figure 2.6B**). Overall, level of endosome disruption increased with both 50B size and ratio. si-NPs comprised of DP150 50B displayed significantly enhanced endosome disruption compared to si-NPs harboring smaller DPs; these trends are consistent with previous work correlating endosomolytic capability to polymer MW.[43] Interestingly in the 50B12 ratio group, there were no significant differences between DP150, DP125, and DP100 si-NPs, indicating that the larger 50B MW benefit may saturate at around DP100. The overall increase in endosome escape activity for DPs of 100 or larger correlates with higher gene silencing activity within our library, where si-NPs containing larger 50B core polymers induced greater silencing (**Figure 2.5A**). Greater levels of endosome escape, which will consequently allow for greater siRNA delivery to the cytosol, is likely a major mechanism for the increased silencing activity seen from si-NPs containing larger 50B DPs. Increasing 50B ratio also increased endosomolytic activity. As an example, 50B8-DP100 si-NPs had >2-fold greater disruptive activity (3.46) over 50B4-DP100 (1.66), while 50B12-DP100 si-NPs had >8-fold greater activity (14.71) compared to 50B4-DP100. In comparison, our binary 50B0 si-NP, comprised solely of the 20kPEG-50B polymer, had less endosome disruptive activity (0.79). These data further suggest that 50B is more potent than 20kPEG-50B at endosome escape and that, even for a given quantity of 50B used in si-NP formulation, endosome escape potency correlates with the 50B MW.

2.2.iv. 50B polymer MW and ratio are critical regulators of ternary si-NP stability

To assess stability of the different si-NPs, siRNA encapsulation was quantified in the presence of heparin salt over time. Heparan sulfate is a negatively charged protein found in the

GBM that can electrostatically interact with positively charged polymers that make up the si-NP carrier.[28, 90] Though si-NPs such as ours are designed with hydrodynamic diameters that bypass the ~10 nm GBM filtration barrier, si-NP disassembly would make the siRNA cargo vulnerable to renal filtration.[28, 91]

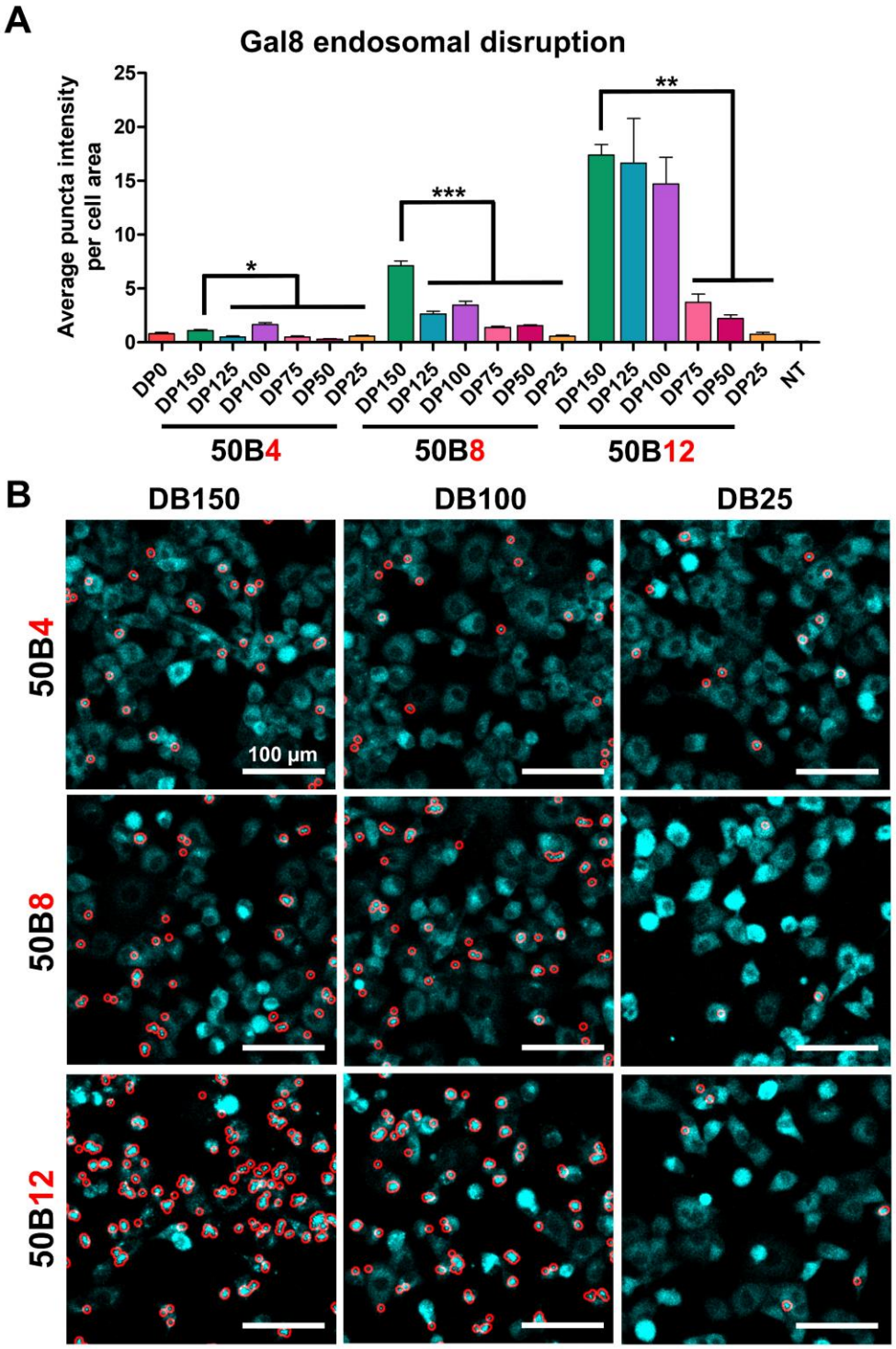

Figure 2.6: Ternary si-NP endosomal disruptive activity is dependent on 50B size and ratio. (A) Gal8-YFP expressing cells were tracked for Gal8 redistribution and puncta formation following si-NP treatment. Average puncta intensity per cell area was calculated for 4 hr after si-NP treatment (N = 3). One-way ANOVA analysis with Tukey's multiple comparison test was used to compare activity differences (*, $p < 0.05$; **, $p < 0.01$; ***, $p < 0.001$). (B) Representative micrographs show automated puncta recognition (encircled in red) by MATLAB script.

si-NPs were therefore challenged with either 0 U/mL, 25 U/mL, or 50 U/mL heparin, and siRNA encapsulation was assessed as a measure of si-NP stability (**Figure 2.7A-C**). Overall, increasing 50B size and ratio in ternary si-NPs improved si-NP stability in heparin. At 0 U/mL heparin, all si-NPs showed slow siRNA release, and 50B0 si-NPs were fully disassembled by 9 hr (**Figure 2.7A**). However, incorporation of core-forming 50B polymer vastly improved stability, and even the minimally stable 50B4 si-NPs retained at least 37% of their siRNA cargo by 9 hr. We observed similar trends when challenging si-NPs with 25 U/mL or 50 U/mL heparin. By 120 min of si-NPs challenged with 50 U/mL heparin, all 50B4 si-NPs were disassembled, whereas all 50B12 si-NPs still retained 35% or more of their cargo (**Figure 2.7C**).To better quantify these data, the area under the curve (AUC) at each heparin condition was calculated (**Figure 2.7D-G**). 50B0 si-NPs had the lowest AUC, matching its data showing quick loss of encapsulated siRNA (**Figure 2.7D**). AUC increased with increasing 50B ratio (**Figure 2.7E-G**), indicating greater siRNA retention. While one may anticipate that 50B12 si-NPs would be more susceptible to heparin-mediated disassembly due to their lower surface PEGylation, this effect was not apparent. These data therefore suggest that free 50B polymer can complex more tightly with siRNA than 20kPEG-50B and that the single block 50 core-forming polymer content is more critical than the PEG content for cargo loading stability across the range of formulations conditions used here.

Within each 50B ratio group, si-NPs harboring larger 50B sizes retained their siRNA cargo for a longer period while DP50 and DP25 si-NPs tended to disassemble the fastest (**Figure 2.7A-C**). AUC data calculated from these kinetic graphs show that increasing 50B size decreased rate of siRNA release. However, DP150 si-NPs do not confer strikingly greater stability over DP125 or DP100 si-NPs. This is reflected in the AUC calculated for the 50 U/mL heparin condition. 50B8-DP100 si-NPs increased AUC appreciably from 50B8-DP75 si-NPs (8300 %min 50B8-DP100 si-

NPs vs. 6573 %min 50B8-DP75 si-NPs); however, 50B8-DP100 si-NPs have a comparable AUC to 50B8-DP150 si-NPs (7929 %min) (**Figure 2.7F**).

Serum proteins can also factor into si-NP destabilization following *in vivo* systemic delivery. In circulation, serum proteins such as albumin, IgGs, and lipoproteins can create a "corona" on the nanoparticles that can trigger recognition and clearance by the RES.[92] To assess stability of our si-NPs in serum, we utilized quencher-based methods where ternary si-NPs were co-loaded with tetramethylrhodamine (TAMRA)-tagged siRNA and non-fluorescent acceptor Black Hole Quencher (BHQ2)-tagged siRNA and challenged with 50% (**Figure 2.8**) fetal bovine serum (FBS). When excited TAMRA is in close proximity to BHQ2 (e.g., co-loaded into an si-NP), its emission is absorbed by the quencher, suppressing the measurable fluorescent signal.[93] However, as the si-NPs disassemble and distance is increased between the two tagged siRNAs, TAMRA emission signal is restored (**Figure 2.8A**). TAMRA fluorescence in the presence of FBS was plotted over time for 50B0 si-NPs and the ternary library (**Figure 2.8B-E**). si-NP stability in FBS was increased both by increasing 50B MW and increasing 50B contribution to the N/P ratio. We calculated the half-time to TAMRA signal plateauing as a measure of si-NP stability, where more stable si-NPs had longer half-times to fluorescence restoration (**Figure 2.8F**). In accordance with stability trends seen following heparin challenge, si-NPs containing DP150, DP125, and DP100 did not significantly differ in half-time, suggesting that these si-NPs conferred similar levels of stability. Furthermore, the effect of 50B MW on si-NP serum stability was more apparent as 50B ratio was increased. For instance, the half-time for 50B8-DP150 si-NPs (63.9 min) was 2-fold greater than 50B8-DP25 (29.1 min) si-NPs, but the half-time for 50B12-DP150 si-NPs (100.4 min) was >3-fold compared to 50B12-DP25 counterparts (32.3 min).

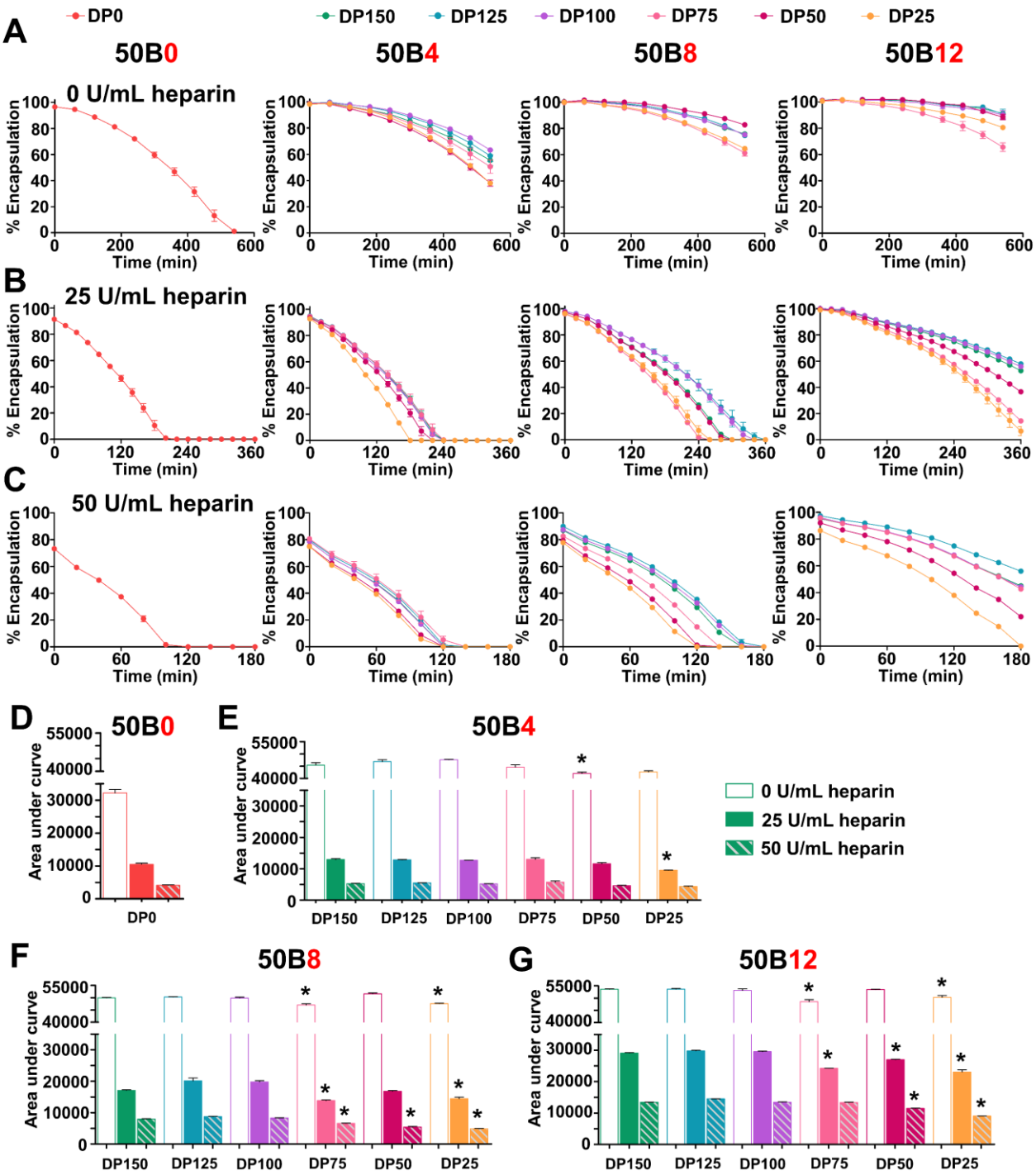

Figure 2.7: Ternary si-NP stability in heparin improves with increasing 50B size and ratio. (A) si-NP stability was assessed by siRNA encapsulation in the presence of 0 u/mL heparin, (B) 25 U/mL heparin, and (C) 50 U/mL heparin over time (N = 3). (D) Area under the curve of plots of %siRNA encapsulation vs. time were calculated for various heparin concentrations for 50B0, (E) 50B4, (F) 50B8, and (G) 50B12 si-NPs. Hollow, solid, and dashed bars represent 0, 25, and 50 U/mL heparin conditions, respectively. One-way ANOVA analysis with Tukey's multiple comparison test was used to compare stability differences; * show si-NPs with AUC significantly lower ($p < 0.05$) from DP150 si-NP within the same heparin condition.

For *in vivo* delivery, this may suggest that the effects of 50B size and 50B ratio are additive and tuning one parameter could compensate for the other. For example, the half-time for 50B12-DP50 si-NPs (65.9 min) may be significantly reduced compared to 50B12-DP150, but it is virtually equivalent to the half-time displayed by 50B8-DP150 si-NPs (64.0 min). Similar trends were observed when TAMRA signal was quantified in the presence of 10% FBS or heparin **(**Figure 2.9**).** These collective data on our si-NP library indicate that 50B4, 50B8, and 50B12 si-NPs containing DP100 are lead candidates most worth of further *in vivo* studies, as they exhibit near maximal gene silencing activity, endosome disruptive ability, and stability, while also limiting toxicity.

2.2.v. Lead ternary si-NPs display a desirable safety response in vivo

Toxicology studies are an important facet of interrogation toward understanding the impact of 50B size and ratio on the *in vivo* use of ternary si-NPs. The above activity and stability studies suggest that 50B4-DP100, 50B8-DP100, and 50B12-DP100 si-NPs may be lead candidates for subsequent *in vivo* studies. However, due to the higher cytotoxicity displayed by 50B12 si-NPs *in vitro* (**Figure 2.5**), preliminary *in vivo* toxicity studies were performed using 50B12 si-NPs to assess mouse survival following treatment. A 1 mg/kg dose of 50B12 si-NPs were injected i.v. into wild-type mice, and mice were observed for any adverse events or succumbing to treatment (**Figure 2.10A**). si-NPs harboring smaller 50B sizes were injected, and mice responded well to 1 mg/kg treatment with 50B12-DP25 si-NPs. Though 50B12-DP100 si-NPs displayed minimal *in vitro* toxicity and enhanced gene silencing activity, we found 50B12-DP25 si-NPs to be the more optimal formulation based on greater safety with i.v. administration *in vivo*. Based on these pilot studies, we moved forward with more rigorous *in vitro* toxicity studies using 50B0 si-NPs as a binary si-NP control and 50B4-DP100, 50B8-DP100, and 50B12-DP25 si-NPs as our lead ternary si-NP candidates.

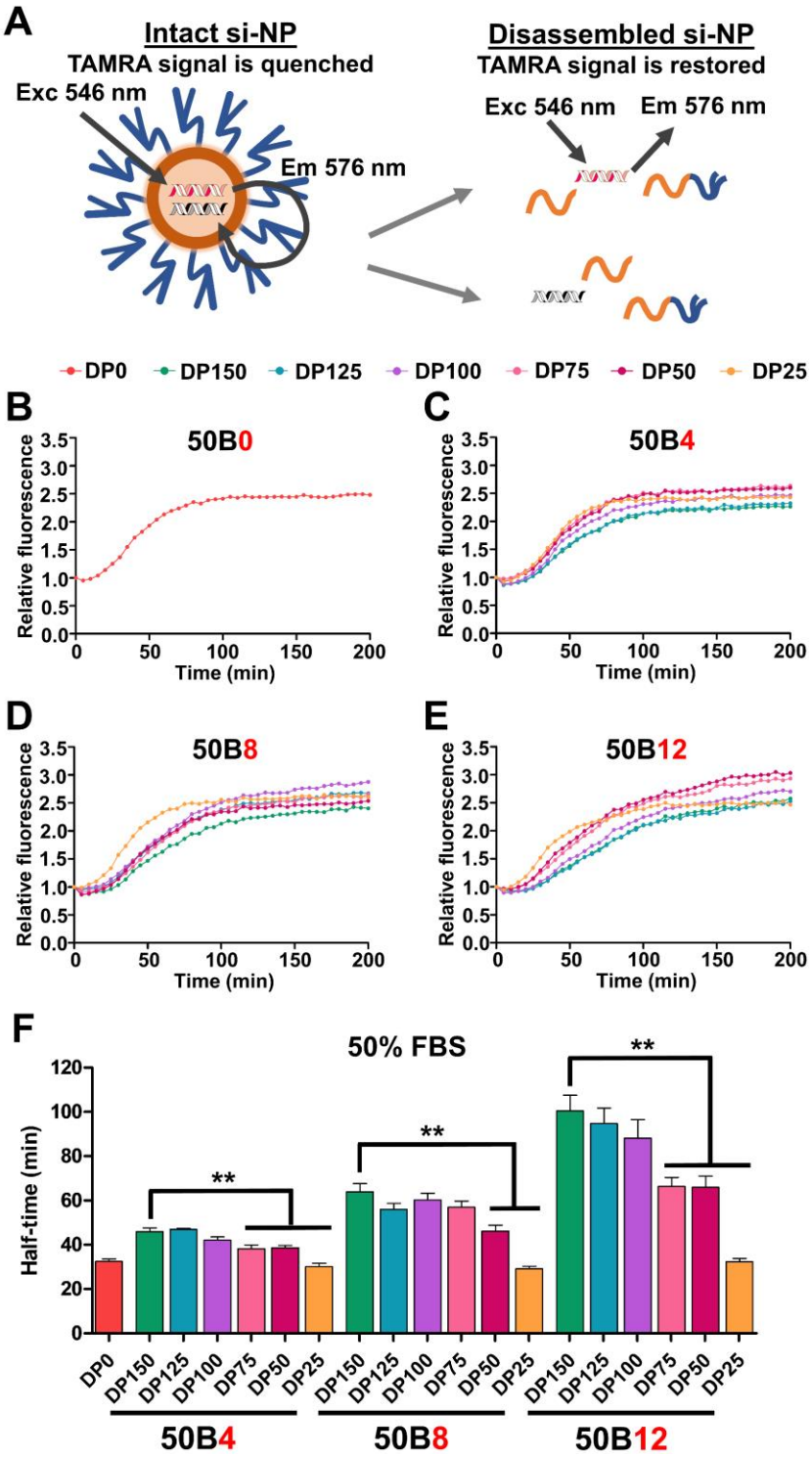

Figure 2.8: Ternary si-NP stability in serum improves with increasing 50B size and ratio. (A) si-NPs were co-loaded with fluorescent TAMRA-siRNA and quencher BHQ2-siRNA. Fluorescence de-quenching was measured to detect cargo release from si-NP destabilization. (B) Relative fluorescence was plotted for 50B0 si-NPs and (C) 50B4, (D) 50B8, and (E) 50B12 ternary si-NPs challenged with 50% FBS over time (N = 6). (F) Half-time to fluorescence signal plateau was calculated for each si-NP as a

measure of relative stability. One-way ANOVA analysis with Tukey's multiple comparison test was used to compare stability differences (**, $p < 0.01$).

An initial *in vitro* viability screen using our lead si-NPs revealed that toxicity was 50B ratio-dependent at high doses; however, si-NPs displayed minimal cytotoxicity overall, with >85% viability for 50 nM doses and lower (**Figure 2.10B**).

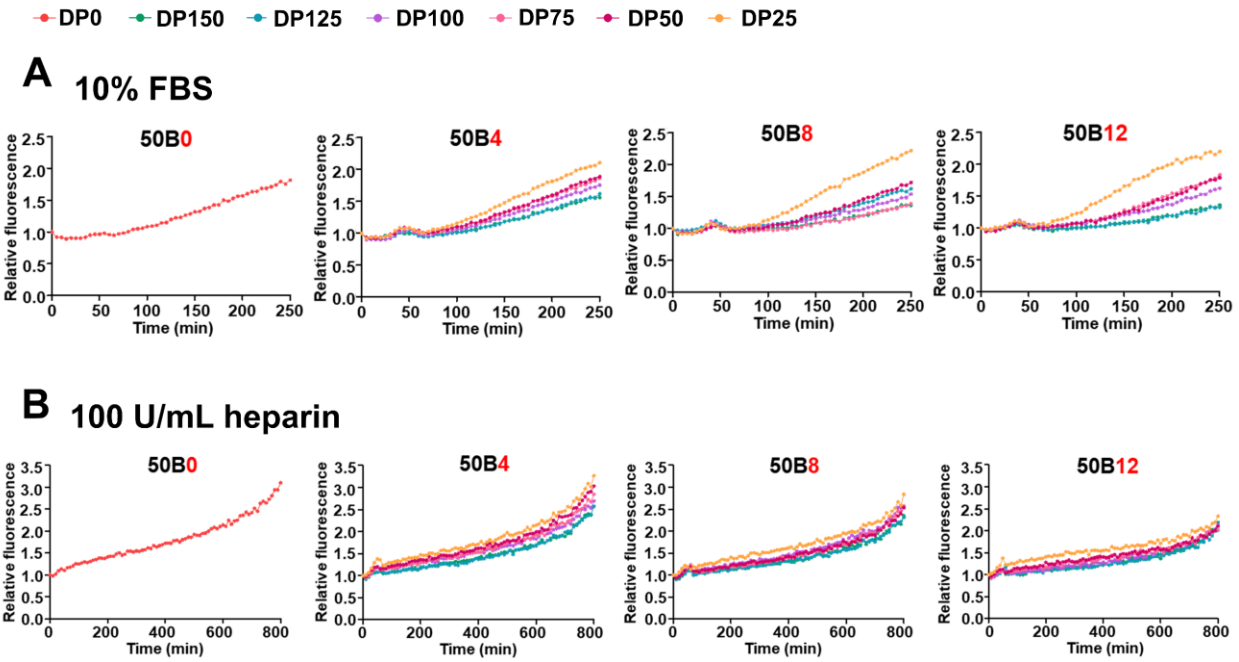

Figure 2.9: Additional TAMRA fluorophore/quencher-based assays to measure si-NP destabilization.
siRNA cargo release was measured in response to (A) 10% FBS and (B) 100 U/mL heparin over time.

Wild-type, immune-competent Balb/C mice were i.v. injected with lead si-NPs and resulting toxicity markers were compared to vehicle control at 30 min following injection. We and others have previously shown that acute dose-limiting nanocarrier and viral toxicities—occurring within 1 hr post-injection—are driven by the release and downstream effects of lipid mediator platelet activating factor (PAF).[33, 94] PAF was therefore used as a marker of acute si-NP toxicities in this work. Because PAF is extremely unstable and difficult to measure, it's levels can be indirectly estimated by measurement of plasma PAF acetyl hydrolase (PAF-AH) activity.

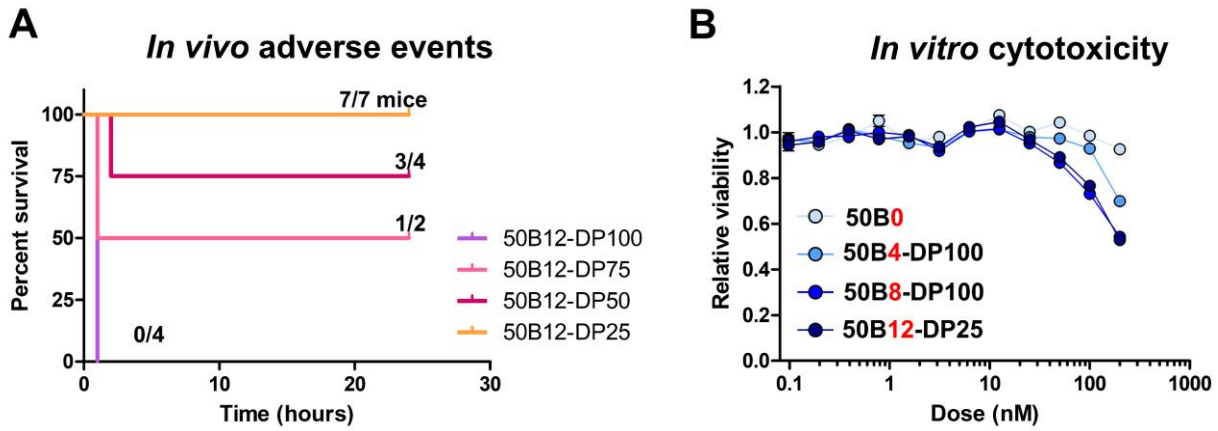

Figure 2.10: si-NP toxicity screening.
(A) Survival was assessed in wild-type mice following 1 mg/kg i.v. injection with ternary formulations from the 50B12 si-NP library. (B) Viability dose curve for 50B0, 50B4-DP100, 50B8-DP100, and 50B12-DP25 lead si-NPs.

PAF-AH hydrolyzes PAF into an inactive form and its activity is negatively correlated with PAF levels.[95, 96] We evaluated mouse plasma for PAF-AH activity 30 minutes after si-NP injection (**Figure 2.11A**). None of the lead si-NPs had significantly decreased PAF-AH activity compared to trehalose vehicle control. This suggests that our lead si-NPs did not induce PAF related nanocarrier toxicities and were well-tolerated. To further confirm these results, we assessed mouse whole blood for elevated hematocrit and red blood cell concentration compared to vehicle. As a major mediator of anaphylaxis, PAF induces shock-like effects such as vascular permeability and hemoconcentration when it is present in the bloodstream.[97] There was no apparent vascular congestion following si-NP injection **(Figure 2.11B-C**). We also examined liver histology following acute si-NP delivery and observed no difference compared to vehicle (**Figure 2.11D**). Other primary si-NP clearance organs, kidneys and spleen, were also observed and displayed normal histology (**Figure 2.11E-F**).

In these studies, 50B0 was used as a benchmark si-NP that has served as a historical standard in our lab and has a desirable safety profile.[33, 44] Though all of our lead ternary si-NPs

were safe upon treatment, there was a slight trend towards decreased plasma PAF-AH activity as 50B core polymer ratio was increased (**Figure 2.11A**).

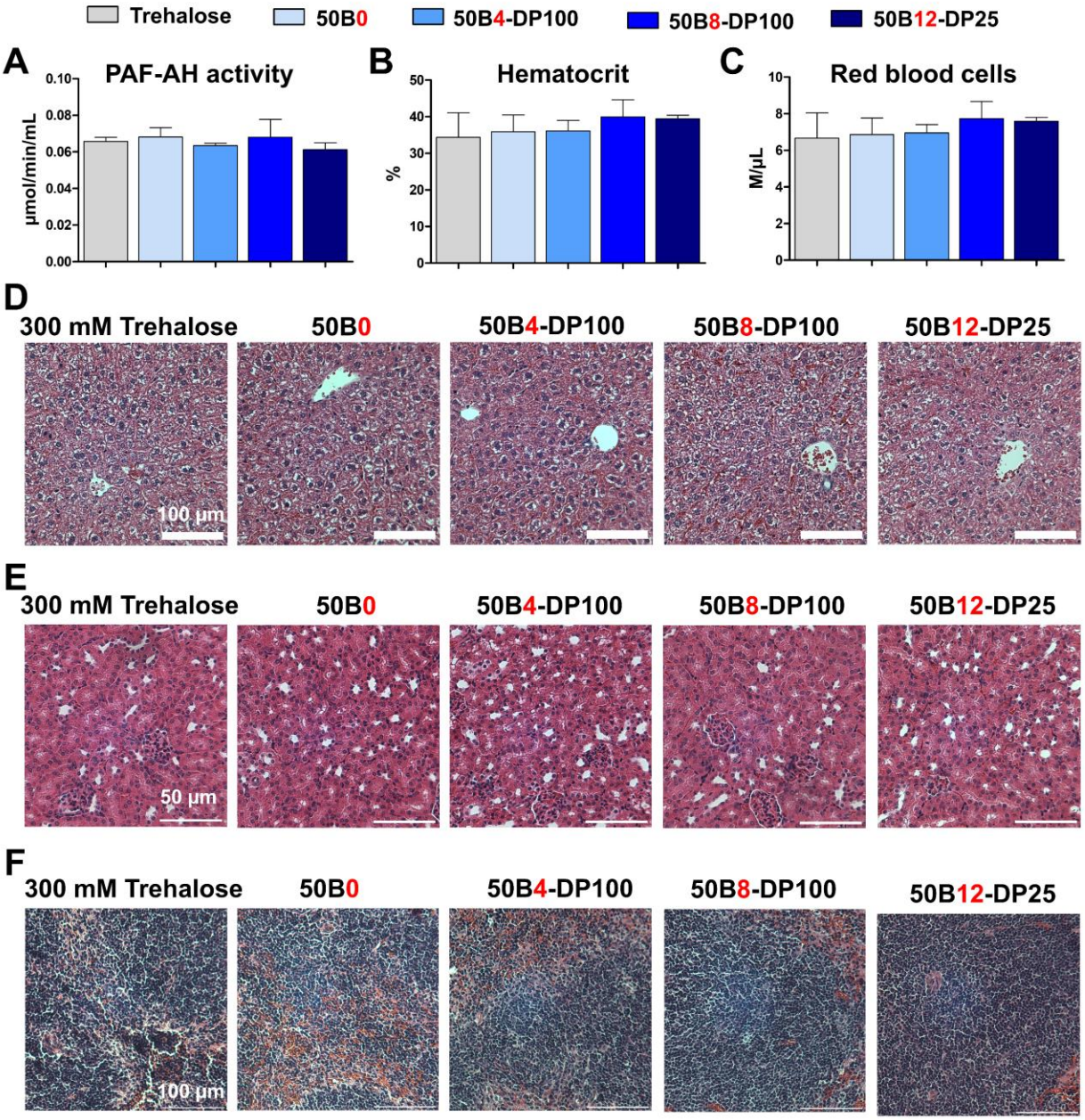

Figure 2.11: Lead ternary si-NPs display minimal acute toxicity.
Mice were i.v. treated with either trehalose vehicle or si-NPs and assessed after 30 min. Plasma PAF-AH activity was measured (A) as an indirect measure of plasma PAF levels, a biomarker for acute liver Kupffer cell toxicity (N = 4-5). Mouse blood was assessed for signs of PAF-induced hemoconcentration by measuring % hematocrit (B) and red blood cell level (C, N = 7-9). Mouse livers (D), kidneys (E), and spleens (F) were evaluated for histological signs of toxicity, in particular vascular congestion, by H&E staining.

Treatment with our ternary si-NPs, however, did not result in significant differences in PAF-AH activity when compared to mice treated with binary 50B0 si-NPs. We previously showed that PAF related nanocarrier toxicities are driven by the level of uptake and endosome disruptive activity by liver Kupffer cells.[33] This is contrary to other cationic carriers, such as the "gold standard" PEI, which can induce toxicity via aggregation with serum proteins and excessive cell membrane disruption upon binding.[98, 99] 50B core polymer size and ratio can both regulate endosome disruptive activity (**Figure 2.6**) which may in turn promote PAF related toxicities. It was found here that balancing the MW and quantity of the 50B component allows development of promising, safe si-NP formulations.

2.2.vi. Lead ternary si-NPs enhance in vivo pharmacokinetics

We next assessed our lead si-NPs for *in vivo* pharmacokinetics and biodistribution. si-NPs were loaded with Cy5-tagged siRNA, and fluorescence of the injected si-NPs was tracked by laser scanning confocal intravital microscopy (IVM) imaging of the mouse ear vasculature (**Figure 2.12A**). This longitudinal fluorescence tracking on a per-second basis enables a robust quantification of pharmacokinetic parameters, revealing increased circulation half-life and area under curve (AUC) upon inclusion of a 50B core-forming polymer in ternary si-NPs compared to binary 50B0 si-NPs (**Figure 2.12B-D**). This finding is consistent with previous studies showing that ternary si-NPs have greater *in vivo* tumor bioavailability than binary si-NPs.[37] Plasma half-lives for 50B0, 50B4-DP100, 50B8-DP100, and 50B12-DP25 si-NPs were 21.2, 70.1, 37.5, and 27.6 min, respectively. Similar relative trends were seen in AUC values calculated for each si-NP, where 50B4-DP100 si-NPs had close to a 3-fold increase in AUC compared to 50B0 si-NPs. The relative benefit of the core-forming 50B polymer decreases as its ratio within the si-NP is increased. While 50B4-DP100 si-NPs exhibited maximal blood circulation pharmacokinetics,

50B8-DP100 si-NPs had a 1.72-fold increase and 50B12-DP25 si-NPs only had a 1.13-fold increase in AUC over 50B0 si-NPs. Similar trends were seen in si-NP clearance, where 50B4-DP100 si-NPs had the lowest values, and 50B0 si-NPs had the greatest clearance (**Table 2.1**). As 50B core polymer ratio is increased, there is a consequent decrease in the 20kPEG-50B surface-forming polymer, necessary for si-NP charge shielding. These data suggest that, in the *in vivo* setting, a balance in core:surface polymer ratio is required for optimal blood circulation and that the lack of a core-forming polymer (50B0) or too much core polymer (50B12) can diminish i*n vivo* bioavailability. To optimize for pharmacokinetics, our ternary si-NPs ideally balance two main competing factors: (1) higher 50B core polymer ratios promote stronger siRNA complexation whereas the 20kPEG-based surface-forming polymer likely sterically hinders electrostatic interactions between the cationic polymer blocks and siRNA. For example, higher packaging stability in the presence of serum is expected to contribute to improved pharmacokinetics, and we indeed observed increased stability in FBS for our ternary si-NPs as we increased 50B ratio (**Figure 2.8**). (2) lower 20kPEG-50B surface polymer ratios, resulting from higher 50B core polymer ratios, minimize stealth shielding and increase si-NP zeta potential and protein adsorption, properties that contribute to rapid clearance and poorer *in vivo* pharmacokinetics.

Organ siRNA biodistribution was also assessed 1 hour after si-NP delivery, revealing similar biodistribution profiles for all si-NPs tested (**Figure 2.12E**). Greatest si-NP accumulation occurred in the liver (>45%), with minimal heart accumulation (<2.5%). Biodistribution to kidneys was ≤20% for all si-NPs, suggesting limited si-NP disassembly in the GBM. 50B12-DP25 si-NPs had greater localization to the liver and spleen, major clearance organs making up the RES, compared to other si-NPs. Since 50B12-DP25 si-NPs have the lowest ratio of surface-forming PEG polymer, this may suggest that they are more vulnerable to recognition and clearance by

phagocytic cells. This underscores the importance of maintaining a threshold level of surface forming PEG polymer in ternary si-NP formulations, in order to minimize recognition and clearance by phagocytic cells.

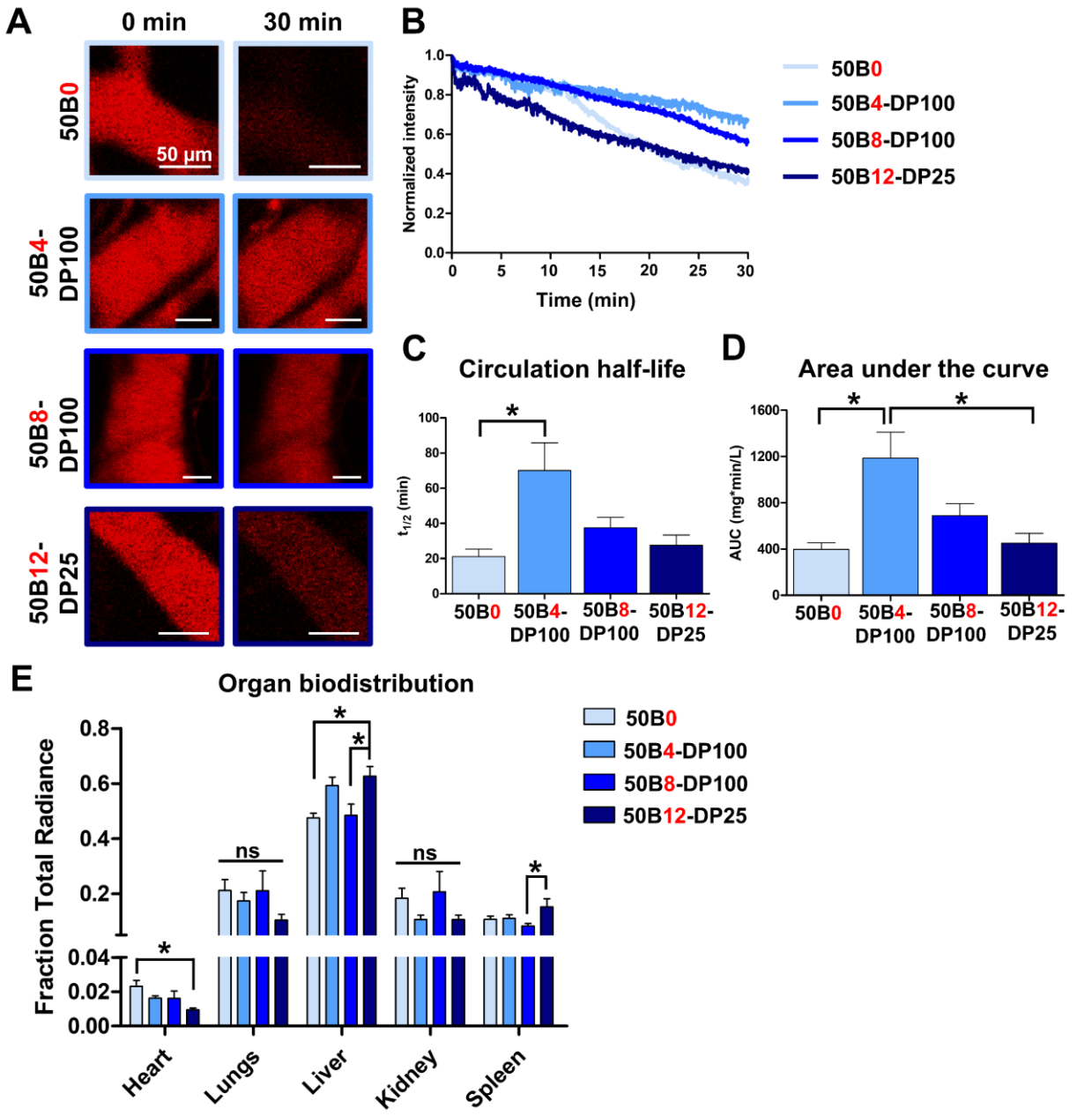

Figure 2.12: Lead ternary si-NPs improve in vivo pharmacokinetics following intravenous si-NP treatment.

(A) Representative intravital microscopy images of fluorescent Cy5 si-NPs in mouse ear vasculature (N = 3-4). (B) Average pharmacokinetic curves of each si-NP formulation. (C) Plasma half-life and (D) area under curve was calculated for each si-NP from intravital microscopy data. One-way ANOVA analysis with Tukey's multiple comparison test was used to compare differences in pharmacokinetic parameters (*,

$p < 0.05$). (E) Tissue biodistribution of si-NPs loaded with Cy5-tagged siRNA was assessed at 1 hr post-injection.

Table 2.1: Pharmacokinetic parameters quantified from intravital imaging of si-NPs. Parameters include half-life ($T_{1/2}$), area under the curve (AUC), and clearance (Cl).

Formulation	$T_{1/2}$ (min)	$AUC_{0\text{-}t}$ (mg*min/L)	$AUC_{0\text{-}inf}$ (mg*min/L)	Cl (mL/min)
50B0	21.2 ± 4.15	264 ± 28	398 ± 56	0.049 ± 0.006
50B4-DP100	70.1 ± 15.67	440 ± 48	1187 ± 224	0.018 ± 0.004
50B8-DP100	37.5 ± 5.8	358 ± 18	688 ± 104	0.029 ± 0.005
50B12-DP25	27.6 ± 5.78	285 ± 39	451 ± 85	0.045 ± 0.010

2.2.vii. Ternary si-NP formulations enable robust knock down of the oncogenic protein Rictor

The favorable toxicity profiles and pharmacokinetic performance displayed by our lead si-NPs justified advancement into studies on *in vivo* tumor target gene silencing activity. *In vitro* data on our full ternary library indicates that si-NP activity improves with increasing 50B size and ratio. We therefore hypothesized that increasing 50B ratio within our lead si-NPs will enhance *in vivo* tumor gene silencing potency, a parameter that has not been studied in our ternary si-NPs. Our previous silencing studies, however, were performed on cells exogenously expressing model gene *LUC*. Moving forward, we assessed si-NP silencing ability on an endogenously expressed tumor driver, choosing specifically to target the known tumor-driver gene *RICTOR*.[17, 62] The protein Rictor has established roles in tumor formation and tumor cell survival. To enable high throughput, protein-level screening of endogenous Rictor expression, CRISPR/Cas9 gene editing was used to introduce a HiBiT peptide tag in frame with Rictor ($Rictor^{HiBiT}$) at the endogenous *RICTOR* gene locus of MDA-MB-231 breast cancer cells.[100] Through split Nano-Luciferase (Nano-Luc) complementation, $Rictor^{HiBiT}$ produces a bioluminescent signal, acting as a quantitative reporter for endogenous Rictor protein levels.

Rictor^{HiBiT} cells were treated with increasing doses of si-NPs loaded with siRICTOR (200 nM to 0.0976 nM) (**Figure 2.13A**). After 72 hours, relative Nano-Luc activity measurements revealed greater endogenous Rictor knockdown in cells treated with 50B8-DP100 and 50B12-DP25 si-NPs. For example, 50B8-DP100 and 50B12-DP25 si-NPs induced >80% Rictor knockdown at a 12.5 nM dose, versus 50B4-DP100 (60%) and 50B0 (34%). Notably, the EC50 values for 50B8-DP100 and 50B12-DP25 si-NPs were both subnanomolar and similar to each other, recorded at >10-fold lower than those seen in 50B4-DP100 si-NPs (**Figure 2.13B**). At high doses, all si-NPs had similar levels of activity, with greater than 80% Rictor knockdown at a 200 nM dose.

In vitro si-NP uptake was quantified in MDA-MB-231 cells using fluorescent TAMRA-tagged siRNA at 4, 8, and 24 hr of treatment. While the percentage of TAMRA+ cells increased over time in all groups (90% TAMRA+ by 24 hr), (**Figure 2.13C**) a greater percentage of 50B12-DP25 treated cells were TAMRA+ at earlier timepoints (**Figure 2.13D**). This result is consistent with previous studies revealing an inverse correlation between PEG coating density and cell uptake. Since 50B12-DP25 si-NPs contain the highest ratio of core 50B polymer, and consequently lowest amounts of PEG shielding (**Figure 2.13C**), it is possible that their decreased PEG coating facilitates rapid cell entry. Overall, these data suggest that all lead formulations tested *in vivo* had robust siRNA delivery to tumor cells.

2.2.viii. Optimized ternary si-NP core polymer content enhances tumor cell uptake in vivo and oncogene targeting in an orthotopic breast cancer model

To assess *in vivo* si-NP gene silencing activity by our lead si-NP candidates, we established orthotopic mammary tumors using MDA-MB-231.Rictor^{HiBiT} cells. Once tumors reached a volume of 50 mm^3 [Day 0] mice were randomized into groups for treatment with ternary si-NPs

(50B0, 50B4-DP100, 50B8-DP100, and 50B12-DP25) loaded with siRNA against *RICTOR* (siRictor) or with non-targeting siRNA (siControl, 50B8-DP100) at 1 mg/kg (**Figure 2.13E**). Treatment with trehalose vehicle served as a control. A second treatment on Day 2 with si-NPs harboring fluorescent non-targeting siRNA (TAMRA si-NPs) enabled measurements of si-NP uptake by tumor cells on Day 3, when tumors were dissociated and analyzed by flow cytometry for mean fluorescent intensity (MFI). These studies revealed that 50B8-DP100 si-NPs exhibited the greatest MFI compared to any other si-NPs (**Figure 2.13F**). This is in contrast to our findings performed in cell culture demonstrating highest cell uptake of 50B12-DP25 si-NPs. This suggests that tumor biodistribution and cell uptake of 50B8-DP100 si-NPs benefit from greater PEG shielding *in vivo* in ways that were not detected from *in vitro* experiments.

Tumors assessed on Day 3 post-treatment for protein levels of Rictor^{HiBiT} revealed that, as compared to tumors from mice treated with vehicle or with siControl-loaded si-NPs, tumors treated with si-NPs loaded with human Rictor-targeting siRNAs (sihRictor-NPs) exhibited Nano-Luc activity that was decreased by >50%, reflecting siRNA-mediated knockdown of endogenous Rictor (**Figure 2.13G**). Consistent with *in vivo* tumor cell uptake data, tumors treated with 50B8-DP100 sihRictor-NP displayed the greatest Rictor knockdown (approx. 80%) relative to tumors treated with siControl-NPs and were significantly more potent than binary 50B0 sihRictor-NPs containing no 50B core polymer. Interestingly, gene silencing activity by 50B8-DP100 si-NPs was modestly, albeit not significantly, greater than 50B12-DP25 si-NPs (70% knockdown), potentially due to greater *in vivo* circulation time (**Figure 2.12G-7H**), *in vivo* tumor cell uptake (**Figure 2.13F**), and endosome disruptive activity (**Figure 2.6**).

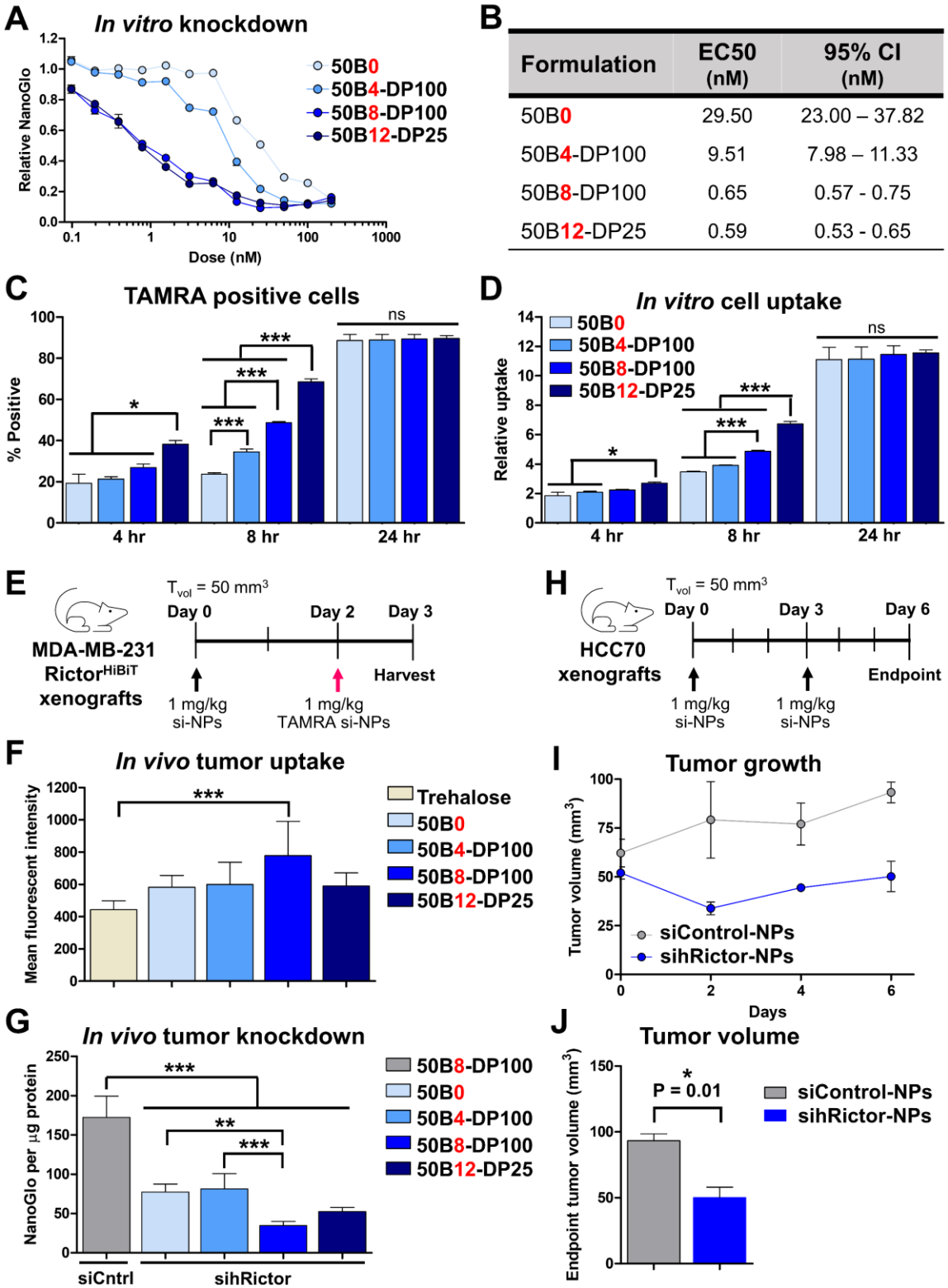

Figure 2.13: 50B8-DP100 si-NPs are the lead formulation for in vivo tumor uptake and tumor gene silencing.

(A) Rictor-HiBiT cells were treated with a subset of si-NPs at a range of siRNA doses, and relative Rictor silencing was assessed by NanoGlo detection of HiBiT (N = 6). (B) EC50 values for each si-NP were

calculated as a measure of si-NP silencing potency. (C-D) si-NPs loaded with fluorescent TAMRA-siRNA were used to assess in vitro uptake at 4, 8, and 24 hr of treatment (N = 3). (E) Mice bearing Rictor-HiBiT tumors were injected with trehalose vehicle, 1 mg/kg siControl-NPs, or 1 mg/kg sihRictor-NPs once tumors reached 50 mm^3 on Day 0. Mice were injected with 1 mg/kg fluorescent TAMRA si-NPs on Day 2. Tumors were harvested for analysis on Day 3. (F) si-NP in vivo tumor uptake at 24 hr after si-NP treatment was measured by flow cytometric quantification of TAMRA fluorescence (N = 5-6 mice). One-way ANOVA analysis with Dunnett's Multiple Comparison Test was used to compare uptake differences to trehalose vehicle-treated mice (***, $p < 0.001$). (G) si-NP in vivo tumor silencing of Rictor at 72 hr after si-NP treatment was quantified by NanoGlo detection of HiBiT levels (N = 4-6 mice). One-way ANOVA analysis with Tukey's multiple comparison test was used to compare silencing differences (**, $p < 0.01$; ***, $p < 0.001$). (H) Mice bearing HCC70 tumors were injected with 1 mg/kg 50B8-DP100 siControl-NPs or sihRictor-NPs once tumors reached 50 mm^3 on Day 0 and again on Day 3. (I-J) Tumor volumes of treated mice were monitored until Day 6 (N = 3). Unpaired t-test analysis was used to compare tumor volume differences on Day 6.

The 50B8-DP100 ternary si-NP formulation therefore exhibits characteristics that overcome multiple siRNA delivery barriers, positioning it as a frontrunner ternary formulation for future exploration of si-NP use in a therapeutic setting. The treatment efficacy of 50B8-DP100 si-NPs was, therefore, next tested in an orthotopic mammary tumor model using HCC70 cells. Once tumors surpassed a volume of 50 mm^3 [Day 0], mice were randomized into groups for i.v. treatment with 50B8-DP100 si-NPs bearing non-targeting siRNA (siControl-NPs) or siRNA targeting the oncogene Rictor in the human genome (sihRictor-NPs) at 1 mg/kg on Days 0 and 3 (**Figure 2.13H**). Tumor volume was monitored throughout the study. Mice treated with sihRictor-NPs had significantly diminished tumor volume (50.22 mm^3) compared to mice treated with siControl-NPs (93.27 mm^3) by the study endpoint (**Figure 2.13I-J**), indicating that 50B8-DP100 si-NPs have high potential for future application in oncological therapy.

2.2.ix. Optimized 50B8-DP100 si-NPs are well-tolerated in a muti-dose treatment setting

After establishing the therapeutic potential of 50B8-DP100 si-NPs in the cancer setting, we next assessed the long-term safety of this formulation following multiple i.v. treatments. Healthy, wild-type Balb/c mice were treated with three injections (Days 0, 3, and 7) of trehalose vehicle or 50B8-DP100 si-NPs harboring siControl or siRNA targeting Rictor in the mouse

genome (simRictor) (**Figure 2.14A-B**). Mice were treated with either siControl- or simRictor-NPs to assess for potential carrier related toxicities of si-NPs or potential toxicities resulting from Rictor silencing in off-target organs. Mice were assessed on Day 8 for kidney and liver toxicity markers, blood urea nitrogen (BUN), alanine aminotransferase (ALT), and aspartate aminotransferase (AST). Both groups of si-NP treated mice possessed plasma marker levels within the normal ranges for healthy mice (**Figure 2.14C**). Treatment with simRictor-NPs has the potential to produce off-target Rictor knockdown in the liver, which could result in hyperglycemia.[34] Mice treated with si-NPs were, therefore, assessed for glucose levels at the study endpoint, and baseline levels were similar to vehicle treated mice (**Figure 2.14D**). We furthermore probed the si-NP treated mice for Rictor knockdown within the liver, kidney, and spleen by western analysis (Figure 2.14**E**). While our si-NPs displayed the greatest biodistribution to the liver (**Figure 2.12**), simRictor-NPs mediated a relatively low level of Rictor protein knockdown (~15%) in this organ. We did not observe Rictor protein knockdown within the kidney, and similar to liver, spleens had a relatively low (~20%) protein knockdown. Finally, histological assessment of the liver, kidney, and spleen produced no signs of tissue damage following si-NP treatment (**Figure 2.14F**). Complete blood count levels following si-NP treatment were also similar to levels seen in vehicle treated mice (**Figure 2.15**). Together, these data indicate that 50B8-DP100 si-NPs display minimal toxicological effects following multiple treatments while also limiting knockdown activity in off-target organs. In the therapeutic setting, efficacious delivery of siRNA is likely to involve repeat si-NP administration.

2.3.Conclusions

Here, we aimed to understand the effect of core polymer content on ternary si-NP function both at the *in vitro* and *in vivo* level. We identified lead si-NP candidates that displayed maximal activity

and stability without sacrificing safety *in vivo* and demonstrated that careful variation of core polymer size and ratio can balance these characteristics for efficacious si-NP tumor delivery. Addition of a core 50B polymer improved si-NP stability and activity in comparison to binary si-NPs across a very broad range of 50B MWs and formulation conditions.

However, si-NP library screening also revealed trends among the ternary si-NPs, consistently showing that increasing 50B MW and ratio improved gene silencing potency, endosome disruptive ability, and stability when challenged with heparin salts or serum. However, increasing 50B content also came at the cost of heightened cytotoxicity. By simultaneously balancing 50B size and ratio, we identified ternary si-NP formulations that enhanced the si-NP therapeutic index, improved *in vivo* pharmacokinetics, and conferred potent tumor gene silencing in an orthotopic mammary tumor model. These studies underline the flexibility of ternary si-NP designs, as they can be easily tuned to overcome multiple delivery barriers. Our findings furthermore generate critical knowledge on the structure-activity relationships driven by ternary si-NP core polymer MW and content. These insights will guide future siRNA nanoparticle design for improved *in vivo* efficacy following systemic delivery.

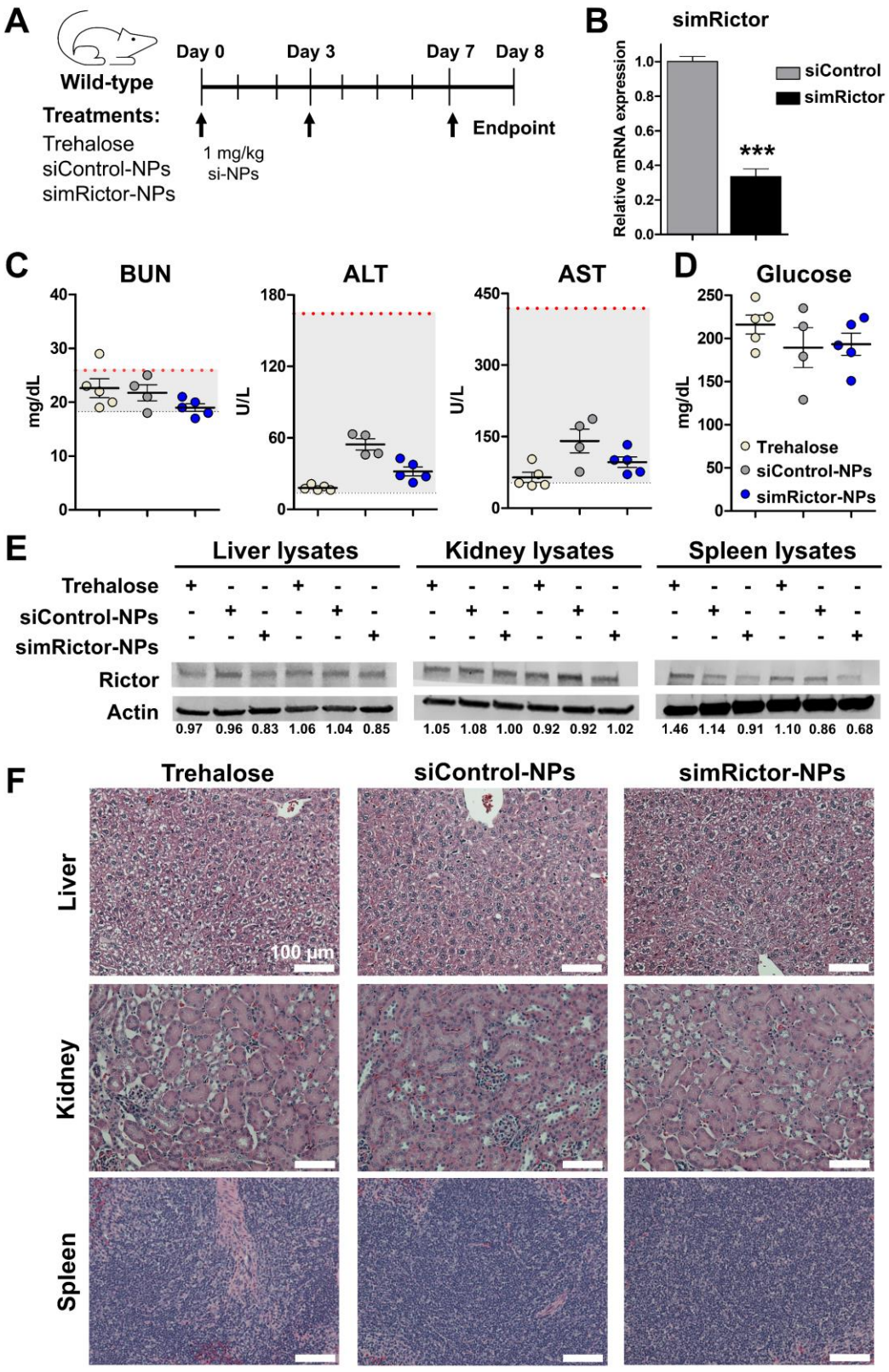

Figure 2.14: 50B8-DP100 si-NPs display minimal toxicological effects following multi-dose treatments.

(A) Healthy, wild-type mice were treated with three injections over the course of a week and analyzed for safety and off-target activity on Day 8, 24 hr after the final injection. (B) Silencing potency of simRictor sequence was confirmed by qPCR in murine EMT6 cells. (C) Plasma BUN, ALT, and AST levels were within the normal ranges following multiple si-NP injections. Normal ranges for each marker are indicated by dotted y-axis lines. (D) simRictor-NP treatment did not result in elevated baseline glucose levels compared to vehicle treatment. (E) Livers, kidneys, and spleens were probed for Rictor protein knockdown by western analysis. Densiometric analysis of bands was calculated relative to average of siControl-NP bands. (F) Livers, kidneys, and spleens were assessed for tissue damage by H&E staining.

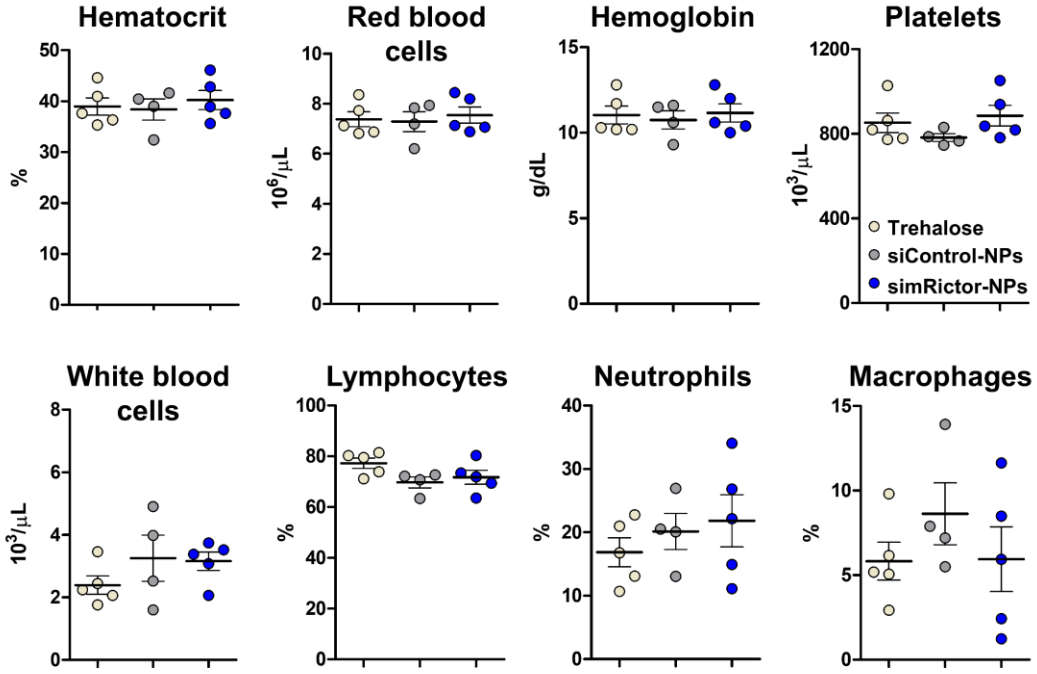

Figure 2.15: Complete blood count analysis following multi-dose si-NP treatments.
si-NP treated mice showed complete blood count levels similar to vehicle treated mice.

2.4.Materials and Methods

2.4.i. Materials and reagents

Unless otherwise noted, chemicals and materials for biological assays were purchased from Sigma-Aldrich or Fisher Scientific. All oligonucleotides used in these studies were synthesized on a MerMade 12 Oligonucleotide Synthesizer (Bioautomation) using modified (2'-OMe and 2'-F) phosphoramidites. Sequences and modifications of all oligonucleotides can be found in **Table 2.2**.

Table 2.2: siRNA sequences.

Oligonucleotide	Sequence (5' to 3')
Control sense	fC*mG*fU mU fA mA fU mC fG mC fG mU fA mU fA mA fU*mA*fC
Control antisense	5PHO mG*fU*mA fU mU fA mU fA mC fG mC fG mA fU mU fA mA*fC*mG
Luciferase sense	fC*mA*fA mU fU mG fC mA fC mU fG mA fU mA fA mU fG*mA*fA
Luciferase antisense	5PHO mU*fU*mC fA mU fU mA fU mC fA mG fU mG fC mA fA mU*fU*mG
hRictor sense	fG*mA*fA mG fA mU fU mU fA mU fU mG fA mG fU mC fC*mU*fA
hRictor antisense	5PHO mU*fA*mG fG mA fC mU fC mA fA mU fA mA fA mU fC mU*fU*mC
mRictor sense	fC*mU*fU mA fG mA fA mG fA mU fC mU fC mG fU mG fA*mA*fA
mRictor antisense	5PHO mU*fU*mU fC mA fC mG fA mG fA mU fC mU fU mC fU mA*fA*mG
Modifications: f = backbone 2'Fluoro; m = backbone 2'O-Methyl; * = phosphorothioate bond; 5PHO = 5' phosphorylation; TAMRA and BHQ2 fluorophores tagged on 3' end of Control sense strands	

2.4.ii. Polymer synthesis and characterization

All polymers were synthesized by RAFT polymerization using 4-cyano-4-(ethylsulfanylthiocarbonyl)sulfanylpentanoic acid (ECT) as the CTA, synthesized as previously described.[101] 50B polymers were synthesized at 50:50 molar ratios of 2-(dimethylamino)ethyl methacrylate (DMAEMA) and butyl methacrylate (BMA) using AIBN as an initiator and a 5:1 ratio of CTA:initiator, in 20% w/v dioxane for 24 hr. 50B polymers were purified by dialysis in water followed by lyophilization.

To synthesize 20kPEG-50B, 20kPEG-ECT was first synthesized by DIC/DMAP coupling of hydroxyl-terminated 20kDa PEG to ECT in dichloromethane for 48 hr, as previously described.[44, 77] A 10 molar excess of ECT, 10 molar excess of DIC, and 5 molar excess of DMAP to 20kDa PEG was used in a 10% w/v reaction. 20kPEG-ECT was purified by precipitation in diethyl ether and dried under vacuum. RAFT polymerization of 50:50 DMAEMA and BMA

was performed as described above. 20kPEG-50B was purified by precipitation in 2:1 pentane:diethyl ether and dried under vacuum.

Polymers were characterized for degree of polymerization and MW using ^{1}H nuclear magnetic resonance spectroscopy (H NMR, Bruker, 400 MHz) and dimethyl formamide mobile phase gel permeation chromatography (GPC, Agilent Technologies).

2.4.iii. **Formulation of lyoprotected si-NPs, characterization of size and surface charge**

All ternary si-NPs were formulated using a 3 mg/mL polymer solution of 20kPEG-50B and 0.5 mg/mL polymer solution of 50B made up of 10% ethanol and 90% 0.1 M citrate buffer (pH 4). Binary si-NP 50B0 contained only the 20kPEG-50B polymer solution. si-NPs were formulated at a total polymer to nucleic acid ratio (N^{+}/P^{-}, calculated using the ratio of protonated amines on DMAEMA polymer to phosphates on the siRNA duplex) of 16. N/P of 50B was varied as 0, 4, 8, or 12 of the total polyplex N/P of 16. siRNA and polymer amounts were calculated as previously described[37], using the formulas below:

$$nmol\ Pol_1 = \frac{(nmol\ siRNA)(bp\ siRNA)(2)\left(\frac{N}{P}\right)}{(RU\ DMAEMA)(0.5)}$$

$$nmol\ Pol_2 = \frac{(nmol\ siRNA)(bp\ siRNA)(2)\left(\frac{N}{P}\right) - (nmol\ Pol_1)(RU\ DMAEMA_1)(0.5)}{(RU\ DMAEMA)(0.5)}$$

where Pol_1 refers to the 50B polymer and Pol_2 refers to the 20kPEG-50B polymer.

After mixing calculated amounts of polymer and siRNA, the solution was allowed to complex for 30 min. Following complexation, 5x v/v 0.2 M phosphate buffer (pH 8) was added to raise solution pH to 7.4.

For *in vitro* experiments, formulated si-NPs were added to Amicon centrifugal tubes (Millipore Sigma) with 50 kDa MW cut-off to concentrate si-NPs and remove excess levels of pH buffers. 7x v/v of 270 mM sucrose solution was added to concentrated si-NPs and si-NPs were

once again spun to a final concentrated dose of 2000 nM. Concentrated si-NPs were flash-frozen, lyophilized overnight, and stored at -80 °C. To reconstitute lyophilized si-NPs, water was first added to si-NP cake at the volume that si-NPs were lyophilized in. si-NPs were allowed to sit for 20 min to rehydrate fully, and media or other buffers were then added to dilute si-NPs to their final working dose needed for respective assays.

For *in vivo* experiments, si-NPs were concentrated in pH buffers as described above and then washed with 7x 300 mM aqueous trehalose solution. si-NPs were spun down to a 1 mg/kg dose in a 100 uL injection volume and frozen and lyophilized as described above. *In vivo* lyophilized si-NPs were reconstituted with 100 uL sterile water to deliver si-NPs i.v. in an isotonic solution.

si-NP hydrodynamic diameter and zeta potential was measured by dynamic light scattering (DLS, Zetasizer Nano ZS, Malvern Instruments).

2.4.iv. Cell culture

All cells used in this work were cultured in Dulbecco's modified eagle's medium (DMEM, Gibco Cell Culture), containing 4.5 g/L glucose, 10% FBS (Gibco), and 1% Antibiotic-Antimycotic (Gibco). All cells were tested for *Mycoplasma* contamination using MycoAlert Mycoplasma Detection Kit (Lonza).

2.4.v. In vitro assessment of si-NP target gene silencing and cell viability following si-NP treatment

Luciferase gene silencing and si-NP cell viability were assessed in Luciferase-expressing MDA-MB-231 cells that were transduced with the *LUCIFERASE* gene as previously described. [44] Cells were seeded in opaque 96-well plates at 4,000 cells/well. After adhering overnight, cells were treated with si-NPs encapsulating either siControl or siLuciferase siRNA. si-NP treatment

was replaced at 24 hr. Luciferase gene knockdown was assessed at 48 and 72 hr through the addition of luciferin-containing media (150 ug/mL) and imaging of luminescence by IVIS (Caliper Life Sciences). Knockdown of luminescence signal was normalized against cells treated with siControl-NPs.

RICTOR gene silencing was assessed in Rictor^{HiBiT}-expressing MDA-MB-231 cells. HiBiT-tagged Rictor cells were generated by CRISPR-Cas9 mediated homology directed repair. A single-stranded oligo donor (ssODN) sandwiching the *RICTOR* STOP codon was used for HiBiT sequence insertion. HiBiT sequence insertion was confirmed by successful Nano-Luc complementation using a Nano-Glo HiBiT Lytic Detection assay (Promega) according to manufacturer's instructions. Cells were dilution cloned as single-cell derived colonies to identify subpopulations with high levels of Nano-Luc complementation. Selected cells were plated and treated for si-NP silencing studies as described above. Rictor gene knockdown was assessed at 72 hr using the Nano-Glo HiBiT Lytic Detection assay, and luminescence was measured by plate reader (Tecan Infinite F500). Knockdown of luminescence signal was normalized against cells treated with siControl-NPs.

siControl-containing si-NPs were used for viability assessment at 24 hr. CellTiter-Glo assay (Promega) was used according to manufacturer's instructions for relative viability assessment normalized to untreated wells.

2.4.vi. In vitro cell uptake

si-NPs harboring fluorescent TAMRA-siRNA were used to assess uptake in MDA-MB-231 cells. 100,000 cells/well were seeded in 12-well plates and allowed to adhere overnight. Cells were treated with 100 nM si-NPs for 4, 8, and 24 hrs, and untreated cells were used as negative controls. At study endpoint, si-NPs were removed, and cells were trypsinized and washed with

PBS three times. Cells were reconstituted a final time in PBS and assessed for TAMRA fluorescence using flow cytometry (Guava easyCyte SL System, Luminex). TAMRA fluorescence was monitored using the Yellow filter off the 488 nm Blue laser (YEL-B parameter). Quantification of geometric mean fluorescence intensity and percent positive cells was performed on FlowJo software.

2.4.vii. In vitro assessment of si-NP endosome disruptive activity

Gal8-YFP measurement were carried out as previously described.[33, 43, 88] Gal8-YFP expressing MDA-MB-231 cells were seeded at 2,000 cells/well in opaque half-area 96-well plates. After allowing cells to adhere for 24 h, cells were treated with 200 nM si-NPs. Cells were imaged for Gal8 recruitment by automated fluorescent microscopy (Nikon C1si + confocal microscope system on a Nikon Eclipse Ti-0E inverted microscope base, Plan Apo VC 20 × objective, Galvano scanner, and 408/488/543 dichroic mirror). Wells were imaged by a software-controlled motorized stage that moved the plate between images. Recruited Gal8 was identified by a MATLAB script recognizing Gal8-YFP fluorescent puncta, and intensity was normalized to total cell area.

2.4.viii. Characterization of si-NP encapsulation, stability against heparin and serum

si-NP encapsulation was assessed using the Quant-iT Ribogreen assay kit (ThermoFisher). Assay reagents were prepared following manufacturer's instructions and heparin salts were added at final concentrations of 0, 25, and 50 U/mL. si-NPs were prepared at a 100 nM final dose. Final well volumes in an opaque 96-well plate were made up of 50 mL si-NPs in TE buffer, 50 uL heparin in TE buffer, and 100 uL Ribogreen reagent. Fluorescence was measured on a plate reader (Tecan Infinite F500) at 520 nm over time, and encapsulation efficiency was calculated against a standard curve of siRNA-only wells containing known levels of siRNA.

si-NP stability in fetal bovine serum (FBS) and heparin salts was assessed using black hole quencher assay. si-NPs were co-loaded with TAMRA-tagged siRNA and Black hole quencher-tagged siRNA (BHQ2, capable of quenching TAMRA emission). To synthesize TAMRA and BHQ-tagged siRNAs, standard controlled pore glass synthesis columns containing the respective fluorophores were purchased from Glen Research (20-5910-41M, 20-5932-42M), and Control sense oligonucleotide strands were grown. 100 nM si-NPs and final FBS concentration of either 10% or 50% were added to opaque 96-well plates. TAMRA was excited at 546 nm and fluorescence was measured at 576 nm. As TAMRA signal was restored following si-NP cargo release and loss of Black hole quenching, rate of relative TAMRA fluorescence increase over time was plotted as a measure of si-NP destabilization kinetics.

2.4.ix. In vivo si-NP toxicology studies

For acute toxicity studies, wild-type immunocompetent Balb/C mice (4-6 week old, Charles River) were injected i.v. in the tail vein with 1 mg/kg si-NPs. 300 mM aqueous trehalose was injected as a vehicle control. Mouse blood was collected via cardiac punch 30 min after injection to assess for acute platelet activating factor (PAF)-related si-NP toxicities. Mouse EDTA-blood samples were spun 1,000×g for 10 min at 4 °C to isolate plasma for analysis using a PAF acetyl hydrolase activity kit (Caymen Chemical). Plasma samples were assayed in duplicate according to the manufacturer's protocol using 10 μL plasma samples in each well.

For multi-dose toxicity studies, wild-type immunocompetent Balb/C mice (4-6 week old, Charles River) were injected i.v. in the tail vein with 1 mg/kg si-NPs bearing siRNA targeting *Rictor* in the mouse genome (simRictor-NPs) on Days 0, 3, and 7. Mouse blood was collected via cardiac punch on Day 8, 24 hr after the final injection. Plasma biochemistry analysis for systemic markers (AST, ALT, BUN, glucose) was performed by Antech GLP through the Vanderbilt

Translational Pathology Shared Resource (TPSR). Biochemistry markers were compared against a normal value range for Balb/C mice, and ranges were referenced from the Mouse Phenome Database by The Jackson Laboratory.

Collected blood was also analyzed for complete blood counts (including hematocrit and red blood cell measures) by TPSR. Mouse organs were harvested (liver, kidney, spleen) and fixed in 10% formalin for H&E histologic analysis of si-NP toxicity.

Western analysis for Rictor protein knockdown was performed on liver, kidney, and spleen tissues. Organs were homogenized in ice-cold lysis buffer (RIPA lysis buffer supplemented with 2% NP-40, 1X protease inhibitor cocktail (Roche), and 1x phosphatase inhibitor cocktail (Roche)). Protein concentration was determined by BCA assay (Pierce), and samples were resolved by SDS-PAGE. Separated proteins were transferred to nitrocellulose membranes, blocked, and probed with primary antibodies Rictor (Sigma-Aldrich), and β-actin (Cell Signaling Technologies).

2.4.x. Intravital microscopy and biodistribution

Anesthetized CD-1 mice were immobilized on a heated stage for fluorescence scanning of the ear vasculature by confocal microscopy. Microscopy was performed using a Nikon Czsi+ system with a Nikon Eclipse Ti-oE inverted microscopy base, Plan ApoVC 20× differential interference contrast N2 objective, 0.75 NA, Galvano scanner, and 543 dichroic mirror. Prior to imaging, mouse ears were depilated and positioned on a glass coverslip using immersion oil. Light microscopy was used to focus upon a prominent ear vein where flowing red blood cells could be easily visualized. Once a vein was in focus, confocal microscopy was initiated, and mice were tail vein injected with si-NPs harboring fluorescent, Cy5-tagged siRNA. Intravital fluorescence decay via laser scanning was monitored as one image per second, with a laser gain of 98 throughout. All image analysis and acquisition were done using Nikon NIS-Elements AR version 4.30.01. For

image analysis, a region of interest (ROI) was highlighted within the mouse ear vasculature, and a fluorescence decay curve from this ROI was generated. Background fluorescence was first subtracted, and fluorescence values were normalized to a maximum initial fluorescence intensity. Fluorescence decay curves were fit to a one-compartment intravenous bolus model in PK Solver[102] to determine pharmacokinetic parameters. A one-compartment model was chosen because it had the greatest fit (R^2 value) compared to other models tested in PK Solver.

2.4.xi. In vivo si-NP tumor studies

Athymic nude Balb/C mice (4-6 weeks, Envigo) were injected with 1e6 HiBiT-tagged Rictor MDA-MB-231 cells in 50:50 Matrigel:serum-free DMEM in the inguinal mammary fat pad. Once tumors reached 50 mm^3 in volume (Day 0), mice were divided into treatment groups and injected i.v. with 1 mg/kg si-NPs bearing siControl or siRNA targeting *RICTOR* in the human genome (sihRictor). Mice injected with 300 mM aqueous trehalose were used as a vehicle control. si-NPs bearing fluorescent TAMRA-tagged siRNAs were injected i.v. on Day 2. On Day 3 (72 hr after siRictor-NP treatment and 24 hr after siTAMRA-NP treatment) tumors were harvested for downstream analysis.

A portion of harvested tumors were assessed for si-NP uptake by flow cytometry (Amnis CellStream, Luminex). Tumors were processed for flow analysis as previously described[44] and quantified for TAMRA fluorescence using a 583 nm filter off the 532 nm laser (D4 laser parameter). Uptake analysis was performed on FlowJo software.

A portion of harvested tumors were assessed for gene silencing by Nano-Luciferase complementation of HiBiT-tagged Rictor. Tumors were lysed and quantified for total protein using BCA Assay (Pierce). HiBiT-tagged Rictor knockdown was assessed in lysates using Nano-Glo HiBiT Lytic Detection assay (Promega) according to manufacturer's instructions.

For therapeutic tumor growth inhibition studies, athymic nude Balb/C mice (4-6 weeks, Envigo) were injected with 1e6 HCC70 cells in 50:50 Matrigel:serum-free RPMI in the inguinal mammary fat pad. Once tumors reached 50 mm^3 in volume (Day 0), mice were divided into treatment groups and injected i.v. with 1 mg/kg si-NPs bearing siControl or sihRictor. Mice were again injected with si-NPs on Day 3. Tumor volumes were monitored by digital caliper measurements (T_{vol} = length x $width^2$ / 2).

2.4.xii. Statistical Analyses

Data were analyzed using GraphPad Prism 8 software (Graphpad Software, Inc.). In most cases, si-NP performance was compared by one-way ANOVA analysis. Specific statistical tests used for data can be found in corresponding figure legends. Data is plotted as average ± SEM. For all figures, * $p \leq 0.05$; ** $p \leq 0.01$; *** $p \leq 0.001$; ns, not significant.

Chapter 3: Assessment of the therapeutic impact of selective mTORC2 inhibition in TNBC

3.1. Introduction

Many strategies to modulate PI3K/mTOR pathway signaling in TNBC have focused their efforts on inhibition of mTORC1. However, mTORC1-specific inhibitors have not shown great success in TNBC, even in combination with chemotherapy.[11, 12] The limited success of mTORC1-specific targeting may be largely attributed to resurgent PI3K signaling due to the inhibition of the negative feedback loop between mTORC1 and IRS-1.[50] Reactivated PI3K can consequently activate mTORC2 signaling, and importantly, phosphorylate Akt to induce survival signaling. Less is known about mTORC2, though emerging studies implicate it in TNBC progression.[103-105] Small molecule inhibitors that are capable of blocking mTORC2 signaling, such as ATP competitive TORKinibs, also inhibit mTORC1, making it difficult to ascertain the specific effects of mTORC2 inhibition. Here, we begin to comprehensively characterize effects of selective and acute mTORC2 inhibition through silencing of Rictor, an obligate cofactor of the complex. In a molecular subtype-specific manner, we show here that certain TNBC subtypes are more sensitive to mTORC2-specific inhibition, making selective mTORC2 inhibition an advantageous therapeutic strategy for *RICTOR*-amplified TNBC. Finally, we also assess the utility of mTORC2 blockade to improve TNBC chemo-response, thus identifying a cooperative treatment regime that may benefit PI3K-active TNBC patients.

3.2. Results and Discussion

3.2.i. mTORC2 signaling promotes oncogenic behaviors in cancer cells and decreases overall survival in patients

Previous meta-analyses report that high tumor *RICTOR* expression correlates with decreased disease-free survival in patients and decreased overall survival in patients with invasive

breast cancer harboring.[17, 62] We further corroborated this data through analysis of TCGA (N = 817; N = 960) and METABRIC (N = 1904) databases where *RICTOR* amplification or over-expression (defined as *RICTOR* altered) decreased overall patient survival (**Figure 3.1A**). In TNBC specifically, previous reports have found high *RICTOR* levels to correlate with decreased progression-free survival in BL1 and BL2 subtypes.[17] This suggests that mTORC2 signaling plays an important pro-oncogenic role in at least some TNBC molecular phenotypes and that mTORC2 inhibition could serve as a beneficial treatment strategy.

Downstream effectors of mTORC2 promote tumor cell survival through mTORC2 phosphorylation of Akt at serine 473 (S473) and regulate tumor cell motility and metastasis through PKCα/Rac1 activation.[106] Furthermore, downstream phosphorylation of targets such as SGK and NDRG1 can promote resistance to chemotherapies as well as PI3K/AKT inhibition (**Figure 3.1B**).[107, 108] We found that Rictor activation, as measured in reverse-phase protein array (RPPA) as T1135, correlates with increased phosphorylation of Akt at S473 and phosphorylation of NDRG1 (**Figure 3.1C**). This suggests that Rictor overexpression promotes mTORC2 signaling and phosphorylation of mTORC2 substrates that play known pro-oncogenic roles. Meanwhile, downstream effectors of mTORC1 control cell processes such as protein translation, proliferation, and metabolism. The mTORC1 signaling complex contains a negative feedback loop to PI3K signaling through S6K inhibition of IRS-1. Any inhibition of mTORC1 through small molecule inhibitors such as rapamycin analogs (conferring mTORC1-selective inhibition) or mTOR kinase inhibitors (conferring dual mTORC1 and mTORC2 inhibition by blocking mTOR catalytic activity) would result in the loss of this negative feedback and consequent resurgence of PI3K signaling that can activate Akt through phosphorylation at threonine 308 (T308). Our RPPA analysis shows that Rictor activation correlates with decreased

phosphorylation of mTORC1/S6K substrate S6 (**Figure 3.1C**), suggesting that Rictor overexpression is associated with decreased mTORC1 activity that could drive resurgent PI3K activity. Together, this data suggests that Rictor amplification can potentiate tumorigenic activities through multiple avenues.

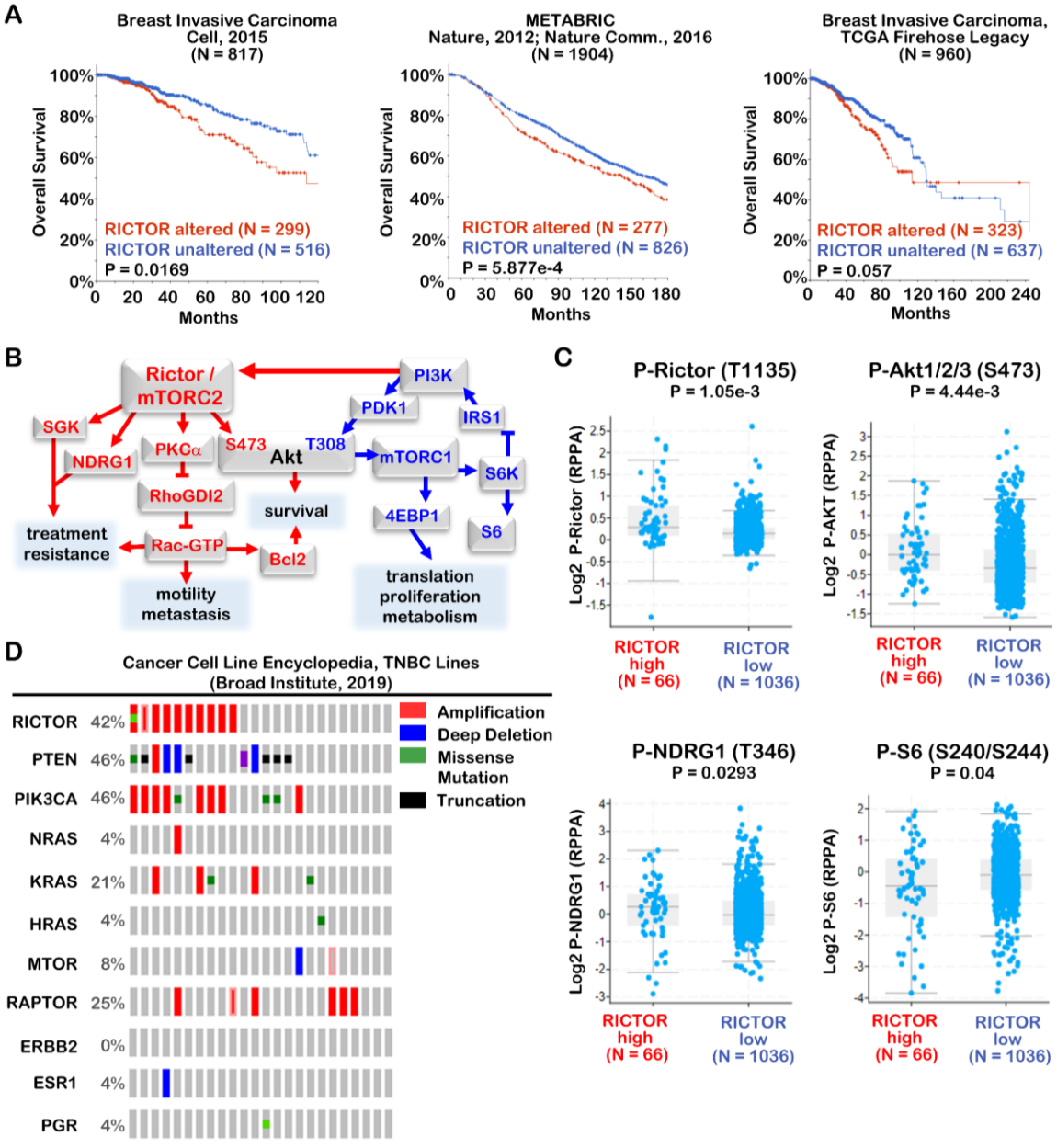

Figure 3.1: Rictor/mTORC2 signaling promotes oncogenic behaviors in cancer cells.
(A) Analysis of breast cancer datasets suggest that RICTOR amplification or over-expression correlates with worse outcome, and (B-C) with phosphorylation of mTORC2 effectors, suggesting that RICTOR amplification increases mTORC2 signaling, which drives tumor malignancy. (D) RICTOR-amplified TNBC cell lines were identified in the CCLE.

We queried the CCLE database for TNBC cell lines (defined as lacking *ESR1*, *PGR*, and *ERBB2*) with corresponding genomic copy number data and found that approximately 42% (10 out of 24 cell lines) of TNBC lines displayed *RICTOR* amplification (**Figure 3.1D**). Interestingly, 9 out of those 10 *RICTOR* amplifications co-occurred with PI3K pathway alterations (either *PTEN* loss/mutation or *PIK3CA* amplification). In contrast, only 5 out of the 24 cell lines harbored *RAPTOR* amplification.

TNBC cell lines displaying *RICTOR* amplification (HCC70, CAL851) or normal *RICTOR* levels (MDA-MB-157) were chosen to assess the therapeutic effects of mTORC2 inhibition and its relativity sensitivity in TNBC molecular phenotypes. Importantly, HCC70 and CAL851 cells lines harbor additional PI3K pathway-related genomic alterations; HCC70 cells display *PTEN* deletion while CAL851 cells display *PIK3CA* mutation. These mutations may promote greater response to mTORC2 therapy. As suggested by the RPPA analysis, cells with *RICTOR* over-expression may over-activate mTORC2 signaling, particularly under stress conditions.

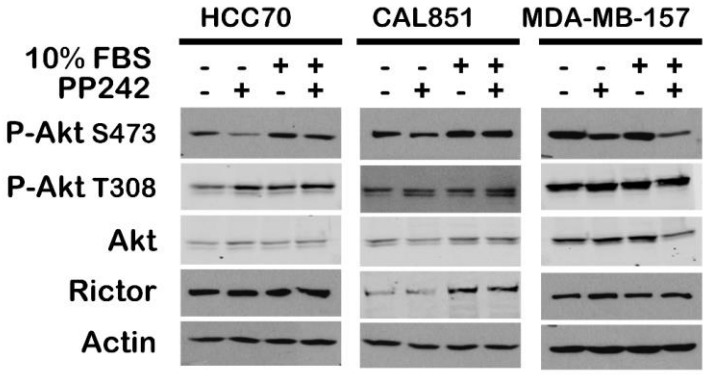

Figure 3.2: TNBC cell lines display differential activation of PI3K/mTOR signaling.
Cell lines amplified for *RICTOR* (HCC70, CAL851) or displaying basal *RICTOR* levels (MDA-MB-157) were treated with mTORC1/2 inhibitor PP242, which blocks mTORC2 activity (i.e., P-Akt S473) but causes increased PI3K signaling (i.e., P-Akt T308), due to mTORC1 inhibition.

This was demonstrated in our chosen TNBC cell lines where treatment with the mTOR kinase inhibitor, PP242, decreased mTORC2 signaling, measured through decreased P-Akt S473,

in MDA-MB-157 cells (**Figure 3.2**). In *RICTOR*-amplified lines, mTORC2 signaling was also decreased with PP242 treatment, but this effect was mitigated in the presence of serum. Our strategy for *RICTOR* silencing to selectively inhibit mTORC2, particularly in RICTOR-amplified TNBC, may prove to be efficacious where other strategies for mTOR inhibition have failed.

3.2.ii. mTORC2 signaling inhibition in RICTOR amplified TNBC potently decreases cell growth and enhances cell killing

In recent years, researchers have begun to uncover the role of mTOR signaling in cancer but a lot remains to be understood on the effects of mTOR inhibition in established TNBC. We probed *RICTOR*-amplified TNBC lines HCC70 and CAL851, as well as a potential non-responder cell line MDA-MB-157, with mTOR inhibitors to elucidate therapeutic and signaling effects of mTOR blockade. Selective mTORC1 inhibition was achieved using the rapamycin analog, RAD001, while dual mTORC1 and mTORC2 inhibition was achieved using the TOR kinase inhibitor, PP242. We treated the 3 cell lines with a dose curve of each drug and assayed relative cell numbers (**Figure 3.3A**). While RAD001 decreased cell growth to some degree even at low doses, the cell lines showed sensitivity to PP242 treatment in a dose-dependent manner, suggesting an increased potency against the mTORC2 pathway. The lack of cell inhibitory response to RAD001 may in part be due to the distinct signaling effects of mTORC1 inhibition, which we assessed by western analysis at early timepoints following inhibitor treatment (**Figure 3.3B-C**). Treatment with RAD001 blocks phosphorylation of P-S6, an mTORC1 substrate; but phosphorylation of Akt at S473 paradoxically increases, indicating only a partial inhibition of Akt and suggesting that mTORC2 activity may compensate for any inhibition of mTORC1 (**Figure 3.3B, D**). PP242 achieves durable inhibition of P-Akt S473 and transient inhibition of P-Akt T308 (**Figure 3.3C**). However, P-Akt T308 resurges over time, suggesting a re-activation of PI3K

signaling following mTORC1 inhibition and release of negative feedback to IRS-1. Increased P-Akt T308 levels were also seen following RAD001 treatment (**Figure 3.3D**). In a consistent manner, both drugs also increase phosphorylation of PDK, an effector of PI3K that commits phosphorylation of Akt at T308. Interestingly, while PP242 decreases P-Akt S473 in HCC70 and CAL851 cells, the inhibition is more complete in MDA-MB-157 cells, again suggesting overactive mTORC2 signaling in *RICTOR*-amplified cell lines.

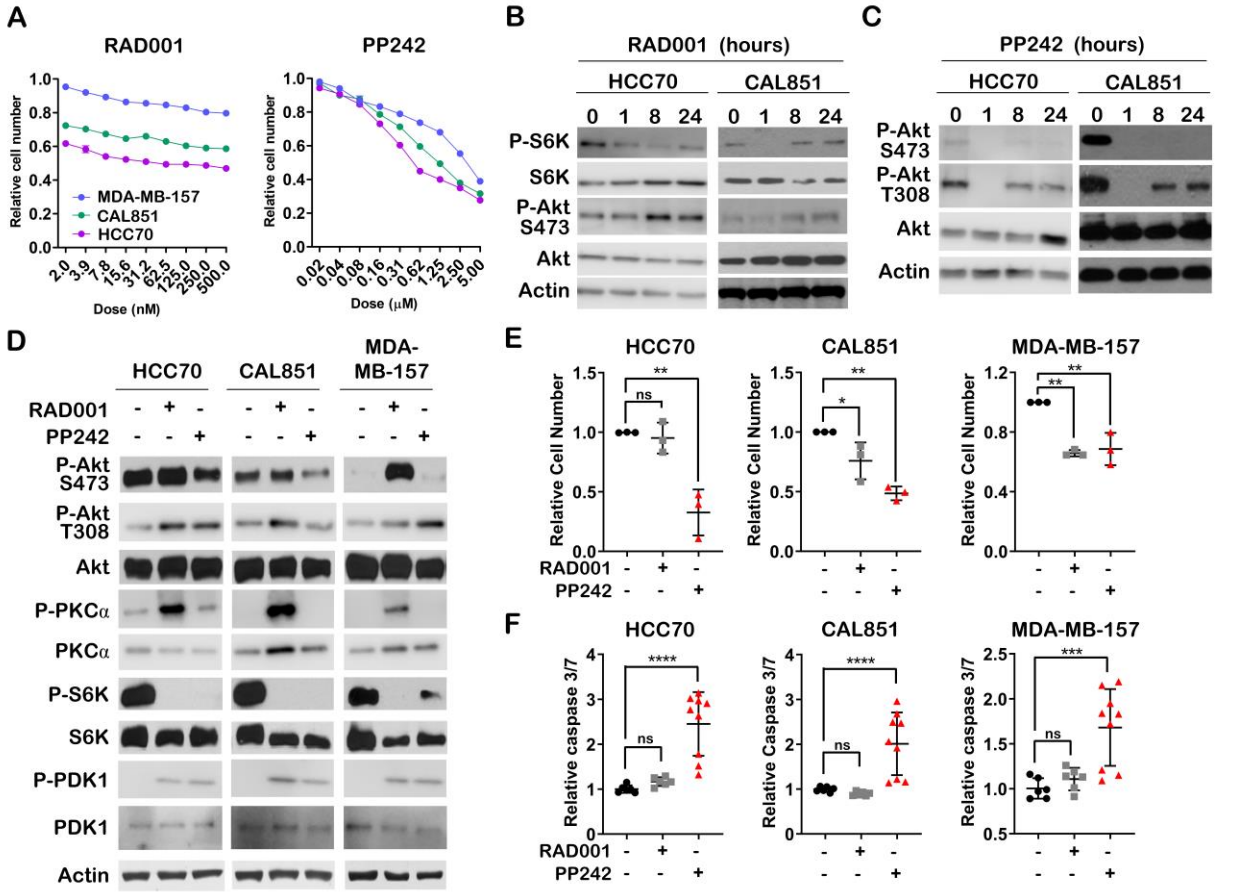

Figure 3.3: The distinct effects of mTORC1 inhibition may not be advantageous in TNBC. (A) The distinct effects of mTORC1 inhibition in TNBC were studied using RAD001 while distinct effects of dual mTORC1/2 inhibition was studied using mTOR kinase inhibitor PP242. (B-D) Both drugs result in increased PI3K signaling. (E) Cell number was assessed in TNBC cells treated with RAD001 and PP242, showing greater growth inhibition and in RICTOR-amplified TNBCs (HCC70 and CAL851) upon PP242 treatment compared to RAD001 treatment. (F) Caspase 3/7 activity was assessed in TNBC cells, showing increased cell apoptosis upon PP242 treatment than RAD001 treatment.

Cell number and cell death were also assessed following RAD001 and PP242 treatment. In *RICTOR*-amplified lines, PP242 significantly decreased cell number while both drugs displayed similar effects in MDA-MB-157 cells (**Figure 3.3E**). Treated cells were also assessed for apoptosis by measuring caspase 3/7 activity. PP242, but not RAD001, enhanced cleaved caspase 3 in all cell lines (**Figure 3.3F**). This may suggest that inhibition of mTORC2, but not mTORC1, activity may enhance therapeutic cell killing. Together, this data establishes an important and distinct role for mTORC2 signaling in TNBC, particularly for *RICTOR*-amplified cases.

3.2.iii. mTORC2 inhibition improves TNBC response to chemotherapy

We next assessed the utility of combining mTOR signaling inhibition with chemotherapy. Neoadjuvant chemotherapy has remained a standard of care for TNBC patients, for a lack of more targeted therapies approved at the early tumor stage. Next-generation sequencing studies on TNBC tumors that have undergone neoadjuvant chemotherapy, however, reveal that a substantial portion of residual tumors comprise mutations in the PI3K/mTOR pathway, correlating it with chemoresistance.[61] We therefore sought to combine small molecules RAD001 and PP242 with paclitaxel and doxorubicin to ascertain whether blockade of certain mTOR signaling arms in TNBC may potentiate chemotherapy-mediated tumor cell killing. All TNBC cell lines displayed sensitivity to chemotherapy with increasing dose (**Figure 3.4A**). Importantly, we could achieve near complete cell growth inhibition with doxorubicin treatment while paclitaxel treatment resulted in a plateaued effect at higher doses. Paclitaxel has been noted to induce a cancer stem cell-like phenotype in BC cells, which can promote resistance in a PI3K/Akt dependent manner.[109-111] Paclitaxel is therefore an important treatment regime to study in TNBC, not only because it is a first-line therapeutic agent for TNBC patients but also because it may be promoting resistance mechanisms that could be mitigated through mTOR blockade. Combination

studies were performed with inhibitors RAD001 and PP242, and cell lines were assessed for viability. PP242 combination with doxorubicin and paclitaxel chemotherapies decreased cell numbers in *RICTOR*-amplified cell lines beyond the chemotherapies alone or chemotherapy combined with RAD001 (**Figure 3.4B-C**). However, RAD001 and PP242 combination did not inhibit cell growth in MDA-MB-157 cells beyond what was achieved with chemotherapy alone. This suggests that mTORC2 inhibition, but not mTORC1 inhibition, plays an important additive role to chemotherapy cell killing in *RICTOR*-amplified TNBC.

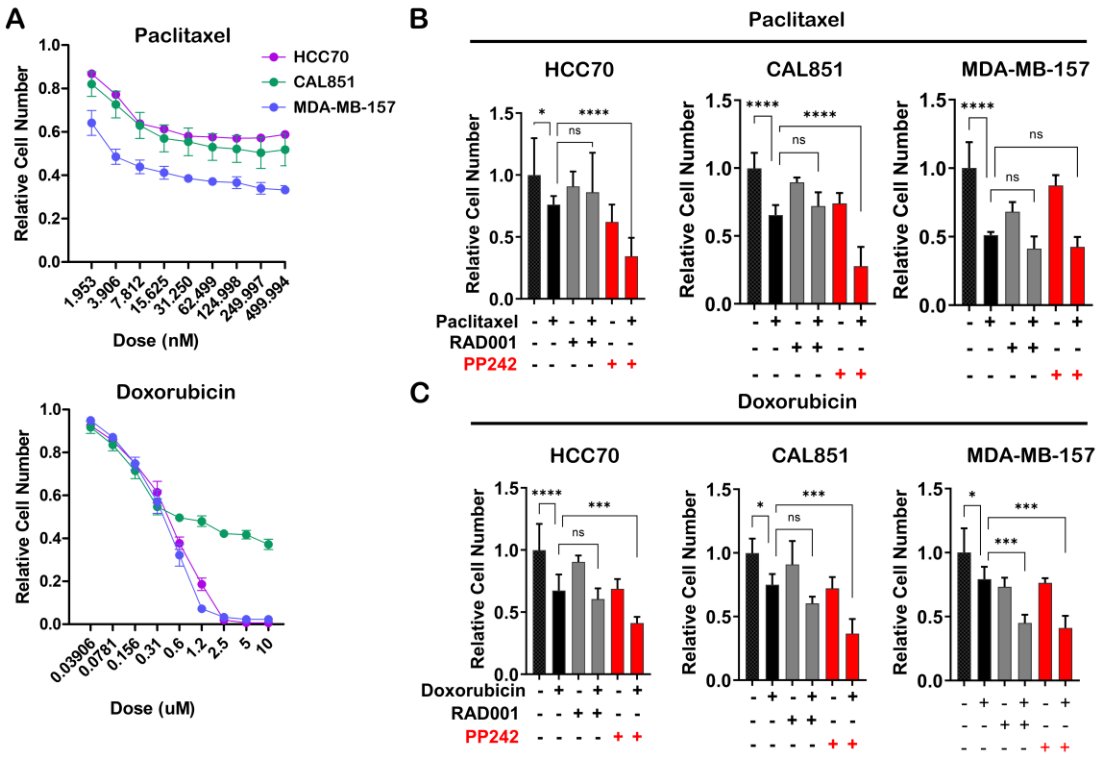

Figure 3.4: mTORC2 blockade improves chemotherapy cell killing in *RICTOR*-amplified TNBC.

(A) TNBC cell lines were treated with a dose curve of doxorubicin and paclitaxel and cell numbers were assessed 2 days post treatment. (B-C) Small molecule inhibitors PP242 and RAD001 were combined with chemotherapy and cell numbers were quantified 2 days post treatment.

3.2.iv. Rictor siRNA as a strategy for selective mTORC2 inhibition blocks Akt and obstructs tumor cell survival

To further understand the distinct effects of blocking mTORC1 versus mTORC2 signaling without the confounding effects of dual signaling inhibition, we designed siRNAs that could potently and selectively block these respective pathways. To accomplish this, we designed and administered siRNAs against *RAPTOR* and *RICTOR* and compared their effects against treatment with a non-targeting control siRNA (siControl) (**Figure 3.5A-C**). Like the effects of RAD001, siRaptor treatment decreased P-S6 levels, a substrate of mTORC1 that confirms efficient inhibition of mTORC1 activity (**Figure 3.5D**). However, siRaptor also increased in P-Akt S473 levels and resulted in the loss of the S6K1-mediated negative feedback loop on PI3K activity, as seen by the increase in P-IRS1. Meanwhile, siRictor treatment selectively inhibited mTORC2 signaling (P-Akt S473 levels) without impacting mTOC1 signaling (P-S6, P-IRS1 levels).

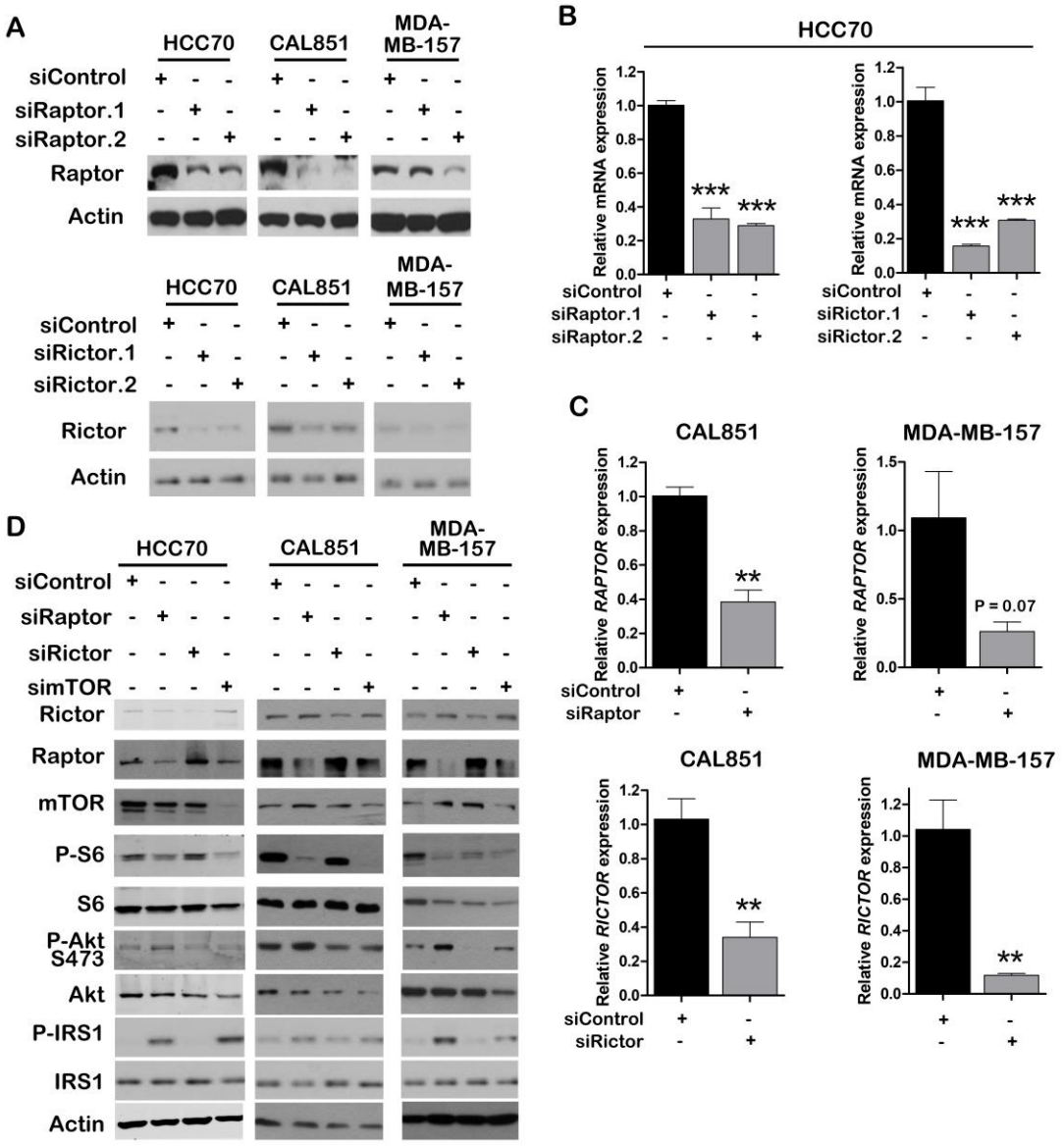

Figure 3.5: The distinct effects of selective mTORC1 vs. mTORC2 inhibition can be assessed by RNAi-mediated protein knockdown.

(A) siRNA sequences designed against RAPTOR and RICTOR were validated by western analysis and (B-C) qPRC for their ability to knockdown target genes. (D) siRictor treatment diminished mTORC2 signaling (P-AKT S473) without affecting mTORC1 signaling (P-S6).

Cell growth and cell death was also assessed following siRNA treatment. In *RICTOR*-amplified cell lines, siRictor, but not siRaptor, significantly diminished cell growth by over 40% compared to cells treated with siControl (**Figure 3.6A**). In MDA-MB-157 cells, siRaptor treatment significantly diminished cell number by approximately 20%, while siRictor treatment had no impact compared to siControl-treated cells. Analysis of caspase 3/7 activity revealed an

approximate 3-fold increase in apoptosis in *RICTOR*-amplified cell lines following siRictor treatment and an approximate 2-fold increased in MDA-MB-157 cells (**Figure 3.6B**). Caspase 3/7 activity was not elevated in siRaptor-treated cells. A lack of cell death induction following siRaptor treatment is expected, as mTORC1 signaling is associated more closely to cell proliferation while mTORC2 can regulate cell survival. Thus, while mTORC1 signaling can promote growth arrest, mTORC2 is more likely to initiate apoptosis.

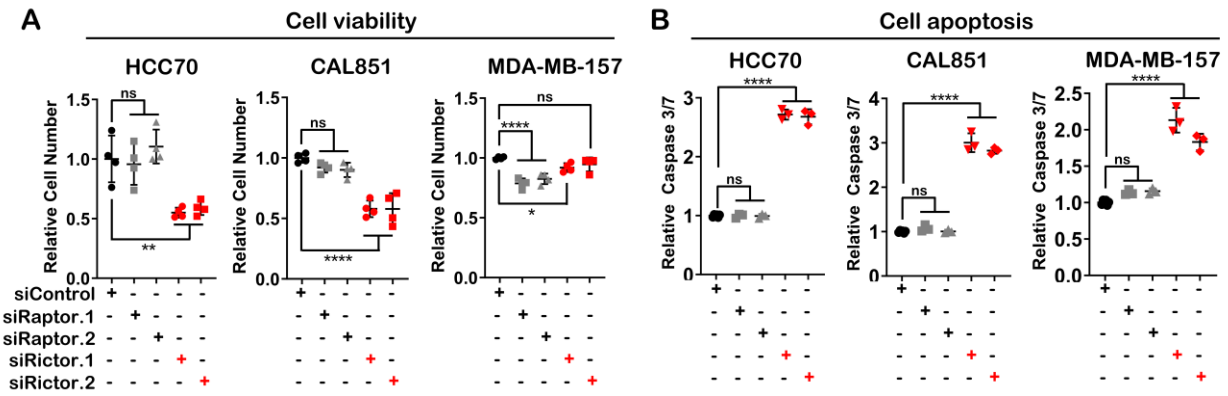

Figure 3.6: Selective mTORC2 inhibition blocks TNBC cell growth.
(A) Cell number was assessed in TNBC cells transfected with RICTOR or RAPTOR siRNA sequences, showing decreased growth in RICTOR-amplified TNBCs (HCC70 and CAL851) upon RICTOR, but not RAPTOR knockdown, and (B) Caspase 3/7 activity assessment showed increased cell apoptosis.

Silencing of *MTOR* was also assessed by simTOR treatment, which sufficiently depleted P-S6 and P-Akt S47 levels but also increased P-IRS1 expression (**Figure 3.7A-B, Figure 3.5D**). Analysis of cell viability indicated a median effect of mTOR knockdown on cell growth (**Figure 3.7C**). While CAL851 and MDA-MB-157 cells showed approximately 30% cell growth reduction, HCC70 cell growth was not inhibited. Feedback signaling from mTORC1 inhibition may explain these incomplete effects.

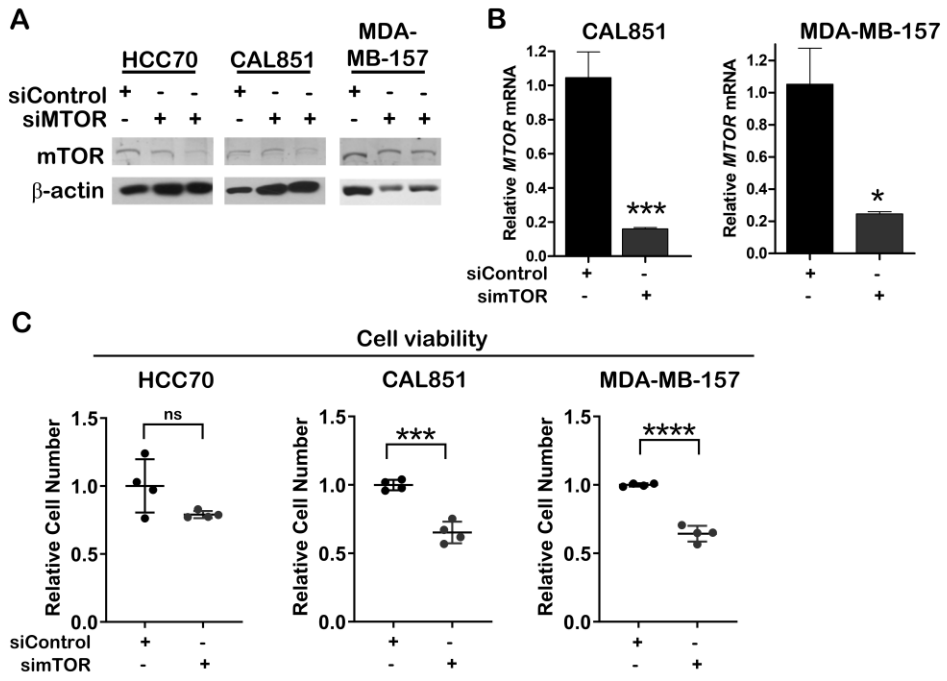

Figure 3.7: Effects of RNAi-mediated mTOR knockdown.
A) Knockdown of *MTOR* was achieved using an simTOR siRNA which was probed by western. B) qRT-PCR was performed in CAL851 and MDA-MB-157 cell lines to confirm mRNA level knockdown. siRNA was delivered at a 50 nM dose and mRNA was harvested for analysis at 48 hr following treatment. C) simTOR effect on cell growth was assessed by CellTiter Glo assay.

Transwell assays performed on HCC70 cells treated with either siRaptor or siRictor showed decreased migration of cells treated with either siRNA, though there was greater sensitivity to siRictor treatment (**Figure 3.8A-C**). Also, 3D culture assays revealed decreased colony sizes and decreased number of protrusions in siRaptor- and siRictor-treated cells compared to siControl-treated cells (**Figure 3.8D-E**). The greater sensitivity to siRictor therapy observed in *RICTOR*-amplified cell lines, compared to TNBC cells that harbor normal *RICTOR* levels, suggests that selective mTORC2 inhibition can be a promising therapeutic strategy for certain molecular subtypes of TNBC. These assays also point to an important therapeutic role for Rictor/mTORC2 in the biological processes of metastasis.

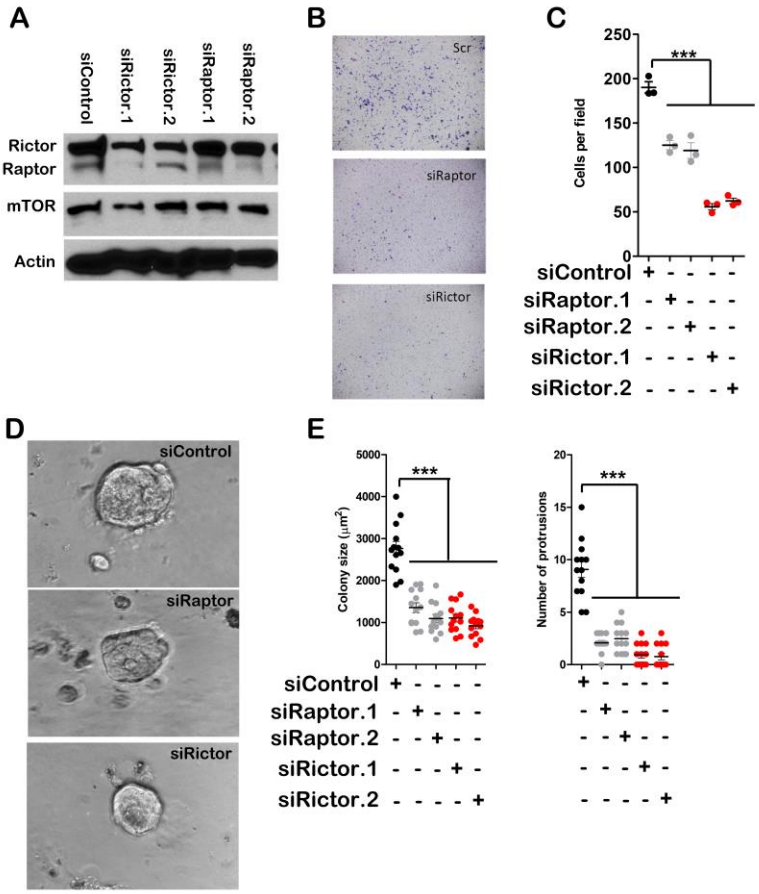

Figure 3.8: The distinct effects of selective mTORC1 vs. mTORC2 inhibition in cell migration.

(A) HCC70 cells were treated with 50 nM siRaptor or siRictor for 72 hours and (B,C) assessed for transwell migrations over the course of 5 hours. (D-E) HCC70 cells were 3D-cultured for 10 days post- siRaptor and siRictor transfection and quantified for colony size and number of protrusions.

After establishing the therapeutic potential of siRictor treatment in *RICTOR*-amplified TNBC, we assessed siRictor combination with chemotherapy. TNBC cell lines HCC70 and MDA-MB-231 were treated with paclitaxel and doxorubicin at a dose curve, and this was combined with siControl or siRictor treatment (**Figure 3.9**). Though MDA-MB-231 cells are not classically mutated for *RICTOR*, [16], multiple studies have found them to over-express Rictor protein and have shown that knockdown of Rictor suppressed tumor cell growth and motility.[112-115] In both cell lines, siRictor combination decreased cell growth and increased cell apoptosis to a greater

extent that chemotherapy alone. This data indicates that mTORC2 inhibition, via Rictor silencing, can enhance chemotherapy cell killing effect.

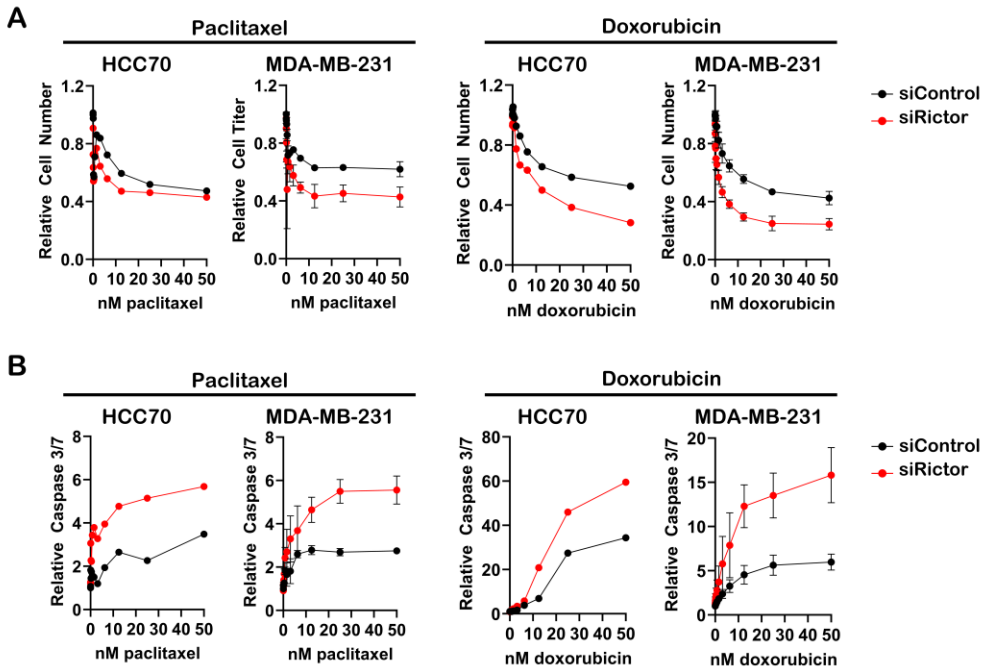

Figure 3.9: siRictor combination with chemotherapy has greater cell killing effects than chemotherapy alone.
A-B) HCC70 and MDA-MB-231 cells were treated with siControl or siRictor combined with chemotherapy and assessed for cell numbers and caspase 3/7 activity.

3.2.v. siRictor as a strategy for assessing the signaling impact of selective mTORC2 inhibition in RICTOR-amplified TNBC

PI3K resurgence upon PP242 treatment, a consequence of mTORC1 signaling inhibition, was directly assessed by ELISA measuring PI3K-mediated conversion of PI(4,5)P2 to PI(3,4,5)P3 (**Figure 3.10A**). Following PP242 treatment, PI(3,4,5)P3 levels were elevated 2.8-fold in HCC70 cells and 3.8-fold in MDA-MB-231 cells. PI(3,4,5)P3 levels remained unchanged after siRictor treatment. This is a key advantage of siRictor therapy over clinical inhibitors such as rapalogs and mTOR kinase inhibitors.

To further quantify signaling effects of siRictor treatment, we performed proteome profiling of HCC70 cells 48 hours and 7 days after siRictor treatment using an antibody array of

kinase phosphorylation (**Figure 3.10B-E**). These samples were also compared to cells 48 hours after PP242 treatment. Phospho-kinase array data largely confirmed our western blot observations. PP242 treatment robustly decreases p70 S6 phosphorylation, and by 48 hours, AKT phosphorylation at T308 is recovering in PP242-treated cells, suggesting feedback activation of PI3K/PDK1 signaling (**Figure 3.10B**). Meanwhile, p70 S6 phosphorylation remains unaffected in siRictor-treated cells, and AKT T308 phosphorylation is robustly decreased up to 7 days after siRictor treatment. Both PP242- and siRictor-treated cells display diminished phosphorylation at AKT S473. However, phosphorylation of PRAS40, a downstream effector of AKT, is not decreased in PP242-treated cells, once again suggesting a partial restoration of Akt signaling (Figure 3.10**C**). PRAS40 phosphorylation remains mitigated for up to 7 days in siRictor-treated cells.

A lack of mTORC2-selective inhibitors has made it difficult to understand the signaling effects that are induced by blockade of this pathway arm, but Rictor RNAi technologies are powerful tools that have been used to gain these insights. The role of Rictor/mTORC2 for phosphorylation of Akt at S473 to promote HER-2-amplified BC survival is well-established,[62] but mTORC2 controls many other effectors such as AGC kinase SGK, and PKC which can propagate effects to related signaling loops.[63, 106, 116] Rictor can also interact with proteins in a manner that is independent of mTORC2 activity.[117] Understanding the signaling events that follow selective mTORC2 inhibition can help identify both the advantages and possible compensatory mechanisms that may exist in this pathway. Our studies begin to probe this in *RICTOR*-amplified TNBC, which may benefit greatly from selective mTORC2 inhibition, through determination of kinase phosphorylation following siRictor treatment. For example, siRictor treatment results in a prolonged inhibition of AKT S473 phosphorylation as well as

phosphorylation of its downstream effector, PRAS40, at T246. Since Akt-mediated phosphorylation of PRAS40 at T246 permits mTORC1 activation,[118, 119] siRictor treatment effectively avoids resurgent mTORC1 activity in this manner. Another Akt target, GSK3α, was unaffected by siRictor treatment, but we did observe a transient increase in GSK3β S9 phosphorylation. Akt-S473 phosphorylation is not required for GSK3,[120] so modulation in this substrate may suggest perturbations in other arms of the PI3K/mTOR pathway following siRictor treatment.

Yet other downstream effectors of Akt and related kinases were also quantified in the phosphor-array, and this data can provide important information on compensatory pathways activated by siRictor treatment, which can inform design of subsequent combination therapies (**Figure 3.10D-E**). For example, siRictor treatment impacted kinase signaling that does not fall directly within the PI3K-mTOR-Akt signaling axis. For instance, siRictor treatment, but not PP242 treatment, increased phosphorylation of ERK at T202/Y185, a member of the mitogen-activated protein kinase (MAPK) signaling pathway that can converge on mTORC1.[121] In such a case, siRictor therapeutic efficacy may be improved by combination with MAPK inhibitors. These and other signaling events can help inform combination therapies that will cooperate with mTORC2 inhibition to combat a heterogeneous disease such as TNBC. However, additional studies are needed to rigorously assess the signaling mechanisms affected by selective mTORC2 inhibition. Together this data suggests that siRictor treatment is a promising strategy to robustly inhibit mTORC2 activity while sparing mTORC1 activity.

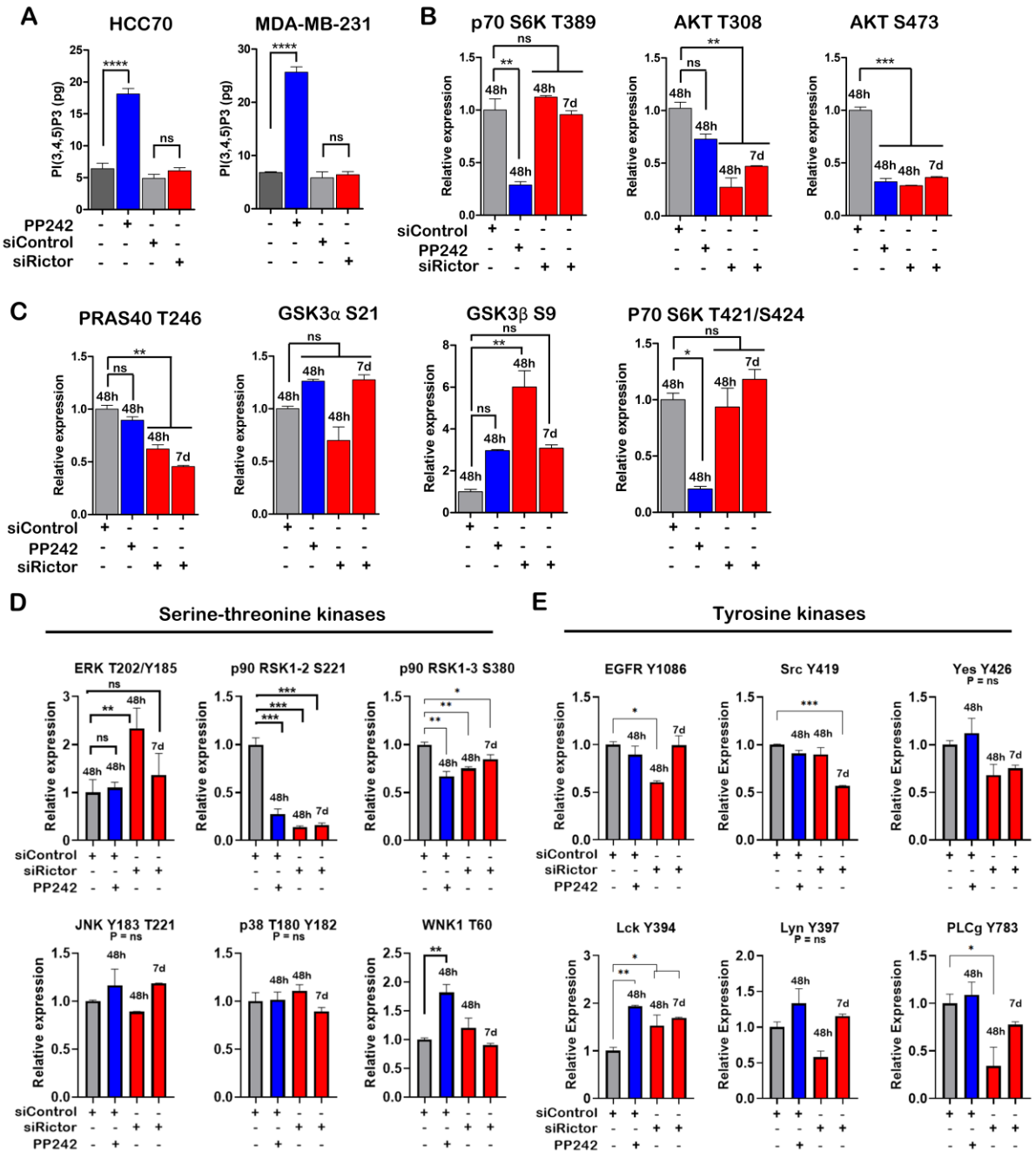

Figure 3.10: RNAi-mediated knockdown of Rictor is an approach to inhibit mTORC2 activity without effecting mTORC1 signaling.

(A) Unlike PP242, siRictor treatment does not result in resurgent PI3K signaling in TNBC cells, as assessed by PIP3 activity 48 hours after treatment. (B-D) Distinct signaling effects of siRictor treatment, compared to PP242, was assessed by kinases arrays, showing inhibition of mTORC2 signaling up to 7 days after transfection.

3.3. Conclusions

In this work, we provided evidence that therapeutic targeting of Rictor to enable selective mTORC2 inhibition can be an efficacious strategy in triple negative breast cancer. We utilized clinically relevant mTOR inhibitors capable mTORC1-selective or dual mTORC1/2 blockade to elucidate the important role of mTORC2 signaling in tumor cell survival and did so in a molecular phenotype-specific manner. Our work showed that *RICTOR*-amplified TNBCs are particularly sensitive to mTORC2 blockade, making this a viable, molecularly targeted therapy for certain subtypes of TNBC. We further validated RNAi-mediated ablation of Rictor as a selective inhibitor of mTORC2 activity that provides therapeutic benefit while also not perturbing mTORC1 signaling to induce resurgent PI3K activity. siRictor was also used here to begin studying the distinct signaling effects of mTORC2 blockade, both within the PI3K/mTOR pathway as well as parallel pathways, which can inform future drug combinations that can synergize with siRictor and serve as potent TNBC therapies.

3.4. Materials and Methods

3.4.i. Materials and reagents

Unless noted, all chemicals and materials for biological assays were purchased from Sigma-Aldrich or Fisher Scientific. A list of oligonucleotide sequences is provided in **Table 3.1**, and chemical modifications, if used, are indicated. Unmodified siRNAs were purchased from Dharmacon. siRNAs bearing modifications, including fluorophore labeling, were synthesized on a MerMade 12 Oligonucleotide Synthesizer (Bioautomation).

Table 3.1: siRNA sequences.

Oligonucleotide	Sequence (5' to 3')
Control sense	fU*mU*fC mU fC mC fG mA fA mC fG mU fG mU fC mA fC*mG*fU
Control antisense	5PHO mA*fC*mG fU mG fA mC fA mC fG mU fU mC fG mG fA mG*fA*mA
Rictor.1 sense	fG*mA*fA mG fA mU fU mU fA mU fU mG fA mG fU mC fC*mU*fA
Rictor.1 antisense	5PHO mU*fA*mG fG mA fC mU fC mA fA mU fA mA fA mU fC mU*fU*mC
Rictor.2 sense	GAC ACA AGC ACU UCG AUU AUU
Rictor.2 antisense	UAA UCG AAG UGC UUG UGU CUU
Raptor.1 sense	fU*mG*fG mC fU mA fG mU fC mU fG mU fU mU fC mG fA*mA*fA
Raptor.1 antisense	5PHO mU*fU*mU fC mG fA mA fA mC fA mG fA mC fU mA fG mC*fC*mA
Raptor.2 sense	fU*mG*fG mA fG mA fA mG fC mG fU mG fU mC fA mG fA*mU*fA
Raptor.2 antisense	5PHO mU*fA*mU fC mU fG mA fC mA fC mG fC mU fU mC fU mC*fC*mA
mTOR sense	fG*mG*fC mC fA mU fA mG fC mU fA mG fC mC fU mC fA*mU*fA
mTOR antisense	5PHO mU*fA*mU fG mA fG mG fC mU fA mG fC mU fA mU fG mG*fC*mC
Modifications: f = backbone 2'Fluoro; m = backbone 2'O-Methyl; * = phosphorothioate bond; 5PHO = 5' phosphorylation; Cy5 fluorophore tagged on 5' end of Control sense strands	

3.4.ii. Cell culture

Human triple negative breast cancer (TNBC) cell lines (HCC70, CAL851, MDA-MB-157, and MDA-MB-231) were purchased from American Tissue Type Collection and were maintained at <50 passages for all experiments. All cell lines were screened regularly for mycoplasma using the MycoAlert Mycoplasma Detection Kit (Lonza). All cells were maintained in 10% fetal bovine serum (FBS, Gibco) and 1% antibiotic-antimycotic (Anti-Anti, Gibco), using Roswell Park Memorial Institute (RPMI) media (Gibco) for HCC70, and Dulbecco's Modified Eagle Medium (DMEM) (Gibco) for CAL851, MDA-MB-157, and MDA-MB-231. All drugs, apart from siRNAs, for cell treatment were purchased from SelleckChem.

Unless otherwise indicated, adhered cells were treated with RAD001 (200 nM), PP242 (500 nM), paclitaxel (dose range from 0-500 nM), or doxorubicin (dose range from 0-5 μM) dissolved in DMSO; an equal volume of DMSO was used as an untreated control. For dose range experiments, cells were treated with a 10-point 2-fold dilution of the given drug. Where indicated, cells were reverse-transfected with 100 nM siRNA complexed with Lipofectamine RNAiMAX (Thermo Fisher Scientific) in OptiMEM media (Gibco) according to manufacturer's instructions.

3.4.iii. Quantitative reverse transcriptase polymerase chain reaction (qRT-PCR)

mRNA was isolated from cell lysates using the RNEasy Mini Kit (Qiagen) and converted to cDNA using the iScript cDNA Synthesis Kit (Bio-Rad), following manufacturer's instructions. mRNA levels were quantified using SYBR Green (Bio-Rad) based qRT-PCR, and mRNA was normalized to the housekeeping gene, GAPDH. A list of primers used is provided in **Table 3.2**.

Table 3.2: qPCR primers.

Primer	Sequence (5' to 3')
GAPDH forward	TCT TTT GCG TCG CCA GCC
GAPDH reverse	TGA CCA GGC GCC CAA TAC
RICTOR forward	GTG CCA CAT ATG GGG GTT CA
RICTOR reverse	GTT CCA GAT GGA AGA CCT CCT G
RAPTOR forward	TCG TCA AGT CCT TCA AGC AG
RAPTOR reverse	GGG TGA TTT GGG TTG ATT GC
MTOR forward	GCT GTG AGG TCT GAG TTT AAG G
MTOR reverse	ATT GCC TTC TGC CTC TTA TGG

3.4.iv. Western blotting

HCC70, CAL851, and MDA-MB-157 cells cultured in 6-well plates were lysed in ice-cold radioimmunoprecipitation assay (RIPA) buffer supplemented with protease inhibitor (cOmplete, Roche) and phosphatase inhibitor (Phos-STOP, Roche) for 15 minutes. Lysates were cleared by 13,000 xg centrifugation for 10 min at 4 °C. Protein concentration was quantified by Pierce BCA

assay (Thermo Fisher Scientific, USA). Proteins were resolved on 4-12% polyacrylamide gels (Novex, Invitrogen) and transferred to nitrocellulose membranes (iBlot2, Invitrogen). Membranes were blocked and probed with following rabbit monoclonal antibodies from Cell Signaling Technologies: Actin, Raptor, Rictor Total Akt, P-Akt S473, P-Akt T308, IRS1, P-IRS1, S6K, P-S6K, PKCα, P-PKCα, PDK1, P-PDK1. Membranes were probed with anti-Rabbit IgG IRDyes (LI-COR). Gels were imaged using the Odyssey Fc Imaging System (LI-COR).

3.4.v. Cell number and Caspase 3/7 activity

HCC70, CAL851, and MDA-MB-157 cells seeded in opaque 96-well plates were treated with RAD001 or PP242 in the presence or absence of paclitaxel or doxorubicin chemotherapies. Cells were reverse-transfect with siControl, siRaptor, or siRictor siRNAs, with transfection media replaced after 24 hours. Caspase 3/7 activity was assessed at 48 hours by Caspase 3/7 Glo assay (Promega). Cell number was assessed at 72 hours by CellTiter Glo assay (Promega). Luminescence for each assay was measured on a Tecan Infinite F500 plate reader. Data was normalized to the average value of untreated control wells.

3.4.vi. Kinase array assays and measurement of phosphatidyl inositol (3,4,5) phosphate [PI(3,4,5)P3]

HCC70 and MDA-MB-231 cells were transfected in OptiMEM with siControl and siRictor sequences, replacing transfection media with OptiMEM 16 hours after transfection. Adhered cells were treated with 500 nM PP242. At 48 hours after treatment, cell lysates were collected in NP-40 lysis buffer supplemented with EDTA-free protease inhibitor cocktail (Roche) and PhosSTOP (Roche), cleared by centrifugation at 14,000 xg for 10 minutes at 4 °C, and assessed for protein concentration using Pierce BCA assay (Thermo Fisher). Lysates were used as directed in PI3-Kinase Activity ELISA: Pico kit (Echelon Biosciences, Inc.), which measures the PI3K-mediated

conversion of PI(4,5)P2 to PI(3,4,5)P3. Kinase reactions were supplemented with 2mM dithiothreitol (DTT) and 100 uM ATP and incubated at 37 °C for 6 hours prior to use in ELISA. Absorbance of ELISA reactions were measured at 450 nm on the plate reader (Tecan Infinite F500). PI(3,4,5)P3 values for each kinase reaction were calculated against a PI(3,4,5)P3 standard curve. Lysates were used as directed in the R&D Systems Proteome Profiler Human Phospho-Kinase Array.

3.4.vii. Human breast cancer dataset analysis

Clinical breast cancer datasets curated by The Cancer Genome Atlas (TCGA) [122] and METABRIC [123, 124] were queried for tumors harboring RICTOR gene amplification or RICTOR mRNA overexpression (defined as >2 SD above the mean RICTOR levels across the entire dataset), collectively defined herein as RICTOR alterations. Kaplan-Meier survival curves were generated using cBio software, [125] comparing overall survival of patients whose tumors harbor RICTOR alterations versus those without RICTOR alterations.

Cell lines curated by the Cancer Cell Line Encyclopedia [126] were queried for triple negative breast cancer characterization (defined as lacking ESR1, PGR, and ERBB2) as assessed by cBioPortal software. Corresponding genomic copy number data was analyzed for cell lines harboring *RICTOR* versus *RAPTOR* gene amplification.

Chapter 4: In vivo therapeutic efficacy of siRictor-NPs in triple negative breast cancer

4.1.Introduction

Beyond some molecularly targeted strategies, such as immunotherapies that are available for subsets of advanced-TNBC patients, NAC followed by tumor resection continues to be the standard of care for early, pre-metastatic TNBC cases. Upregulation of mTORC2 may be driving chemoresistance in these tumors, suggesting that combination of mTORC2 inhibition with chemotherapy may improve TNBC tumor cell killing. Beyond the pro-tumor roles regulated by mTORC2 signaling, Rictor itself has been implicated in breast cancer progression. Immunohistochemical (IHC) staining of clinical invasive breast carcinomas for Rictor found that Rictor staining intensity correlated with increased tumor grade; *RICTOR* gene alterations in invasive breast carcinomas patients also correlated with decreased overall survival.[62] Furthermore, investigators have shown that blocking mTORC2 signaling, through Rictor ablation, can inhibit mTORC2/Akt-dependent tumor cell survival and metastasis in *in vivo* tumor models.[62, 106] RNAi nanoparticles have furthermore been used to silence Rictor in HER2-amplified breast tumor models, which decreased Akt phosphorylation and decreased tumor growth, and this effect was enhanced when the nanoparticles were combined with the HER2 inhibitor, lapatinib.[17] These previous studies establish selective mTORC2 targeting, particularly through Rictor ablation, as an efficacious strategy for BC, but its effects in the TNBC setting continue to be understudied.

Using our si-NPs optimized for *in vivo* tumor gene silencing in Aim 1, here was assess the performance of siRictor-NPs as a therapy alone and in combination with paclitaxel. While other work in this field has utilized genetic ablation of Rictor to provide fundamental understanding of its potential therapeutic benefits, here we show that delivery of Rictor-targeting si-NPs (siRictor-

NPs) to an existing, actively growing TNBC tumor can potently inhibit mTORC2 activity and block tumor growth. Finally, we provide evidence that combining siRictor-NPs with chemotherapies can provoke an enhanced antitumor effect against TNBCs. Overall, work in this Aim identifies a nanotechnology that can enable RNAi delivery to the tumor and provide therapeutic benefit to PI3K-active TNBC.

4.2.Results and Discussion

4.2.i. Intravenously administered ternary siRNA nanoparticles provide siRNA delivery to the tumor

To achieve *in vivo RICTOR* silencing in the tumor, we utilized the 50B-DP100 siRNA-carrying ternary nanoparticle (si-NP) that we optimized for safe and potent systemic siRNA delivery in Aim 1.[127] si-NPs were first formulated with siRNA tagged with fluorescent tetramethylrhodamine (TAMRA), and siRNA uptake was confirmed in HCC70 cells *in vitro* by flow cytometry, which increased over the 24 hour treatment time (**Figure 4.1A**). More importantly, we wanted to assess si-NP biodistribution and tumor delivery in a tumor-bearing mouse. si-NPs were formulated with Cy5-tagged siRNA and 1 mg/kg were intravenously injected into mice bearing 100-200 mm^3 HCC70 tumors (**Figure 4.1B**). At 24 hr after injection, organs and tumor were harvested for biodistribution analysis (**Figure 4.1C**). The greatest siRNA accumulation was observed in the liver (36%), followed by the kidney (30%) and tumor (16%). This is a significant improvement to previous ternary si-NP formulations, where a majority of siRNA accumulation was found in the kidney[37], indicating a destabilized si-NP that is resulting in the excretion of free siRNA into the urine. HCC70 tumors were then digested to a single cell suspension and quantified for Cy5 si-NP uptake against vehicle treated tumors by flow cytometry (**Figure 4.1D-E**). Over 35% of the tumor cells were positive for Cy5 signal following this single si-NP treatment,

and Cy5 si-NP treated tumors had >2.5-fold increase in Cy5 mean fluorescent intensity (MFI) compared to vehicle treated tumors. A portion of the tumors were also prepared for cryo-histology and imaged by confocal microscopy to visualize Cy5 signal and confirm Cy5 si-NP accumulation in the tumor (**Figure 4.1F**). Cryo-histology revealed pockets of high accumulation around the tumor area, perhaps suggesting that the si-NPs may act as a depot that allows for siRNA uptake over an extended period.

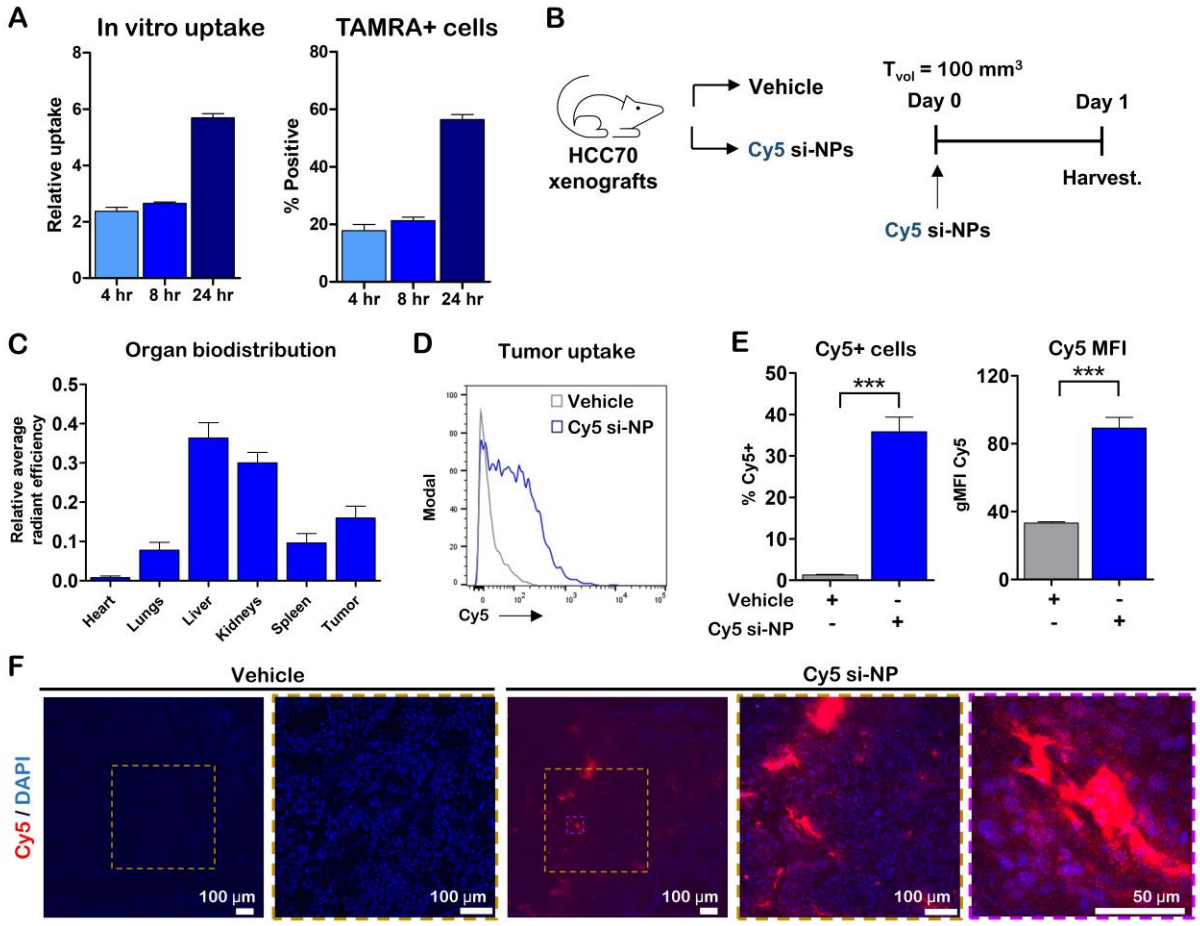

Figure 4.1: Ternary si-NP carrier technology enables siRNA delivery to the tumor.
(A) si-NP uptake was quantified in HCC70 cells over time by flow cytometric detection of the fluorescent TAMRA-tagged siRNA. (B) si-NPs containing Cy5-labeled siRNA were used to assess organ (C) biodistribution in HCC70 tumor-bearing mice and (D-E) tumor uptake was quantified by flow cytometry. (F) Confocal microscopy was used to visualize Cy5 fluorescence within tumor sections.

4.2.ii. siRictor-NP selectively inhibits mTORC2 activity and provides therapeutic benefit when intravenously administered to triple negative breast cancer xenografts

After confirming siRNA delivery to the tumor with our ternary carrier, we loaded si-NPs with siRNA targeting *RICTOR* (siRictor-NPs) and assessed the therapeutic implications of selective mTORC2 targeting in TNBC. Silencing activity of siRictor-NPs in TNBC cell lines was first confirmed by western blot probed for Rictor (**Figure 4.2A**), and diminished Akt phosphorylation at S473 was also verified following siRictor-NP treatment. TNBC cell lines were treated with siRictor-NPs and cell viability was compared against siControl-NPs at 2-days and 7-days following treatment. In *RICTOR*-amplified cell lines, HCC70 and CAL851, siRictor-NP treatment decreased cell growth 2 days post treatment, and this effect was enhanced 7 days post treatment where cell numbers in both lines were diminished by approximately 40% relative to siControl-NPs (**Figure 4.2B**). siRictor-NP treatment did not impact MDA-MB-157 cell growth at either timepoint but, interestingly, reduced MBA-MB-231 cell numbers following 7 days of treatment. Though MDA-MB-231 cells are not classically mutated for *RICTOR*,[16] multiple studies have found them to over-express Rictor protein and have shown that knockdown of Rictor suppressed tumor cell growth and motility.[112-115] HCC70 and MDA-MB-231 cells were furthermore treated with a dose curve of siRictor-NPs, and siRictor-NPs inhibited cell growth in both cell lines with increasing si-NP dose (**Figure 4.2C**). *RICTOR*-amplified HCC70 cells were, in particular, robustly inhibited with increasing siRictor-NP dose, with approximately 60% cell number inhibition at 200 nM siRictor-NP treatment relative to siControl-NP treatment. PI3K activity was once again quantified by ELISA measuring PI3K-mediated conversion of PI(4,5)P2 to PI(3,4,5)P3, and PP242, but not siRictor-NPs, increased PI(3,4,5)P3 at 72 hours post treatment (**Figure 4.2D**). Together, these data confirm that Rictor siRNA, when loaded into our ternary si-

NPs, potentiate mTORC2 signaling inhibition and confer long-lasting therapeutic effects in *RICTOR*-amplified TNBC cell lines.

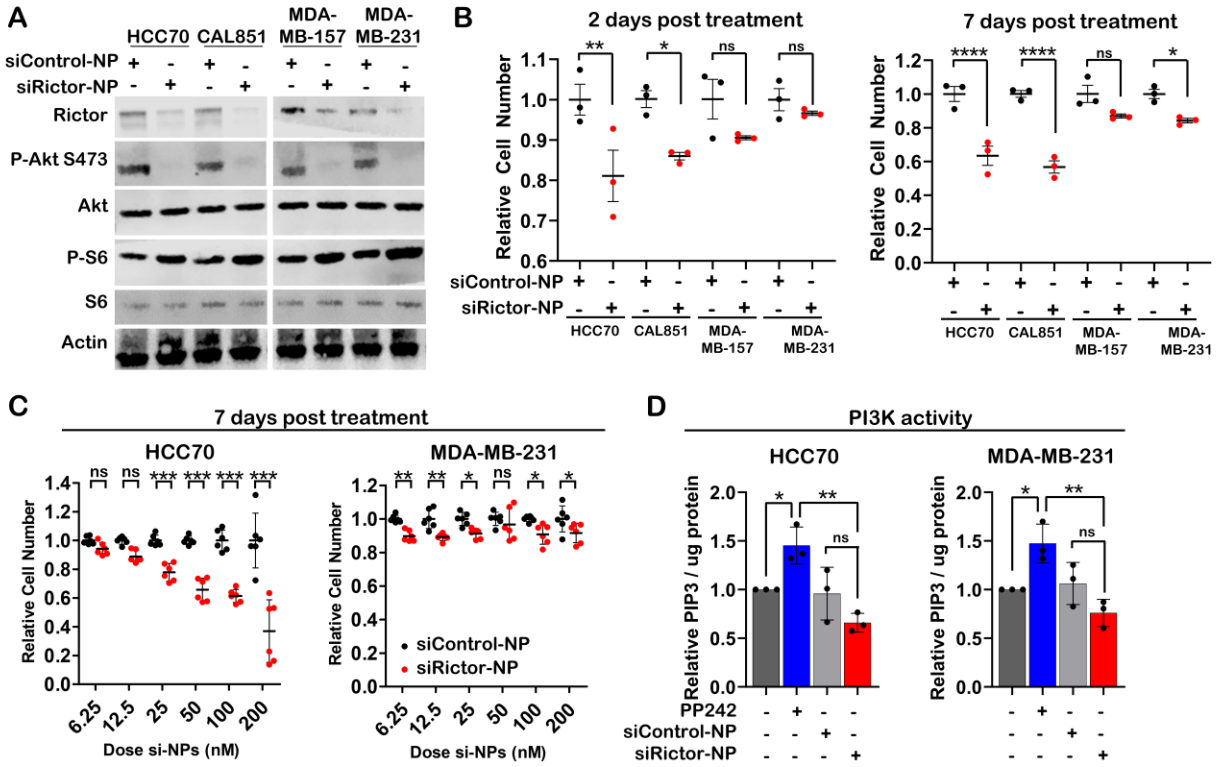

Figure 4.2: Ternary si-NPs harboring siRictor confer therapeutic benefit particularly to *RICTOR*-amplified TNBC.
(A) si-NPs loaded with siRictor (siRictor-NPs) were confirmed for Rictor silencing and mTORC2 inhibition in multiple TNBC cell lines. (B-C) siRictor-NPs inhibit TNBC cell growth up to 7 days following treatment. (D) siRictor-NP treatment does not result in resurgent PI3K signaling in TNBC cells, as assessed by PIP3 activity 72 hours after treatment.

Using our siRictor-NPs, which are optimized for *in vivo* tumor siRNA delivery, we next wanted to assess the therapeutic effects of mTORC2 inhibition in an established TNBC tumor. We generated orthotopic mammary tumors using HCC70 cells, and, once tumors reach 100 mm^3 (Day 0), intravenously treated mice with either 1 mg/kg siControl-NPs or siRictor-NPs on Days 0, 2, and 5 (**Figure 4.3A-B**). Tumors were harvested on Day 7, 48 hours after the final si-NP treatment, for analysis. Rictor silencing in treated tumors was confirmed by western blot analysis, which also showed a substantial diminishment in Akt phosphorylation at S473 (**Figure 4.3C**). Following confirmation of mTORC2 activity inhibition in siRictor-NP treated tumors, siControl-NP and

siRictor-NP treated tumors were assessed for proliferation and cell death by immunohistochemical analysis of Ki67 and cleaved caspase-3, respectively (**Figure 4.3C-D**). IHC revealed reduced cell proliferation in siRictor-NP treated tumors, and a >4-fold induction of caspase-3 cleavage compared to siControl-NP treated tumors. This result correlated with the increased relative necrotic area quantified in scanned H&E of siRictor-NP treated tumors, compared to siControl-NP treated tumors (**Figure 4.3E**).

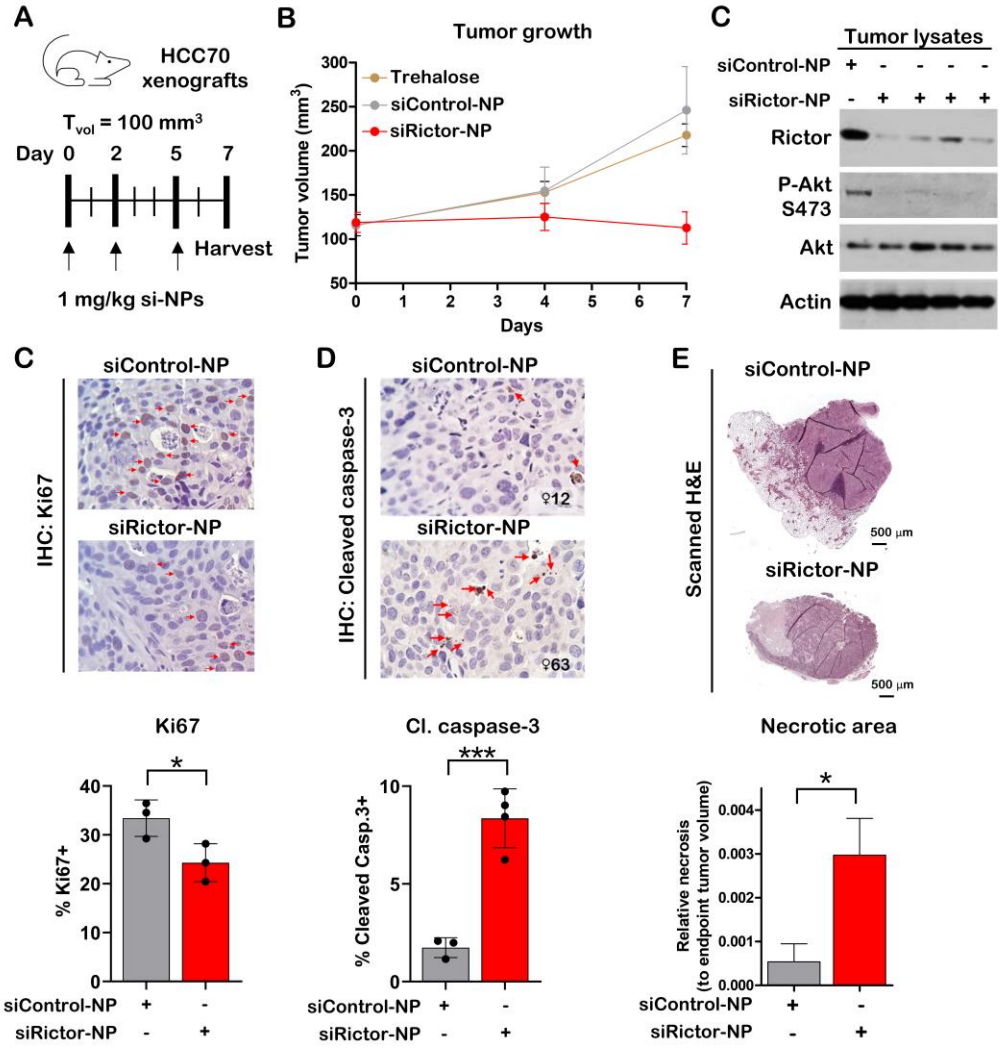

Figure 4.3: Ternary si-NP mediated delivery of siRictor siRNA to the tumor provides therapeutic efficacy.

(A-B) HCC70 tumor-bearing mice (N = 4-5) were i.v. treated with siRictor-NPs on Days 0, 2, and 5 and tumors were harvested for molecular analysis on Day 7. (C) Tumors were confirmed for Rictor knockdown by western analysis. (C) Tumors were assessed by IHC for Ki67 and (D) cleaved caspase-3 induction. (E) Regions of acellularity in tumor H&E staining were quantified as a measure tumor necrosis.

We also confirmed the safety of our si-NPs following multi-dose treatment in a tumor-bearing mouse model. Mouse plasma was also collected during the Day 7 harvest and assessed for elevations in kidney (blood urea nitrogen, BUN) and liver (alanine aminotransferase, ALT; aspartate aminotransferase, AST) which remained at basal levels in si-NP treated mice and also did not exhibit modulations in glucose levels (**Figure 4.4**). This collective data indicates that siRictor-NPs support the delivery of active Rictor siRNA to the tumor and, upon mTORC2 activity inhibition, provide therapeutically beneficial effects such as induction of cell death.

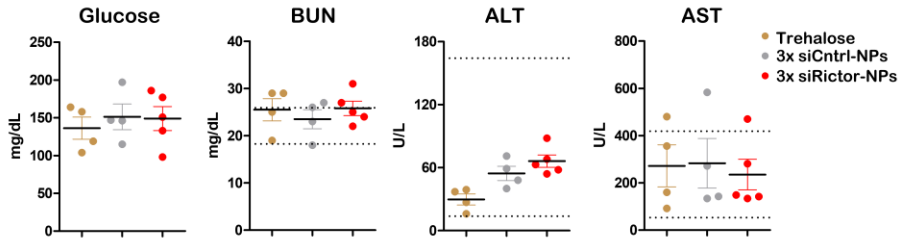

Figure 4.4: siRictor-NPs are safe upon systemic administration to tumor-bearing mice.
Mouse plasma collected on Day 7 was assessed for changes in glucose levels following si-NP treatment, as well as elevation in kidney and liver damage markers.

*4.2.iii.*siRictor-NP combination with paclitaxel inhibits tumor growth beyond paclitaxel alone in xenografts

After establishing the therapeutic potential of *in vivo* Rictor targeting using our siRictor-NPs, we next assessed the utility of combining siRictor-NP therapy with chemotherapy. Neoadjuvant chemotherapy has remained a standard of care for TNBC patients, for a lack of more targeted therapies approved at the early tumor stage. We therefore sought to combine our siRictor-NP therapy with paclitaxel with the motivation that blockade of mTORC2 signaling in TNBC tumors may potentiate chemotherapy-mediated tumor cell killing. HCC70 cells were treated with a dose curve of doxorubicin and paclitaxel which was combined with siControl-NP or siRictor-NP (**Figure 4.5A-B**). Combination with siRictor-NP decreased cell number and increased cell apoptosis to a greater extent than chemotherapy alone. This coincided with combination studies

performed with inhibitors RAD001 and PP242, where PP242 combination with doxorubicin and paclitaxel chemotherapies decreased cell numbers in *RICTOR*-amplified cell lines beyond the chemotherapies alone or chemotherapy combined with RAD001 (**Figure 3.4**).

To ascertain the long-term therapeutic effects of siRictor-NP treatment in *RICTOR*-amplified TNBC *in vivo*, we generated orthotopic mammary tumor xenografts using HCC70 cells. Once tumors reached 100 mm^3 (Day 0), mice were treated with 1 mg/kg i.v. siControl- or siRictor-NPs on Days 0, 3, and 7 and then weekly thereafter (**Figure 4.5C**). si-NP therapy was combined with paclitaxel or vehicle treatment, which was given as a 12 mg/kg dose intraperitoneally twice weekly starting on Days 2 and 5. Tumor growth was monitored through Day 52, and siRictor-NP treatment inhibited tumor growth to 57% compared to control tumors (**Figure 4.5D-E**). Paclitaxel monotherapy minimally inhibited growth to 70% relative to the control group. This limited response is perhaps expected, as next-generation sequencing of residual TNBC patient tumors point to a correlation between PI3K pathway mutations and chemoresistance. However, paclitaxel combination with siRictor-NP strongly inhibited tumor growth to 44% relative to control tumors. Chemo-response was further interrogated through Kaplan-Meier analysis defining survival as tumor volume under 500 mm^3 (**Figure 4.5F**). Paclitaxel monotherapy inhibited growth in 5/11 mice while paclitaxel combination with siRictor-NPs inhibited growth in 7/8 mice. Body weight monitored throughout the study indicate that chemotherapy and si-NP treatments did not result in significant toxicities (**Figure 4.5G**). Together, these data indicate that siRictor-NP therapy confers greater chemosensitivity to *RICTOR*-amplified TNBC, making it a promising cooperative therapy for TNBC patients.

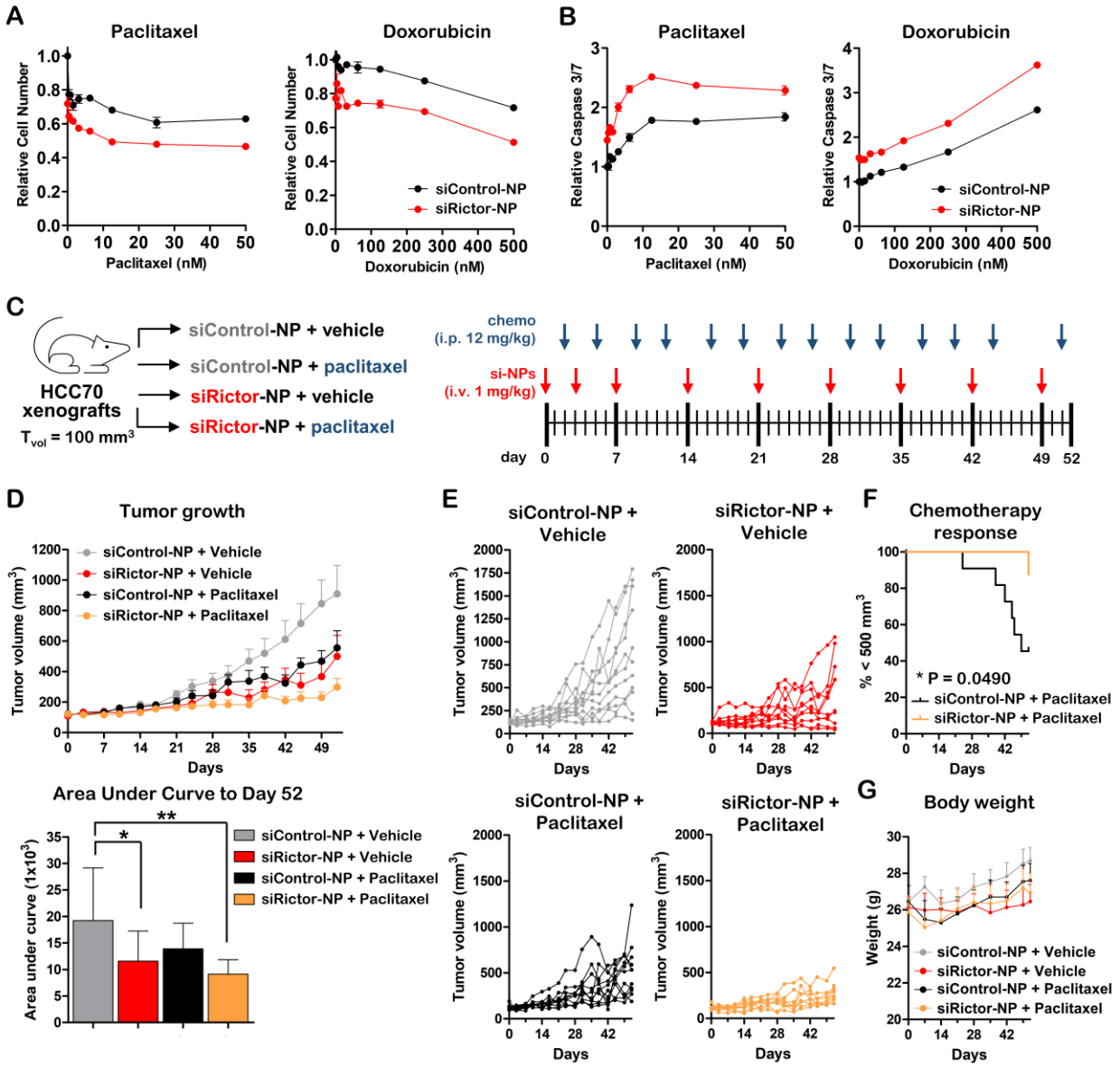

Figure 4.5: Rictor silencing combined with chemotherapy diminishes tumor cell survival and tumor growth.

(A) siRictor-NP combination with paclitaxel and doxorubicin inhibits TNBC cell growth and (B) increases cell apoptosis compared to chemotherapy alone. (C) HCC70 tumor-bearing mice were treated i.v. with siControl- or siRictor-NPs and i.p. with vehicle or paclitaxel to assess the therapeutic efficacy of combination chemotherapy in TNBC (N = 8-11 per group). (D-E) Tumor growth was monitored with through Day 52 and (F) siRictor-NP combination with paclitaxel diminished tumor growth beyond paclitaxel when given alone. (G) Body weight was monitored as a measure of toxicity.

4.3.Conclusions

In this work, we provide evidence of the efficacy of our ternary si-NP developed in Aim 1 when it is directed to deliver siRictor for the therapeutic inhibition of mTORC2 activity in TNBC. When

administered intravenously, our si-NPs deliver efficacious levels of siRNA to TNBC tumor models, and this delivery converts to robust Rictor and P-Akt S472 inhibition within the tumor. siRictor-NP mediated mTORC2 blockade correlated with decreased tumor cell proliferation and significant induction of cell apoptosis. These promising results with siRictor-NP monotherapy warranted longer-term efficacy studies where this nanomedicine was combined with chemotherapy. We demonstrate that siRictor-NP not only inhibits TNBC tumor growth as a sole therapy but also cooperates with paclitaxel to block growth to a greater extent than either agent alone. Collectively, these findings identify an siRictor nanomedicine that confers therapeutic benefit to *RICTOR*-amplified TNBC and potentiates chemotherapy cell killing.

4.4. Materials and Methods

4.4.i. Materials

Unless noted, all chemicals and materials for biological assays were purchased from Sigma-Aldrich or Fisher Scientific. A list of oligonucleotide sequences is provided in **Table 3.1**, and chemical modifications, if used, are indicated. siRNAs bearing modifications, including fluorophore labeling, were synthesized on a MerMade 12 Oligonucleotide Synthesizer (Bioautomation). Polymer synthesis and si-NP formulation was performed as previously published and described in Aim 1 (Chapter 2).[127]

4.4.ii. Cell culture and cell-based assays

Cell-based assays were performed similarly to methods described in Aim 2 (Chapter 3) Materials and Methods section. For brevity, only adjustments made for si-NP treatment are described below. Unless otherwise indicated, adhered cells were treated with 100 nM si-NPs in OptiMEM, and media was replenished after 24 hr.

Cell number and Caspase 3/7 activity: Seeded cells were treated with siControl- or siRictor-NPs. Cell number was assessed at 2 or 7 days after treatment. For chemotherapy

combination studies, cells were treated with 100 nM si-NPs and then treated with chemotherapy 24 hours later. CellTiter Glo (Promego) was assessed 2 days after chemotherapy treatment and Caspase Glo (Promega) was assessed 1 day after chemotherapy treatment. Luminescence for each assay was measured on a Tecan Infinite F500 plate reader. Data was normalized to the average value of wells treated with siControl-NPs.

PI3K activity measurement of phosphatidyl inositol (3,4,5) phosphate [PI(3,4,5)P3]: For siRictor-NP experiments, adhered cells were treated with either 100 nM si-NPs or 250 nM PP242, and lysates were collected at 72 hours. Lysates were used as directed in PI3-Kinase Activity ELISA: Pico kit (Echelon Biosciences, Inc.), which measures the PI3K-mediated conversion of PI(4,5)P2 to PI(3,4,5)P3.

4.4.iii. Flow cytometry, organ biodistribution, and fluorescence imaging for si-NP uptake into TNBC xenografts

Athymic nude Balb/C mice (4-6 weeks, Envigo) will be injected with 1e6 HCC70 cells in 100 µL Matrigel (Corning) in the inguinal mammary fat pad. Once tumors reached 100 mm^3, mice were i.v. injected with either a 300 mM trehalose vehicle control or 1 mg/kg si-NPs harboring Cy5-tagged siRNAs. Organs and tumors were harvested 24 hours after treatment to assess Cy5-NP distribution and uptake. Organs were imaged for Cy5 fluorescence on an IVIS System (Caliper Life Sciences) and baseline autofluorescence of each organ was normalized to vehicle treated organs.

To assess Cy5-NP tumor uptake, tumors were digested using a Mouse Tumor Dissociation Kit (Miltenyi Biotec) following manufacturer's instructions. Following digestion, cells were strained through a 70 µm filter, and red blood cells were lysed for 2 minutes at room temperature using ACK Lysis solution (Gibco). Cells were then resuspended in fluorescence-activated cell

sorting (FACS) buffer (PBS containing 1% FBS and 2 mM EDTA) to a concentration of 5e6 cells per mL. 1e6 cells were incubated with 4′,6-diamidino-2-phenylindole (DAPI) and analyzed on a Guava easyCyte HT flow cytometer (Luminex). Flow cytometry data was analyzed on FlowJo software, where Cy5 uptake was quantified against vehicle treated tumors.

To visualize Cy5 signal within the tumor, tumor samples were snap frozen in OCT embedding medium. Cryosections were stained with DAPI and imaged on a Nikon Eclipse Ti inverted confocal microscope.

4.4.iv. siRictor-NP monotherapy or combination chemotherapy in TNBC xenografts

Athymic nude mice (4-6 weeks, Envigo) were injected with 1e6 HCC70 cells in 100 µL Matrigel in their inguinal mammary fat pad. Once tumors reach 100 mm^3 (Day 0), mice were randomized into treatment groups: siControl-NPs+vehicle, siRictor-NPs+vehicle, siControl-NPs+paclitaxel, and siRictor-NPs+paclitaxel. Mice were treated i.v. with 1 mg/kg si-NPs thrice in the first week (Days 0, 3, and 7) and weekly thereafter. Mice were treated i.p. with 12 mg/kg paclitaxel twice a week, starting on Days 2 and 5. Tumor volume was monitored using digital caliper measurements (T_{vol} = length x $width^2/2$). Tumors were harvested at study endpoint for molecular analysis.

4.4.v. Histological analysis

Tumors were harvested and fixed in 10% neutral-buffered formalin. Tissue processing and embedding was performed by the Vanderbilt Translation Pathology Shared Resource. Paraffin sections were stained with hematoxylin and eosin for relative necrotic area analysis. Immunohistochemistry was performed using Ki67 (Abcam) and cleaved caspase-3 (Cell Signaling Technologies) antibodies, and the average percentage of Ki67 or cleaved caspase-3 stain positive tumor cells was quantified for each tumor using 3-4 representative fields per tumor.

Chapter 5: Conclusion

5.1. Chapter summaries and impact

In the first aim of this dissertation (Chapter 2), our overall objective was to develop an siRNA carrier that can promote robust siRNA accumulation and target gene silencing to the tumor following a systemic injection. Polymeric, electrostatically complexes siRNA nanoparticles (si-NPs) have been developed previously in our lab that enable robust siRNA cargo loading and actively promote endosome escape through incorporation of a core-forming 50:50 poly(DMAEMA-coBMA) (50B) polymer block.[37-39, 44, 45, 77] However, incorporation of cationic polymers that also induce endosome disruption for intracellular delivery can result in *in vivo* dose-limiting toxicities.[33] Here, we systematically screened a library of ternary si-NPs that contained the 50B polymer at varying molecular weights and ratios to identify an optimal si-NP that was both stable and active but also non-toxic, in the *in vivo* setting. Importantly, our si-NP library screening revealed important structure-function relationships regarding endosome-disruptive polymers such as 50B, and this can inform future nanomedicine design. Specifically, we show that increasing the molecular weight of cationic/endosome-disruptive polymers can increase toxicity both *in vitro* and *in vivo*. si-NP gene silencing activity also increases with molecular weight, but this effect does plateau at a certain molecular weight. Furthermore, in a ternary si-NP carrier, the ratio of core-forming polymer requires a balance between ample surface-forming polymer coverage to enhance pharmacokinetics that also does not impede si-NP cellular uptake and consequent gene silencing. These insights into si-NP carrier design are important for the continued development of systemically administered nanomedicines that target extra-hepatic tissues, such as the tumor.

The second aim of this dissertation (Chapter 3) is strongly focused on dissecting the signaling and therapeutic effects of selective mTORC2 targeting in triple negative breast cancer (TNBC) and how this targeting strategy may compare to clinically available inhibitors that also block mTOR. Because TNBC is a heterogenous disease, we assessed therapeutic mTORC2 targeting in the context of molecular phenotypes that displayed PI3K-activating mutations. We used small molecular inhibitors, RAD001 and PP242, to show that PI3K-active TNBC phenotypes are particularly sensitive to mTORC2 blockade. Though studies utilizing genetically-engineered models that deplete mTORC2 activity show that mTORC2 plays an important role in BC, small molecule inhibitors that selectively inhibit mTORC2 do not exist. This has made it difficult to study the therapeutic effects of selective mTORC2 inhibition in a clinically relevant setting where this signaling node is targeted in an actively growing tumor. Here, we used siRNA-mediated *RICTOR* ablation to study the therapeutic utility of mTORC2 blockade in TNBC. Importantly, *RICTOR* silencing inhibits mTORC2 activity in a manner that does not perturb mTORC1 signaling, a major downfall of mTORC1 inhibitors that induce resurgent PI3K signaling through release of an IRS-1-mediated feedback loop downstream of mTORC1.[50] *RICTOR* silencing furthermore induces robust tumor cell apoptosis, an effect that is particularly enhanced in PI3K-active TNBC models and cooperates with chemotherapy-based cell killing, which is the clinical standard-of-care for TNBCs. Altogether, the work in this aim provides strong evidence for selective mTORC2 inhibition, through Rictor ablation, as a promising treatment strategy for TNBC, a disease which suffers from a lack of molecularly targeted therapies.

In the third aim of this work (Chapter 4), we assessed the therapeutic utility of our optimized si-NP system in targeting *RICTOR* for selective mTORC2 inhibition in TNBC. Previous attempts to target mTOR signaling, using drugs such as Everolimus/RAD001, have not shown

clinical efficacy in TNBC, even when combined with standard-of-care chemotherapy.[11-13] Here, we demonstrate that our systemically-administered si-NPs harboring siRNA targeting *RICTOR* (siRictor-NPs) deliver efficacious levels of siRNA to the tumor and robustly inhibit mTORC2 activity in orthotopic TNBC xenografts. Therapeutic mTORC2 blockade results in reduced tumor cell proliferation and a prominent increase in tumor cell apoptosis, indicating that mTORC2 targeting is a promising strategy to extinguish TNBC cell survival. Furthermore, combination of our siRictor-NPs with paclitaxel induced chemosensitivity in TNBC xenografts. While longer-term treatment of siRictor-NPs or paclitaxel monotherapies resulted in notable tumor growth inhibition, combination treatment resulted in a greater response than what was achieved by either therapy alone. Thus, the work in this aim identifies a translational RNAi nanomedicine for delivery and treatment of PI3K-active TNBC which also cooperates with chemotherapy.

Overall, this work elucidates important structure-function relationships for the design of safe and efficacious tumor-tropic si-NPs. Interrogation of the effect of core-forming polymer content on *in vivo* si-NP performance resulted in the discovery of an optimized si-NP that induces maximal tumor gene silencing while also being well-tolerated in a multi-treatment setting. This work additionally interrogates the therapeutic implications of selective mTORC2 inhibition in TNBC and its promising efficacy in treating PI3K-active TNBC. Ultimately, we demonstrate the therapeutically beneficial effects of *RICTOR* targeting in TNBC, which were achieved using our optimized si-NP carrier.

5.2. Shortcomings

Throughout this work, we have used a standard 1 mg/kg intravenous dose for *in vivo* treatment with our si-NP. Early generation siRictor-NPs developed in our lab have shown success in decreasing Rictor and P-Akt expression, reducing tumor volume, and increasing tumor cell

death in TNBC MDA-MB-231 xenografts using this 1 mg/kg dose.[17] In the work presented here, a single 1 mg/kg dose resulted in potent 80% knockdown of Rictor protein in orthotopic MDA-MB-231 xenografts[127] and mediated tumor growth inhibition in *RICTOR*-amplified HCC70 xenografts, suggesting that this dosing level is sufficient for our leading siRictor-NP formulation to bestow therapeutic efficacy. However, our therapeutic studies utilize frequent si-NP dosing (up to thrice in one week), and there is a strong possibility that higher siRictor-NP doses could drive greater therapeutic outcomes. Others have shown that increasing nanoparticle dose can drive tumor delivery, in part through saturation of clearance organs.[128, 129] However, other work interrogating si-NP dose-dependent effects on tumor growth found that increasing siRNA dose did not significantly impact growth inhibition.[130] Overall, the dose-dependency effects of si-NP tissue biodistribution are not yet well-understood.

Dose-escalation studies are furthermore essential to understanding the dose-limiting toxicities of our optimized si-NPs. Our si-NPs incorporate the cationic and endosome-disruptive polymer, 50B, which potentiates gene silencing activity but also inevitably correlates with toxicity. We have previously shown that the maximum tolerated dose of si-NPs can be improved through prophylactic treatment with the platelet-activating factor receptor (PAFR) inhibitor, ABT-491.[33] While we may be able to mitigate carrier-related toxicities through ABT-491 pre-treatment, we first need to ascertain the upper-limit of our therapeutic window to then design treatment regimes that balance si-NP dose and dosing frequency.

Furthermore, tumor delivery of our si-NPs relies on the enhanced permeation and retention (EPR) effect that is often associated with actively growing tumors.[25, 26, 131] However, emerging studies indicate that the heterogeneous nature of tumors, particularly in human patients, would not necessarily abide by this paradigm, therefore potentially limiting efficacious and

uniform delivery of our si-NPs.[132] Addition of tumor-targeting moieties onto our si-NPs may therefore promote greater on-target cellular uptake, though they would not necessarily enhance tumor tropism following an intravenous si-NP injection.

Despite the important advancements made by this work on understanding the therapeutic effects of selective mTORC2 inhibition in TNBC, we continue to have a preliminary understanding of the global signaling effects that may result from mTORC2 blockade. We importantly show in this work that *RICTOR* targeting achieves mTORC2 inhibition in a manner that spares mTORC1 signaling. However, TNBCs, and many other cancers, are prone to resistance mechanisms which may be embedded in unidentified feedback loops that could exist in the PI3K/mTOR/Akt signaling axis. Dual-targeting strategies are likely necessary to improve therapeutic efficacy against TNBC; one such option could be the dual inhibition of Rictor and IRS-1 through co-loading si-NPs, to further limit PI3K re-activation. Activation of currently unknown compensatory signaling loops is further complicated by parallel pathways that also integrate with the PI3K signaling axis, including the MAPK pathway[121] and JAK/STAT pathway.[133] Robust gene expression panels are necessary to identify biological processes that may be altered by *RICTOR* ablation and which may dampen the long-term efficacy of mTORC2 targeting.

In this vein, the therapeutic efficacy studies performed in this work were solely in immune-deficient, human xenograft mouse models. While these models were necessary to study the key molecular phenotypes that are found in PI3K-active and inactive TNBC patients, they do not fully re-capitulate the tumor microenvironment, which is rich in immune cells. We therefore currently have a limited understanding of compensatory mechanisms that may be enacted by other cell populations within the tumor following *RICTOR* silencing.

5.3. Future work and potential applications

Future work on the continued optimization of our ternary si-NP carrier could focus on enhancing the surface-forming polymer for greater non-fouling effects and increased tumor cell uptake. Our si-NP system utilizes a 20k Da PEG surface polymer for stealth-shielding, but PEG-based materials show significant incidences of immunogenicity and complement activation, resulting in accelerated blood clearance (ABC) of PEG moeities.[134, 135] Our lab has previously shown zwitterionic poly(2-methacryloyloxyethyl phosphorylcholine (PMPC)-based si-NP coronas to decrease fouling and consequently improve pharmacokinetics and tumor uptake compared to PEG coronas of the same molecular weight.[44] This surface-polymer could be adapted to our si-NPs for drive greater tumor cell delivery while minimizing ABC effects that may occur in a multi-dose treatment setting such as cancer.

The molecular and pathological underpinnings of selective mTORC2 therapy continue to be understudied. Excitingly, our siRictor-NPs could serve as a clinically-relevant platform to continue studying the effects of Rictor ablation in TNBC, particularly the effects of Rictor silencing on tumor metastasis as well as modulations in the tumor microenvironment following Rictor knockdown. mTORC2 has known roles in motility and metastasis through regulation of downstream effectors PKCα/Rac1.[106] Furthermore, downstream phosphorylation of targets such as SGK and NDRG1 can promote metastasis; NDRG1 is a known suppressor of tumor cell invasion.[107, 108] mTORC2 has been furthermore implicated in immune cell motility, such as neutrophil chemotaxis.[136] Lung metastasis models can be treated with our optimized siRictor-NPs to assess the impact of mTORC2 blockade on the development of metastatic nodules. Additionally, orthotopic mammary tumors can be treated and assessed for local invasion to tumor-draining lymph nodes.

siRictor-NPs can also be used as a platform to characterize the TNBC tumor immune microenvironment following selective mTORC2 inhibition. Emerging literature has found mTORC2 to play a major role in immune cell metabolic reprogramming and consequent immune cell activation, polarization, and responses.[137-139] Preliminary studies would focus on the development of mouse TNBC models that displays potent *RICTOR* knockdown and would allow for studying the tumor microenvironment in an immune-competent setting. It is essential to first characterize the cell-specific delivery of our si-NPs to various compartments of the tumors, including endothelial cells, fibroblasts, and immune cells. Following si-NP treatment, tumors would be analyzed for immune-related signatures such as PD-L1 expression, which has been found to be increased in cancer cells displaying hyper-activated mTOR/Akt signaling.[140] It is anticipated that siRictor-NPs treatment will modulate the immune microenvironment towards an antitumor phenotype, as mTORC2 inhibition has been reported to decrease M2 (anti-inflammatory) polarization of macrophages and improve CD8+ T cell effector response.[141-144] The aforementioned PMPC-based si-NPs may be particularly interesting in this setting, as they may promote delivery to tumor-associated macrophages and drive M1-like (anti-tumor) macrophage polarization to enhance tumor cell killing effects.

Altogether, we have developed an siRNA nanoparticle system that holds high promise for cancer therapy. Additionally, we have uncovered the therapeutic utility of Rictor ablation as a strategy for selective mTORC2 blockade in TNBC. Our si-NP platform, when harboring siRictor, can serve as an efficacious nanomedicine to continue probing the effects of mTORC2 targeting in the TNBC disease setting.

Appendix A: Extended Methods

Ternary siRNA nanoparticle formulation:

For *in vivo* applications, we delivered a 1 mg/kg dose of siRNA in a final volume of 100 µL per injection. The binary si-NP, 50B0, contained only the 20kPEG-50B polymer solution. All si-NPs were formulated at a total polymer to nucleic acid ratio (N^+/P^-, calculated using the ratio of protonated amines on the DMAEMA polymer to phosphates on the siRNA duplex) of 16. For ternary si-NPs, N/P of 50B was varied as 0, 4, 8, or 12 of the total polyplex N/P of 16. siRNA and polymer amounts are calculated using the formulas below:

$$nmol\ Pol_1 = \frac{(nmol\ siRNA)(bp\ siRNA)(2)\left(\frac{N}{P}\right)}{(RU\ DMAEMA)(0.5)}$$

$$nmol\ Pol_2 = \frac{(nmol\ siRNA)(bp\ siRNA)(2)\left(\frac{N}{P}\right) - (nmol\ Pol_1)(RU\ DMAEMA_1)(0.5)}{(RU\ DMAEMA)(0.5)}$$

Pol_1 refers to the 50B polymer

Repeats units for DMAEMA in this polymer should be known and calculated by NMR

For the ternary system in this work, N/P could be 0, 4, 8, or 12

Pol_2 refers to the 20kPEG-50B polymer

Repeat units for DMAEMA should be known and calculated by NMR

For the ternary system in this work, N/P would be set to 16 (total si-NP N/P)

bp siRNA refers to the base pairs of siRNA

Our zipper siRNA are traditionally 19mers, and this value is multiplied by 2 since we encapsulate a duplex

nmol siRNA refers to the total nmol of siRNA to be complexed

Average weight of mouse is known, which is used to calculate the mg of siRNA to encapsulate (a single 1 mg/kg dose to a 24 g mouse is a total of 0.024 mg siRNA)

mg of siRNA can be converted to *nmol siRNA* when divided by the molecular weight of the siRNA duplex

After solving for *nmol* Pol_1 and *nmol* Pol_2, mass (mg) of each polymer can be converted when multiplied by the respective molecular weight of each polymer.

Calculated masses of the 20kPEG-50B and 50B polymers were weighed out. The 20kPEG-50B polymer was dissolved to a 3 mg/mL final polymer solution and the 50B polymer was dissolved to a 0.5 mg/mL polymer solution. To do this, we first dissolved each polymer in EtOH that was 10% v/v of the final solution. (Example: 3 mg of 20kPEG-50B was weighed out, and this mass needs to be dissolved in a total volume of 1 mL to achieve a 3 mg/mL final polymer solution. We would first dissolve it in 100 μL of EtOH). Polymers were brought up to their final dilution by the addition of 0.1 M citrate buffer (pH 4), which made up 90% v/v of the final solution. (Example: The aforementioned 3 mg of 20kPEG-50B polymer would receive 900 μL of pH 4 buffer, added to the 100 μL of EtOH that the polymer is already dissolved in).

Calculated amounts of each polymer were first mixed together to (calculated to achieve a desired N/P), and then the calculated amount of siRNA was added. The solution was allowed to complex for 30 min. Following complexation, 5x v/v 0.2 M phosphate buffer (pH 8) was added to raise solution pH to 7.4. (Example: 500 uL of pH 8 buffer would be added to a 100 μL complexing solution).

Formulated si-NPs were added to Amicon centrifugal tubes (Millipore Sigma) with 50 kDa MW cut-off to concentrate si-NPs and remove excess levels of pH buffers. si-NPs were concentrated to 1/8 of their final volume. (Example: A final 100 μL injection solution would be concentrated to 12.5 μL). Concentrated si-NPs were transferred to a new tube and were brought up to their final volume with 300 mM trehalose solution. si-NPs were aliquoted as 100 μL single

injections per tube, flash-frozen, lyophilized overnight, and stored at -80°C thereafter. To reconstitute lyophilized si-NPs, water was first added to the si-NP cake at the volume that si-NPs were lyophilized in (100 μL per tube). si-NPs were allowed to sit for 30 min to rehydrate fully and then pipet mixed prior to being filled into a syringe for injection.

Western blotting of tumor tissue:

During harvest, tumor tissue was flash-frozen and stored at -80 °C until further use. Ice-cold radioimmunoprecipitation assay (RIPA) buffer was supplemented with protease inhibitor (cOmplete, Roche) and phosphatase inhibitor (Phos-STOP, Roche). Approximately 10 mg of tumor tissue was quickly weighed, placed on ice, and covered with 300 μL RIPA. A 5 mm stainless steel bead was added to tubes and tissues were homogenized at max frequency for 5 min on a Qiagen TissueLyser II. Nonidet P-40 (NP-40) solution was added to homogenate at a 2% v/v and tissues were further disrupted by pulling through a 200 μL pipet tip. Lysates were incubated on ice for at least one hr and cleared by 14,000 xg centrifugation for 15 min at 4°C. Protein concentration was quantified by Pierce BCA assay and 20 μg lysates were used as a general standard.

Proteins were resolved on 4-20% Mini-PROTEAN TGX gels (Bio-Rad) for ~1.5 hrs at 100 V and transferred to nitrocellulose membranes (iBlot2, Invitrogen) for 7 min at 20 V. Membranes were blocked with TBS-based blocking buffer (LI-COR) for 1 hr at room temperature and probed with antibodies from Cell Signaling Technologies overnight at 4°C. Membranes were probed with anti-Rabbit IgG IRDyes (LI-COR) for 1 hr at room temperature the next day. Gels were imaged using the Odyssey Fc Imaging System (LI-COR).

qRT-PCR of tumor tissue:

During harvest, tumor tissue was placed in tubes containing a 5x volume of RNALater and further snipped in the solution so that tissues were only 5 mm long in any direction. Tissues were incubated in RNALater solution overnight at room temperature and then stored at -80°C until

further use. A maximum of 20 mg of tumor tissue was placed in an RNAse-free tube and covered with 1 mL QIAzol Lysis Reagent. A 5 mm stainless steel bead was added to tubes and tissues were homogenized at max frequency for 5 min on a Qiagen TissueLyser II. Lysates were centrifuged at 12,000 xg for 8 min at 4°C to clear debris. Lysates were moved to a new tube and incubated at room temperature for 5 min before adding 200 μL chloroform and shaking vigorously for 15 s. Samples were centrifuged at 12,000 xg for 15 min at 4°C, and the upper aqueous layer of the 3 phases was moved to a fresh tube. An equal volume of 70% EtOH was added. mRNA extraction was then performed according to Qiagen the RNEasy Mini Kit with an additional Buffer RPE wash step added prior to mRNA elution into water. mRNA was eluted with 50 μL water and then an additional 50 μL of water was added to column to elute any extra mRNA (total elution volume was 100 μL). RNA was quantified by reading 260 absorbance, with confirmation that 260/280 and 260/230 absorbance ratios were in the ~2.0 range as a measure of contamination.

1 μg of cDNA was synthesized using the iScript cDNA Synthesis Kit (Bio-Rad), following manufacturer's instructions. The resulting cDNA was diluted to final stock of 0.0125 μg/μL, and 0.025 ug of RNA was added to each PCR well. 6 pmol each of forward and reverse primers was added to each well. mRNA levels were quantified using 2x SYBR Green (Bio-Rad) based qRT-PCR, where the total volume of each well was 20 μL.

When performing qRT-PCR to measure gene knockdown in xenograft tumors (human cells engrafted into mice), it is essential to design housekeeping and target gene primers that only amplify in the human genome while not amplifying the mouse genome. It is also important to confirm that the housekeeping gene that is used does not fluctuate in its expression between treatment groups.

Appendix B: References

1. Morris, G.J., et al., *Differences in breast carcinoma characteristics in newly diagnosed African–American and Caucasian patients.* Cancer, 2007. **110**(4): p. 876-884.
2. Haffty, B.G., et al., *Locoregional Relapse and Distant Metastasis in Conservatively Managed Triple Negative Early-Stage Breast Cancer.* Journal of Clinical Oncology, 2006. **24**(36): p. 5652-5657.
3. Dent, R., et al., *Triple-Negative Breast Cancer: Clinical Features and Patterns of Recurrence.* Clinical Cancer Research, 2007. **13**(15): p. 4429.
4. Carey, L.A., et al., *The Triple Negative Paradox: Primary Tumor Chemosensitivity of Breast Cancer Subtypes.* Clinical Cancer Research, 2007. **13**(8): p. 2329.
5. Rouzier, R., et al., *Breast Cancer Molecular Subtypes Respond Differently to Preoperative Chemotherapy.* Clinical Cancer Research, 2005. **11**(16): p. 5678.
6. Lin, N.U., et al., *Sites of distant recurrence and clinical outcomes in patients with metastatic triple-negative breast cancer: high incidence of central nervous system metastases.* Cancer, 2008. **113**(10): p. 2638-2645.
7. Foulkes, W.D., et al., *The Prognostic Implication of the Basal-Like (Cyclin Ehigh/p27low/p53+/Glomeruloid-Microvascular-Proliferation+) Phenotype of BRCA1-related breast cancer.* Cancer Research, 2004. **64**(3): p. 830.
8. Sivina, E., et al., *Pathological complete response to neoadjuvant chemotherapy in triple negative breast cancer – single hospital experience.* Hereditary Cancer in Clinical Practice, 2023. **21**(1): p. 4.
9. Koboldt, D.C., et al., *Comprehensive molecular portraits of human breast tumours.* Nature, 2012. **490**(7418): p. 61-70.
10. Verret, B., et al., *Efficacy of PI3K inhibitors in advanced breast cancer.* Annals of Oncology, 2019. **30**: p. x12-x20.
11. Gonzalez-Angulo, A.M., et al., *Open-label randomized clinical trial of standard neoadjuvant chemotherapy with paclitaxel followed by FEC versus the combination of paclitaxel and everolimus followed by FEC in women with triple receptor-negative breast cancer†.* Annals of oncology : official journal of the European Society for Medical Oncology, 2014. **25**(6): p. 1122-1127.
12. Huober, J., et al., *Neoadjuvant chemotherapy with paclitaxel and everolimus in breast cancer patients with non-responsive tumours to epirubicin/cyclophosphamide (EC) ± bevacizumab – Results of the randomised GeparQuinto study (GBG 44).* European Journal of Cancer, 2013. **49**(10): p. 2284-2293.
13. Jovanović, B., et al., *A Randomized Phase II Neoadjuvant Study of Cisplatin, Paclitaxel With or Without Everolimus in Patients with Stage II/III Triple-Negative Breast Cancer (TNBC): Responses and Long-term Outcome Correlated with Increased Frequency of DNA Damage Response Gene Mutations, TNBC Subtype, AR Status, and Ki67.* Clin Cancer Res, 2017. **23**(15): p. 4035-4045.
14. Powles, T., et al., *A Randomised Phase 2 Study of AZD2014 Versus Everolimus in Patients with VEGF-Refractory Metastatic Clear Cell Renal Cancer.* Eur Urol, 2016. **69**(3): p. 450-6.
15. Schmid, P., et al., *Fulvestrant Plus Vistusertib vs Fulvestrant Plus Everolimus vs Fulvestrant Alone for Women With Hormone Receptor-Positive Metastatic Breast Cancer: The MANTA Phase 2 Randomized Clinical Trial.* JAMA Oncol, 2019. **5**(11): p. 1556-1564.

16. Lehmann, B.D., et al., *Identification of human triple-negative breast cancer subtypes and preclinical models for selection of targeted therapies.* The Journal of clinical investigation, 2011. **121**(7): p. 2750-2767.
17. Werfel, T.A., et al., *Selective mTORC2 Inhibitor Therapeutically Blocks Breast Cancer Cell Growth and Survival.* Cancer research, 2018. **78**(7): p. 1845-1858.
18. Betker, J.L., S.G. Tilden, and T.J. Anchordoquy, *Escaping to silence using an endosome-disrupting polymer.* Mol Ther, 2021. **29**(10): p. 2893-2894.
19. Nogueira, D.R., et al., *The role of counterions in the membrane-disruptive properties of pH-sensitive lysine-based surfactants.* Acta Biomater, 2011. **7**(7): p. 2846-56.
20. Blanco, E., H. Shen, and M. Ferrari, *Principles of nanoparticle design for overcoming biological barriers to drug delivery.* Nature Biotechnology, 2015. **33**(9): p. 941-951.
21. Whitehead, K.A., R. Langer, and D.G. Anderson, *Knocking down barriers: advances in siRNA delivery.* Nature Reviews Drug Discovery, 2009. **8**(2): p. 129-138.
22. Papahadjopoulos, D., et al., *Sterically stabilized liposomes: improvements in pharmacokinetics and antitumor therapeutic efficacy.* Proceedings of the National Academy of Sciences of the United States of America, 1991. **88**(24): p. 11460-11464.
23. Gabizon, A. and F. Martin, *Polyethylene Glycol-Coated (Pegylated) Liposomal Doxorubicin.* Drugs, 1997. **54**(4): p. 15-21.
24. Gabizon, A., H. Shmeeda, and Y. Barenholz, *Pharmacokinetics of Pegylated Liposomal Doxorubicin.* Clinical Pharmacokinetics, 2003. **42**(5): p. 419-436.
25. Torchilin, V., *Tumor delivery of macromolecular drugs based on the EPR effect.* Advanced Drug Delivery Reviews, 2011. **63**(3): p. 131-135.
26. Maeda, H., H. Nakamura, and J. Fang, *The EPR effect for macromolecular drug delivery to solid tumors: Improvement of tumor uptake, lowering of systemic toxicity, and distinct tumor imaging in vivo.* Advanced Drug Delivery Reviews, 2013. **65**(1): p. 71-79.
27. Albanese, A., P.S. Tang, and W.C.W. Chan, *The Effect of Nanoparticle Size, Shape, and Surface Chemistry on Biological Systems.* Annual Review of Biomedical Engineering, 2012. **14**(1): p. 1-16.
28. Zuckerman, J.E., et al., *Polycation-siRNA nanoparticles can disassemble at the kidney glomerular basement membrane.* Proceedings of the National Academy of Sciences of the United States of America, 2012. **109**(8): p. 3137-3142.
29. Moghimi, S.M. and H.M. Patel, *Serum-mediated recognition of liposomes by phagocytic cells of the reticuloendothelial system – The concept of tissue specificity.* Advanced Drug Delivery Reviews, 1998. **32**(1): p. 45-60.
30. Moghimi, S.M., A.C. Hunter, and J.C. Murray, *Long-Circulating and Target-Specific Nanoparticles: Theory to Practice.* Pharmacological Reviews, 2001. **53**(2): p. 283.
31. Leu, D., et al., *Distribution and Elimination of Coated Polymethyl [2-¹⁴C]Methacrylate Nanoparticles After Intravenous Injection in Rats.* Journal of Pharmaceutical Sciences, 1984. **73**(10): p. 1433-1437.
32. Göppert, T.M. and R.H. Müller, *Polysorbate-stabilized solid lipid nanoparticles as colloidal carriers for intravenous targeting of drugs to the brain: Comparison of plasma protein adsorption patterns.* Journal of Drug Targeting, 2005. **13**(3): p. 179-187.
33. Jackson, M.A., et al., *Kupffer cell release of platelet activating factor drives dose limiting toxicities of nucleic acid nanocarriers.* Biomaterials, 2021. **268**: p. 120528.
34. Hagiwara, A., et al., *Hepatic mTORC2 activates glycolysis and lipogenesis through Akt, glucokinase, and SREBP1c.* Cell Metab, 2012. **15**(5): p. 725-38.

35. Owen, S.C., D.P.Y. Chan, and M.S. Shoichet, *Polymeric micelle stability.* Nano Today, 2012. **7**(1): p. 53-65.
36. Gaucher, G., et al., *Block copolymer micelles: preparation, characterization and application in drug delivery.* Journal of Controlled Release, 2005. **109**(1): p. 169-188.
37. Werfel, T.A., et al., *Combinatorial optimization of PEG architecture and hydrophobic content improves ternary siRNA polyplex stability, pharmacokinetics, and potency in vivo.* Journal of Controlled Release, 2017. **255**: p. 12-26.
38. Jackson, M.A., et al., *Dual carrier-cargo hydrophobization and charge ratio optimization improve the systemic circulation and safety of zwitterionic nano-polyplexes.* Biomaterials, 2019. **192**: p. 245-259.
39. Sarett, S.M., et al., *Hydrophobic interactions between polymeric carrier and palmitic acid-conjugated siRNA improve PEGylated polyplex stability and enhance in vivo pharmacokinetics and tumor gene silencing.* Biomaterials, 2016. **97**: p. 122-132.
40. Oe, Y., et al., *Actively-targeted polyion complex micelles stabilized by cholesterol and disulfide cross-linking for systemic delivery of siRNA to solid tumors.* Biomaterials, 2014. **35**(27): p. 7887-7895.
41. Ambardekar, V.V., et al., *The modification of siRNA with 3′ cholesterol to increase nuclease protection and suppression of native mRNA by select siRNA polyplexes.* Biomaterials, 2011. **32**(5): p. 1404-1411.
42. Nishina, K., et al., *Efficient In Vivo Delivery of siRNA to the Liver by Conjugation of α-Tocopherol.* Molecular Therapy, 2008. **16**(4): p. 734-740.
43. Kilchrist, K.V., et al., *Gal8 Visualization of Endosome Disruption Predicts Carrier-Mediated Biologic Drug Intracellular Bioavailability.* ACS nano, 2019. **13**(2): p. 1136-1152.
44. Jackson, M.A., et al., *Zwitterionic Nanocarrier Surface Chemistry Improves siRNA Tumor Delivery and Silencing Activity Relative to Polyethylene Glycol.* ACS Nano, 2017. **11**(6): p. 5680-5696.
45. Miteva, M., et al., *Tuning PEGylation of mixed micelles to overcome intracellular and systemic siRNA delivery barriers.* Biomaterials, 2015. **38**: p. 97-107.
46. Castaneda, C.A., et al., *The phosphatidyl inositol 3-kinase/AKT signaling pathway in breast cancer.* Cancer and Metastasis Reviews, 2010. **29**(4): p. 751-759.
47. Hennessy, B.T., et al., *Characterization of a naturally occurring breast cancer subset enriched in epithelial-to-mesenchymal transition and stem cell characteristics.* Cancer research, 2009. **69**(10): p. 4116-4124.
48. Agoulnik, I.U., et al., *INPP4B: the new kid on the PI3K block.* Oncotarget, 2011. **2**(4): p. 321-328.
49. Miller, T.W., et al., *Mutations in the phosphatidylinositol 3-kinase pathway: role in tumor progression and therapeutic implications in breast cancer.* Breast cancer research : BCR, 2011. **13**(6): p. 224-224.
50. O'Reilly, K.E., et al., *mTOR inhibition induces upstream receptor tyrosine kinase signaling and activates Akt.* Cancer research, 2006. **66**(3): p. 1500-1508.
51. Bhola, N.E., et al., *Treatment of Triple-Negative Breast Cancer with TORC1/2 Inhibitors Sustains a Drug-Resistant and Notch-Dependent Cancer Stem Cell Population.* Cancer research, 2016. **76**(2): p. 440-452.
52. Hatem, R., et al., *Targeting mTOR pathway inhibits tumor growth in different molecular subtypes of triple-negative breast cancers.* Oncotarget, 2016. **7**(30): p. 48206-48219.

53. Guichard, S.M., et al., *AZD2014, an Inhibitor of mTORC1 and mTORC2, Is Highly Effective in ER+ Breast Cancer When Administered Using Intermittent or Continuous Schedules.* Molecular Cancer Therapeutics, 2015. **14**(11): p. 2508.
54. Bendell, J.C., et al., *A phase I dose-escalation study to assess safety, tolerability, pharmacokinetics, and preliminary efficacy of the dual mTORC1/mTORC2 kinase inhibitor CC-223 in patients with advanced solid tumors or multiple myeloma.* Cancer, 2015. **121**(19): p. 3481-3490.
55. Isakoff, S.J., *Triple-negative breast cancer: role of specific chemotherapy agents.* Cancer journal (Sudbury, Mass.), 2010. **16**(1): p. 53-61.
56. Lebert, J.M., et al., *Advances in the systemic treatment of triple-negative breast cancer.* Current oncology (Toronto, Ont.), 2018. **25**(Suppl 1): p. S142-S150.
57. Gradishar, W.J., et al., *Phase III Trial of Nanoparticle Albumin-Bound Paclitaxel Compared With Polyethylated Castor Oil–Based Paclitaxel in Women With Breast Cancer.* Journal of Clinical Oncology, 2005. **23**(31): p. 7794-7803.
58. Park, I.H., et al., *An Open-Label, Randomized, Parallel, Phase III Trial Evaluating the Efficacy and Safety of Polymeric Micelle-Formulated Paclitaxel Compared to Conventional Cremophor EL-Based Paclitaxel for Recurrent or Metastatic HER2-Negative Breast Cancer.* Cancer research and treatment : official journal of Korean Cancer Association, 2017. **49**(3): p. 569-577.
59. O'Brien, M.E.R., et al., *Reduced cardiotoxicity and comparable efficacy in a phase IIItrial of pegylated liposomal doxorubicin HCl(CAELYX/Doxil) versus conventional doxorubicin forfirst-line treatment of metastatic breast cancer.* Annals of Oncology, 2004. **15**(3): p. 440-449.
60. Sparano, J.A., et al., *Pegylated Liposomal Doxorubicin Plus Docetaxel Significantly Improves Time to Progression Without Additive Cardiotoxicity Compared With Docetaxel Monotherapy in Patients With Advanced Breast Cancer Previously Treated With Neoadjuvant-Adjuvant Anthracycline Therapy: Results From a Randomized Phase III Study.* Journal of Clinical Oncology, 2009. **27**(27): p. 4522-4529.
61. Balko, J.M., et al., *Molecular profiling of the residual disease of triple-negative breast cancers after neoadjuvant chemotherapy identifies actionable therapeutic targets.* Cancer discovery, 2014. **4**(2): p. 232-245.
62. Morrison Joly, M., et al., *Rictor/mTORC2 Drives Progression and Therapeutic Resistance of HER2-Amplified Breast Cancers.* Cancer research, 2016. **76**(16): p. 4752-4764.
63. Kamada, Y., et al., *Tor2 directly phosphorylates the AGC kinase Ypk2 to regulate actin polarization.* Mol Cell Biol, 2005. **25**(16): p. 7239-48.
64. Jacinto, E., et al., *Mammalian TOR complex 2 controls the actin cytoskeleton and is rapamycin insensitive.* Nat Cell Biol, 2004. **6**(11): p. 1122-8.
65. Tsuji-Tamura, K. and M. Ogawa, *Dual inhibition of mTORC1 and mTORC2 perturbs cytoskeletal organization and impairs endothelial cell elongation.* Biochemical and Biophysical Research Communications, 2018. **497**(1): p. 326-331.
66. Nair, J.K., et al., *Impact of enhanced metabolic stability on pharmacokinetics and pharmacodynamics of GalNAc-siRNA conjugates.* Nucleic Acids Res, 2017. **45**(19): p. 10969-10977.
67. Akinc, A., et al., *The Onpattro story and the clinical translation of nanomedicines containing nucleic acid-based drugs.* Nature Nanotechnology, 2019. **14**(12): p. 1084-1087.

68. Zhang, X., et al., *Patisiran Pharmacokinetics, Pharmacodynamics, and Exposure-Response Analyses in the Phase 3 APOLLO Trial in Patients With Hereditary Transthyretin-Mediated (hATTR) Amyloidosis.* Journal of clinical pharmacology, 2020. **60**(1): p. 37-49.
69. Gilleron, J., et al., *Image-based analysis of lipid nanoparticle–mediated siRNA delivery, intracellular trafficking and endosomal escape.* Nature Biotechnology, 2013. **31**(7): p. 638-646.
70. Miao, L., et al., *Delivery of mRNA vaccines with heterocyclic lipids increases anti-tumor efficacy by STING-mediated immune cell activation.* Nature Biotechnology, 2019. **37**(10): p. 1174-1185.
71. Kulkarni, J.A., et al., *Lipid Nanoparticle Technology for Clinical Translation of siRNA Therapeutics.* Accounts of Chemical Research, 2019. **52**(9): p. 2435-2444.
72. Zhu, X., et al., *Long-circulating siRNA nanoparticles for validating Prohibitin1-targeted non-small cell lung cancer treatment.* Proceedings of the National Academy of Sciences, 2015. **112**(25): p. 7779-7784.
73. Gujrati, M., et al., *Multifunctional Cationic Lipid-Based Nanoparticles Facilitate Endosomal Escape and Reduction-Triggered Cytosolic siRNA Release.* Molecular Pharmaceutics, 2014. **11**(8): p. 2734-2744.
74. Liu, S., et al., *Zwitterionic Phospholipidation of Cationic Polymers Facilitates Systemic mRNA Delivery to Spleen and Lymph Nodes.* Journal of the American Chemical Society, 2021. **143**(50): p. 21321-21330.
75. Leu, D., et al., *Distribution and Elimination of Coated Polymethyl [2-14C]Methacrylate Nanoparticles After Intravenous Injection in Rats.* Journal of Pharmaceutical Sciences, 1984. **73**(10): p. 1433-1437.
76. Urits, I., et al., *A Review of Patisiran (ONPATTRO®) for the Treatment of Polyneuropathy in People with Hereditary Transthyretin Amyloidosis.* Neurology and therapy, 2020. **9**(2): p. 301-315.
77. Nelson, C.E., et al., *Balancing Cationic and Hydrophobic Content of PEGylated siRNA Polyplexes Enhances Endosome Escape, Stability, Blood Circulation Time, and Bioactivity in Vivo.* ACS Nano, 2013. **7**(10): p. 8870-8880.
78. Paunovska, K., et al., *A Direct Comparison of in Vitro and in Vivo Nucleic Acid Delivery Mediated by Hundreds of Nanoparticles Reveals a Weak Correlation.* Nano Lett, 2018. **18**(3): p. 2148-2157.
79. Mishra, P., B. Nayak, and R.K. Dey, *PEGylation in anti-cancer therapy: An overview.* Asian Journal of Pharmaceutical Sciences, 2016. **11**(3): p. 337-348.
80. Caliceti, P. and F.M. Veronese, *Pharmacokinetic and biodistribution properties of poly(ethylene glycol)–protein conjugates.* Advanced Drug Delivery Reviews, 2003. **55**(10): p. 1261-1277.
81. Yamaoka, T., Y. Tabata, and Y. Ikada, *Distribution and Tissue Uptake of Poly(ethylene glycol) with Different Molecular Weights after Intravenous Administration to Mice.* Journal of Pharmaceutical Sciences, 1994. **83**(4): p. 601-606.
82. Wang, Y. and D.W. Grainger, *Lyophilized liposome-based parenteral drug development: Reviewing complex product design strategies and current regulatory environments.* Advanced Drug Delivery Reviews, 2019. **151-152**: p. 56-71.
83. Cavallaro, G., et al., *Polymeric nanoparticles for siRNA delivery: Production and applications.* International Journal of Pharmaceutics, 2017. **525**(2): p. 313-333.

84. Radmanovic, N., et al., *Understanding the Freezing of Biopharmaceuticals: First-Principle Modeling of the Process and Evaluation of Its Effect on Product Quality.* Journal of Pharmaceutical Sciences, 2013. **102**(8): p. 2495-2507.
85. Fonte, P., et al., *Effect of cryoprotectants on the porosity and stability of insulin-loaded PLGA nanoparticles after freeze-drying.* Biomatter, 2012. **2**(4): p. 329-339.
86. Veronese, F.M., P. Caliceti, and O. Schiavon, *Branched and Linear Poly(Ethylene Glycol): Influence of the Polymer Structure on Enzymological, Pharmacokinetic, and Immunological Properties of Protein Conjugates.* Journal of Bioactive and Compatible Polymers, 1997. **12**(3): p. 196-207.
87. Sahay, G., et al., *Efficiency of siRNA delivery by lipid nanoparticles is limited by endocytic recycling.* Nature biotechnology, 2013. **31**(7): p. 653-658.
88. Kilchrist, K.V., J.W. Tierney, and C.L. Duvall, *Genetically Encoded Split-Luciferase Biosensors to Measure Endosome Disruption Rapidly in Live Cells.* ACS Sensors, 2020. **5**(7): p. 1929-1936.
89. Kilchrist, K.V., et al., *Mechanism of Enhanced Cellular Uptake and Cytosolic Retention of MK2 Inhibitory Peptide Nano-polyplexes.* Cellular and molecular bioengineering, 2016. **9**(3): p. 368-381.
90. Kanwar, Y.S. and M.G. Farquhar, *Presence of heparan sulfate in the glomerular basement membrane.* Proceedings of the National Academy of Sciences, 1979. **76**(3): p. 1303-1307.
91. Choi, H.S., et al., *Renal clearance of quantum dots.* Nature biotechnology, 2007. **25**(10): p. 1165-1170.
92. Rampado, R., et al., *Recent Advances in Understanding the Protein Corona of Nanoparticles and in the Formulation of "Stealthy" Nanomaterials.* Frontiers in Bioengineering and Biotechnology, 2020. **8**.
93. Chen, J., et al., *Nonfluorescent quenchers to correlate single-molecule conformational and compositional dynamics.* Journal of the American Chemical Society, 2012. **134**(13): p. 5734-5737.
94. Xu, Z., et al., *Induction of Shock After Intravenous Injection of Adenovirus Vectors: A Critical Role for Platelet-activating Factor.* Molecular Therapy, 2010. **18**(3): p. 609-616.
95. Ohnishi, T., et al., *Serum platelet-activating factor acetylhydrolase activity in patients with atopic dermatitis.* Journal of Dermatological Science, 2003. **33**(1): p. 70-72.
96. Graham, R.M., et al., *Plasma degradation of platelet-activating factor in severely ill patients with clinical sepsis.* Critical Care Medicine, 1994. **22**(2).
97. Kelefiotis, D. and C. Vakirtzi-Lemonias, *In vivo responses of mouse blood cells to platelet-activating factor (PAF): role of the mediators of anaphylaxis.* Agents Actions, 1993. **40**(3-4): p. 150-6.
98. Jäger, M., et al., *Branched and linear poly(ethylene imine)-based conjugates: synthetic modification, characterization, and application.* Chem Soc Rev, 2012. **41**(13): p. 4755-67.
99. Godbey, W.T., K.K. Wu, and A.G. Mikos, *Poly(ethylenimine)-mediated gene delivery affects endothelial cell function and viability.* Biomaterials, 2001. **22**(5): p. 471-80.
100. Schwinn, M.K., et al., *CRISPR-Mediated Tagging of Endogenous Proteins with a Luminescent Peptide.* ACS Chemical Biology, 2018. **13**(2): p. 467-474.
101. Convertine, A.J., et al., *Development of a novel endosomolytic diblock copolymer for siRNA delivery.* Journal of controlled release : official journal of the Controlled Release Society, 2009. **133**(3): p. 221-229.

102. Zhang, Y., et al., *PKSolver: An add-in program for pharmacokinetic and pharmacodynamic data analysis in Microsoft Excel.* Comput Methods Programs Biomed, 2010. **99**(3): p. 306-14.
103. Aleskandarany, M.A., et al., *Clinicopathologic and molecular significance of phospho-Akt expression in early invasive breast cancer.* Breast Cancer Research and Treatment, 2011. **127**(2): p. 407-416.
104. Guertin, D.A., et al., *Ablation in Mice of the mTORC Components raptor, rictor, or mLST8 Reveals that mTORC2 Is Required for Signaling to Akt-FOXO and PKCa, but Not S6K1*. Developmental Cell, 2006. **11**(6): p. 859-871.
105. Sarbassov, D.D., et al., *Phosphorylation and Regulation of Akt/PKB by the Rictor-mTOR Complex.* Science, 2005. **307**(5712): p. 1098.
106. Morrison, M.M., et al., *mTOR Directs Breast Morphogenesis through the PKC-alpha-Rac1 Signaling Axis.* PLoS genetics, 2015. **11**(7): p. e1005291-e1005291.
107. Weiler, M., et al., *mTOR target NDRG1 confers MGMT-dependent resistance to alkylating chemotherapy*. Proc Natl Acad Sci U S A, 2014. **111**(1): p. 409-14.
108. Bakker, W.J., I.S. Harris, and T.W. Mak, *FOXO3a is activated in response to hypoxic stress and inhibits HIF1-induced apoptosis via regulation of CITED2.* Mol Cell, 2007. **28**(6): p. 941-53.
109. Knuefermann, C., et al., *HER2/PI-3K/Akt activation leads to a multidrug resistance in human breast adenocarcinoma cells.* Oncogene, 2003. **22**(21): p. 3205-3212.
110. Hirschmann-Jax, C., et al., *A distinct "side population" of cells with high drug efflux capacity in human tumor cells.* Proceedings of the National Academy of Sciences, 2004. **101**(39): p. 14228-14233.
111. Dean, M., T. Fojo, and S. Bates, *Tumour stem cells and drug resistance.* Nature Reviews Cancer, 2005. **5**(4): p. 275-284.
112. Watanabe, R., M. Miyata, and C. Oneyama, *Rictor promotes tumor progression of rapamycin-insensitive triple-negative breast cancer cells.* Biochemical and Biophysical Research Communications, 2020. **531**(4): p. 636-642.
113. Li, H., et al., *Targeting of mTORC2 prevents cell migration and promotes apoptosis in breast cancer*. Breast Cancer Res Treat, 2012. **134**(3): p. 1057-66.
114. Zhang, F., et al., *mTOR complex component Rictor interacts with PKCzeta and regulates cancer cell metastasis.* Cancer Res, 2010. **70**(22): p. 9360-70.
115. Daulat, A.M., et al., *PRICKLE1 Contributes to Cancer Cell Dissemination through Its Interaction with mTORC2.* Dev Cell, 2016. **37**(4): p. 311-325.
116. García-Martínez, J.M. and D.R. Alessi, *mTOR complex 2 (mTORC2) controls hydrophobic motif phosphorylation and activation of serum- and glucocorticoid-induced protein kinase 1 (SGK1).* Biochem J, 2008. **416**(3): p. 375-85.
117. Gao, D., et al., *Rictor forms a complex with Cullin-1 to promote SGK1 ubiquitination and destruction.* Mol Cell, 2010. **39**(5): p. 797-808.
118. Sancak, Y., et al., *PRAS40 Is an Insulin-Regulated Inhibitor of the mTORC1 Protein Kinase*. Molecular Cell, 2007. **25**(6): p. 903-915.
119. Kovacina, K.S., et al., *Identification of a proline-rich Akt substrate as a 14-3-3 binding partner.* J Biol Chem, 2003. **278**(12): p. 10189-94.
120. Jacinto, E., et al., *SIN1/MIP1 Maintains rictor-mTOR Complex Integrity and Regulates Akt Phosphorylation and Substrate Specificity.* Cell, 2006. **127**(1): p. 125-137.

121. Mendoza, M.C., E.E. Er, and J. Blenis, *The Ras-ERK and PI3K-mTOR pathways: cross-talk and compensation.* Trends in Biochemical Sciences, 2011. **36**(6): p. 320-328.
122. Ciriello, G., et al., *Comprehensive Molecular Portraits of Invasive Lobular Breast Cancer.* Cell, 2015. **163**(2): p. 506-519.
123. Pereira, B., et al., *The somatic mutation profiles of 2,433 breast cancers refine their genomic and transcriptomic landscapes.* Nature Communications, 2016. **7**(1): p. 11479.
124. Curtis, C., et al., *The genomic and transcriptomic architecture of 2,000 breast tumours reveals novel subgroups.* Nature, 2012. **486**(7403): p. 346-352.
125. Cerami, E., et al., *The cBio cancer genomics portal: an open platform for exploring multidimensional cancer genomics data.* Cancer discovery, 2012. **2**(5): p. 401-404.
126. Ghandi, M., et al., *Next-generation characterization of the Cancer Cell Line Encyclopedia.* Nature, 2019. **569**(7757): p. 503-508.
127. Patel, S.S., et al., *Core polymer optimization of ternary siRNA nanoparticles enhances in vivo safety, pharmacokinetics, and tumor gene silencing.* Biomaterials, 2023. **297**: p. 122098.
128. Ouyang, B., et al., *The dose threshold for nanoparticle tumour delivery.* Nature Materials, 2020. **19**(12): p. 1362-1371.
129. Davis, M.E., et al., *Evidence of RNAi in humans from systemically administered siRNA via targeted nanoparticles.* Nature, 2010. **464**(7291): p. 1067-1070.
130. Bartlett, D.W. and M.E. Davis, *Impact of tumor-specific targeting and dosing schedule on tumor growth inhibition after intravenous administration of siRNA-containing nanoparticles.* Biotechnology and Bioengineering, 2008. **99**(4): p. 975-985.
131. Perry, J.L., et al., *Mediating Passive Tumor Accumulation through Particle Size, Tumor Type, and Location.* Nano Lett, 2017. **17**(5): p. 2879-2886.
132. Danhier, F., *To exploit the tumor microenvironment: Since the EPR effect fails in the clinic, what is the future of nanomedicine?* J Control Release, 2016. **244**(Pt A): p. 108-121.
133. Hu, X., et al., *The JAK/STAT signaling pathway: from bench to clinic.* Signal Transduction and Targeted Therapy, 2021. **6**(1): p. 402.
134. Armstrong, J.K., et al., *Antibody against poly(ethylene glycol) adversely affects PEG-asparaginase therapy in acute lymphoblastic leukemia patients.* Cancer, 2007. **110**(1): p. 103-111.
135. Hamad, I., et al., *Poly(ethylene glycol)s generate complement activation products in human serum through increased alternative pathway turnover and a MASP-2-dependent process.* Molecular Immunology, 2008. **46**(2): p. 225-232.
136. Liu, L., et al., *mTORC2 regulates neutrophil chemotaxis in a cAMP- and RhoA-dependent fashion.* Dev Cell, 2010. **19**(6): p. 845-57.
137. Guri, Y., T.M. Nordmann, and J. Roszik, *mTOR at the Transmitting and Receiving Ends in Tumor Immunity.* Frontiers in immunology, 2018. **9**: p. 578-578.
138. Powell, J.D., et al., *Regulation of immune responses by mTOR.* Annual review of immunology, 2012. **30**: p. 39-68.
139. Weichhart, T., M. Hengstschläger, and M. Linke, *Regulation of innate immune cell function by mTOR.* Nature reviews. Immunology, 2015. **15**(10): p. 599-614.
140. Lastwika, K.J., et al., *Control of PD-L1 Expression by Oncogenic Activation of the AKT–mTOR Pathway in Non–Small Cell Lung Cancer.* Cancer Research, 2016. **76**(2): p. 227.
141. Chen, W., et al., *Macrophage-Induced Tumor Angiogenesis Is Regulated by the TSC2–mTOR Pathway.* Cancer Research, 2012.

142. Li, K., et al., *Rheb1 deletion in myeloid cells aggravates OVA-induced allergic inflammation in mice.* Scientific reports, 2017. **7**: p. 42655-42655.
143. Huang, Stanley C.-C., et al., *Metabolic Reprogramming Mediated by the mTORC2-IRF4 Signaling Axis Is Essential for Macrophage Alternative Activation.* Immunity, 2016. **45**(4): p. 817-830.
144. Raïch-Regué, D., et al., *Intratumoral delivery of mTORC2-deficient dendritic cells inhibits B16 melanoma growth by promoting CD8+ effector T cell responses.* OncoImmunology, 2016. **5**(6): p. e1146841.